2013-12

Climate analysis of evaporation ducts in the South China Sea

McKeon, Brian D.

Monterey, California. Naval Postgraduate School

NAVAL POSTGRADUATE SCHOOL

MONTEREY, CALIFORNIA

THESIS

CLIMATE ANALYSIS OF EVAPORATION DUCTS IN THE SOUTH CHINA SEA

by

Brian D. McKeon

December 2013

Thesis Advisor: Tom Murphree
Co-Advisor: Paul Frederickson

THIS PAGE INTENTIONALLY LEFT BLANK

REPORT DOCUMENTATION PAGE			Form Approved OMB No. 0704–0188
Public reporting burden for this collection of information is estimated to average 1 hour per response, including the time for reviewing instruction, searching existing data sources, gathering and maintaining the data needed, and completing and reviewing the collection of information. Send comments regarding this burden estimate or any other aspect of this collection of information, including suggestions for reducing this burden, to Washington headquarters Services, Directorate for Information Operations and Reports, 1215 Jefferson Davis Highway, Suite 1204, Arlington, VA 22202–4302, and to the Office of Management and Budget, Paperwork Reduction Project (0704–0188) Washington DC 20503.			
1. AGENCY USE ONLY *(Leave blank)*	**2. REPORT DATE** December 2013	**3. REPORT TYPE AND DATES COVERED** Master's Thesis	
4. TITLE AND SUBTITLE CLIMATE ANALYSIS OF EVAPORATION DUCTS IN THE SOUTH CHINA SEA		**5. FUNDING NUMBERS**	
6. AUTHOR(S) Brian D. McKeon			
7. PERFORMING ORGANIZATION NAME(S) AND ADDRESS(ES) Naval Postgraduate School Monterey, CA 93943–5000		**8. PERFORMING ORGANIZATION REPORT NUMBER**	
9. SPONSORING /MONITORING AGENCY NAME(S) AND ADDRESS(ES) N/A		**10. SPONSORING/MONITORING AGENCY REPORT NUMBER**	
11. SUPPLEMENTARY NOTES The views expressed in this thesis are those of the author and do not reflect the official policy or position of the Department of Defense or the U.S. Government. IRB Protocol number N/A.			
12a. DISTRIBUTION / AVAILABILITY STATEMENT Approved for public release; distribution is unlimited		**12b. DISTRIBUTION CODE**	

13. ABSTRACT (maximum 200 words)

Evaporation ducts have important implications for U.S. Naval activities involving electromagnetic propagation. The presence of an evaporation duct can affect naval operations involving communications, surveillance, electronic warfare, and detection of low-flying missiles, surface ships, or submarine periscopes.

We conducted a climate scale analysis of evaporation duct heights (EDH) in the northern South China Sea (SCS), including how EDH varies throughout the year, how environmental variables affect EDH differently in each season, and how regional and global-scale climate variations are related to EDH. We identified climate variations that may enable skillful long-range forecasts of EDH at lead times of up to three months using anomalies in sea surface temperature, geopotential height, and outgoing longwave radiation (OLR) as potential predictors. SCS EDH showed significant correlations with several climate variation indices, including the Multivariable El Nino Southern Oscillation Index, Nino 4, and the Summer Asian Monsoon OLR Indices.

Improved understanding and skillful predictions of seasonal and climate scale variations in EDH will aid in operational planning in locations for which real-time observations are sparse, and for interseasonal to seasonal lead times for which existing predictions are presently very limited. Knowledge of EDH in the SCS may become critically important given the increasing significance of the eastern and southeastern Asian area, and particularly for operations involving protection of high-value units and anti-submarine warfare.

14. SUBJECT TERMS Climate, Climatology, Evaporation Duct, Electromagnetic Propagation, South China Sea, EM, EDH, Long-Range Forecasting			**15. NUMBER OF PAGES** 111
			16. PRICE CODE
17. SECURITY CLASSIFICATION OF REPORT Unclassified	**18. SECURITY CLASSIFICATION OF THIS PAGE** Unclassified	**19. SECURITY CLASSIFICATION OF ABSTRACT** Unclassified	**20. LIMITATION OF ABSTRACT** UU

NSN 7540–01–280–5500 Standard Form 298 (Rev. 2–89)
Prescribed by ANSI Std. 239–18

THIS PAGE INTENTIONALLY LEFT BLANK

Approved for public release; distribution is unlimited

CLIMATE ANALYSIS OF EVAPORATION DUCTS IN THE SOUTH CHINA SEA

Brian D. McKeon
Lieutenant Commander, United States Navy
B.S., Western Michigan University, 2003

Submitted in partial fulfillment of the
requirements for the degree of

MASTER OF SCIENCE IN METEOROLOGY AND PHYSICAL OCEANOGRAPHY

from the

NAVAL POSTGRADUATE SCHOOL
December 2013

Author: Brian D. McKeon

Approved by: Tom Murphree
Thesis Advisor

Paul Frederickson
Co-Advisor

Wendell Nuss
Chair, Department of Meteorology

THIS PAGE INTENTIONALLY LEFT BLANK

ABSTRACT

Evaporation ducts have important implications for U.S. Naval activities involving electromagnetic propagation. The presence of an evaporation duct can affect naval operations involving communications, surveillance, electronic warfare, and detection of low-flying missiles, surface ships, or submarine periscopes.

We conducted a climate scale analysis of evaporation duct heights (EDH) in the northern South China Sea (SCS), including how EDH varies throughout the year, how environmental variables affect EDH differently in each season, and how regional and global-scale climate variations are related to EDH. We identified climate variations that may enable skillful long-range forecasts of EDH at lead times of up to three months using anomalies in sea surface temperature, geopotential height, and outgoing longwave radiation (OLR) as potential predictors. SCS EDH showed significant correlations with several climate variation indices, including the Multivariable El Nino Southern Oscillation Index, Nino 4, and the Summer Asian Monsoon OLR Indices.

Improved understanding and skillful predictions of seasonal and climate scale variations in EDH will aid in operational planning in locations for which real-time observations are sparse, and for interseasonal to seasonal lead times for which existing predictions are presently very limited. Knowledge of EDH in the SCS may become critically important given the increasing significance of the eastern and southeastern Asian area, and particularly for operations involving protection of high-value units and anti-submarine warfare.

THIS PAGE INTENTIONALLY LEFT BLANK

TABLE OF CONTENTS

LIST OF FIGURES

THIS PAGE INTENTIONALLY LEFT BLANK

LIST OF TABLES

THIS PAGE INTENTIONALLY LEFT BLANK

LIST OF ACRONYMS AND ABBREVIATIONS

AREPS	Advanced Refractive Effects Prediction System
ASTD	air-sea temperature difference
ASW	anti-submarine warfare
AT	air temperature
CoF	cut-off frequency
DoD	Department of Defense
ECS	East China Sea
EDH	evaporation duct height
EM	electromagnetic
EN	El Nino
ENLN	El Nino–La Nina
ENSO	El Nino Southern Oscillation
ESRL	Earth System Research Laboratory
hPa	hector-Pascal
HVU	high-value unit
IO	Indian Ocean
IOD	Indian Ocean Dipole
IOZM	Indian Ocean Zonal Mode
LN	La Nina
LRF	long-rage forecast
LTM	long-term mean
M	modified refractive index
mb	millibar
MEI	Multivariate ENSO Index
MJO	Madden-Julian Oscillation
MOS	Monin-Obukhov similarity theory
NCEP	National Centers for Environmental Prediction
NCAR	National Center for Environmental Research
NOAA	National Oceanic and Atmospheric Administration
NPS	Naval Postgraduate School

OLR	outgoing longwave radiation
Psfc	surface pressure
RDR	radar detection range
RH	relative humidity
SCS	South China Sea
SLP	sea-level pressure
SST	sea surface temperature or surface skin temperature
TDA	tactical decision aid
U.S.	United States
WNP	Western North Pacific
WS	wind speed

ACKNOWLEDGMENTS

I would like to thank my advisers, Dr. Tom Murphree and Mr. Paul Frederickson, for their patience and guidance throughout the process of this study. I could not have hoped for a better research experience.

Special thanks also go to Dr. Peter Guest for allowing me to take his electromagnetic propagation course remotely when it was not offered at NPS as an elective class. I'd also like thank Bruce Ford for his assistance in data collection and processing, and David Ramsaur for his previous work and enthusiasm on the subject.

Lastly, I owe my parents a debt of gratitude for their support and encouragement throughout my entire life, and my friends and classmates for their support during my time at NPS.

THIS PAGE INTENTIONALLY LEFT BLANK

I. INTRODUCTION

A. MOTIVATION

The purpose of this study is to provide a basis for more accurate short and long-range predictions of evaporation duct height (EDH) in the South China Sea (SCS). The presence and height of an evaporation duct influence a range of naval operations, particularly anti-submarine warfare (ASW) and the protection of high-value units (HVUs) from low-flying cruise missiles. In a region where boundary layer observations are sparse, using modern climate analysis to produce more skillful forecasts will improve military decision-makers' ability to determine things such as asset placement, or if over-the-horizon (OTH) detection of a near-surface threat is possible.

With the elimination of the U.S. Navy's radiosonde program, in-situ observations are often not available for model verification, or input into tactical decision aids (TDAs). During times of limited communication or bandwidth, model data may be unavailable all together, leaving no means of predicting electromagnetic propagation. Knowledge of the variation in EDH with changes in environmental variables and climate indices can provide useful assessments of existing conditions and forecasts at lead times several months.

A major motivation for this study was to build on the work of Twigg (2007) and Ramsaur (2009) by employing recent advances in climate analysis, such as the Advanced Climate Analysis and Forecasting (ACAF) tool and the Climate Forecast System Reanalysis (CFSR) data set. In addition, advances in the modeling of EDH have been made with the development of the Navy Atmospheric Vertical Surface Layer Model (NAVSLaM). The combination of improvements in reanalysis data and the modeling of EDH allow for a much more detailed and accurate examination of spatial and temporal variations in EDH, as well as an improved understanding of how environmental variables affect EDH in a specific region. Figure 1 depicts some of the improvements in EDH climate analysis capabilities since Ramsaur (2009). The data used to create Figure 1b has more than five times the spatial resolution of the data used to create Figure 1a.

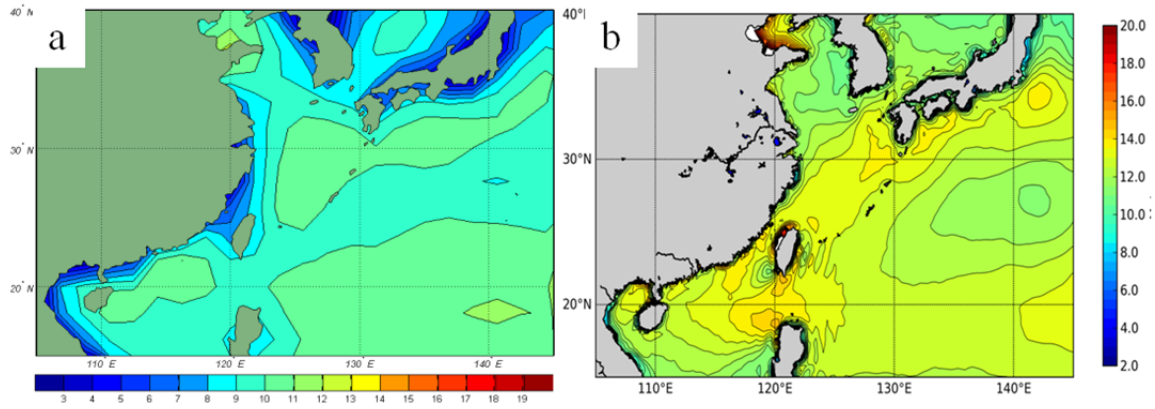

Figure 1. Long-term mean (LTM) evaporation duct height (EDH, in m) for October from: (a) Ramsaur (2009) using NCEP/NCAR R1 data with the NPS bulk model of EDH and (b) current analysis methods and tools: ACAF, CFSR data, and the NAVSLaM model of EDH. Figure (b) created at the ACAF website (October 2013).

B. REFRACTION, DUCTING, AND RADAR DETECTION RANGE

Just as with light or sound, radio-frequency electromagnetic (EM) waves refract with changes in the density of the medium in which they are propagating. Refractivity is used to describe the vertical and horizontal changes in the speed of EM waves, and the direction and degree to which they bend. Since the atmosphere fluctuates in density due to changes in temperature, pressure, and humidity, refractivity changes in both the vertical and horizontal affecting the way EM waves propagate. Understanding how refractivity changes with density, and how density varies in space and time, is necessary to predict the propagation path of an EM wave.

1. Modified Refractivity and Ducting Layers

Modified refractivity (M) is used to describe this refraction relative to the curvature of Earth's surface and is useful when describing the potential of EM waves to propagate though trapping layers in the atmosphere. M is defined as:

$$M = 77.6\frac{p}{T} - 5.6\frac{e}{T} + 375000\frac{e}{T^2} + 0.1568z$$

where p (hPa) is atmospheric pressure, T (K) is temperature, *e* (hPa) is the water vapor pressure at height z (m), and constants have been determined empirically.

The type of refraction is determined from the vertical gradient of M. When the gradient of M is positive (dM/dz >0), EM waves experience sub-refraction or bend upward away from Earth's surface. When the gradient of M is negative (dM/dz<0), EM waves experience super-refraction or bend downward toward Earth's surface. When dM/dz = 0, EM waves are undergoing refraction equal to the curvature Earth and propagate parallel Earth's surface.

In typical conditions over the open ocean, relative humidity decreases rapidly with height from near saturation conditions at the surface, thus tending to create a negative M gradient. As the decrease in relative humidity with height from the very rapid decrease at the surface, the negative M gradient becomes positive at some height (z) above the surface. If the negative M gradient extends sufficiently high, a waveguide will be created and EM waves will refract downward and bounce off the ocean surface in a repetitive manner. This waveguide depicted in Figure 2 is referred to as an evaporation duct and can greatly extend near-surface radar detection ranges (RDR; Frederickson 2008). Though several other types of ducting can occur, it is the evaporation duct that is the focus of this study.

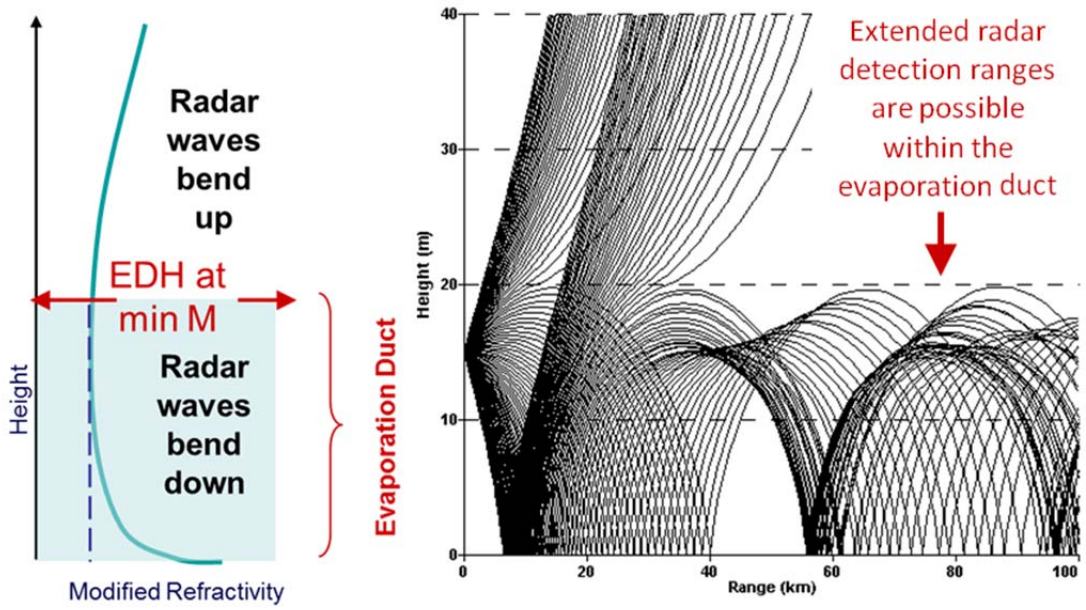

Figure 2. A vertical M profile for an evaporation duct and its associated height versus range ray trace plot of X-band waves emitted from an antenna at 15 m in height propagating through an atmosphere with an evaporation duct height (EDH) of 20 m, after Frederickson, Davidson, and Goroch 2000).

2. The Effects of Environmental Factors on EDH

Variations in EDH over the ocean come primarily from variations in four environmental variables: sea surface temperature (SST), air temperature (AT) relative humidity (RH), and near-surface wind speed (WS). The response of the EDH to changes in these variables is dependent on the air-sea temperature difference (ASTD). When ASTD is negative (warmer SST and unstable conditions), as we typically observe in the SCS, EDH generally increases with an increase in SST, AT, or WS, or a decrease in RH. When ASTD is positive (warmer AT and stable conditions), the response of EDH is less straightforward. In stable conditions, EDH still tends to increase with an increase in SST, AT, or a decrease in RH, but will instead decrease with an increase in WS. Furthermore, the evaporation duct tends to reach a maximum height when the ASTD is between 0.5^{o} and 3^{o} C and decreases rapidly at higher and lower values of ASTD. In this range of ASTD, along with calm winds or very low RH, EDH can reach extremely high values or become undefined (Frederickson 2008). Conditions such as these are very uncommon in the open ocean, but can be observed in coastal waters near desert regions.

Figures 3 and 4 are plots of EDH predicted by NAVSLaM versus ASTD for various values of wind speed and relative humidity, respectively. The difference in behavior between positive and negative values of ASTD (stable versus unstable conditions) is significant. Conditions in the SCS are normally unstable, so modeling of EDH is rather straightforward. Conditions in coastal regions or in other parts of the world can experience stable conditions, where EDH is much more variable in space and time.

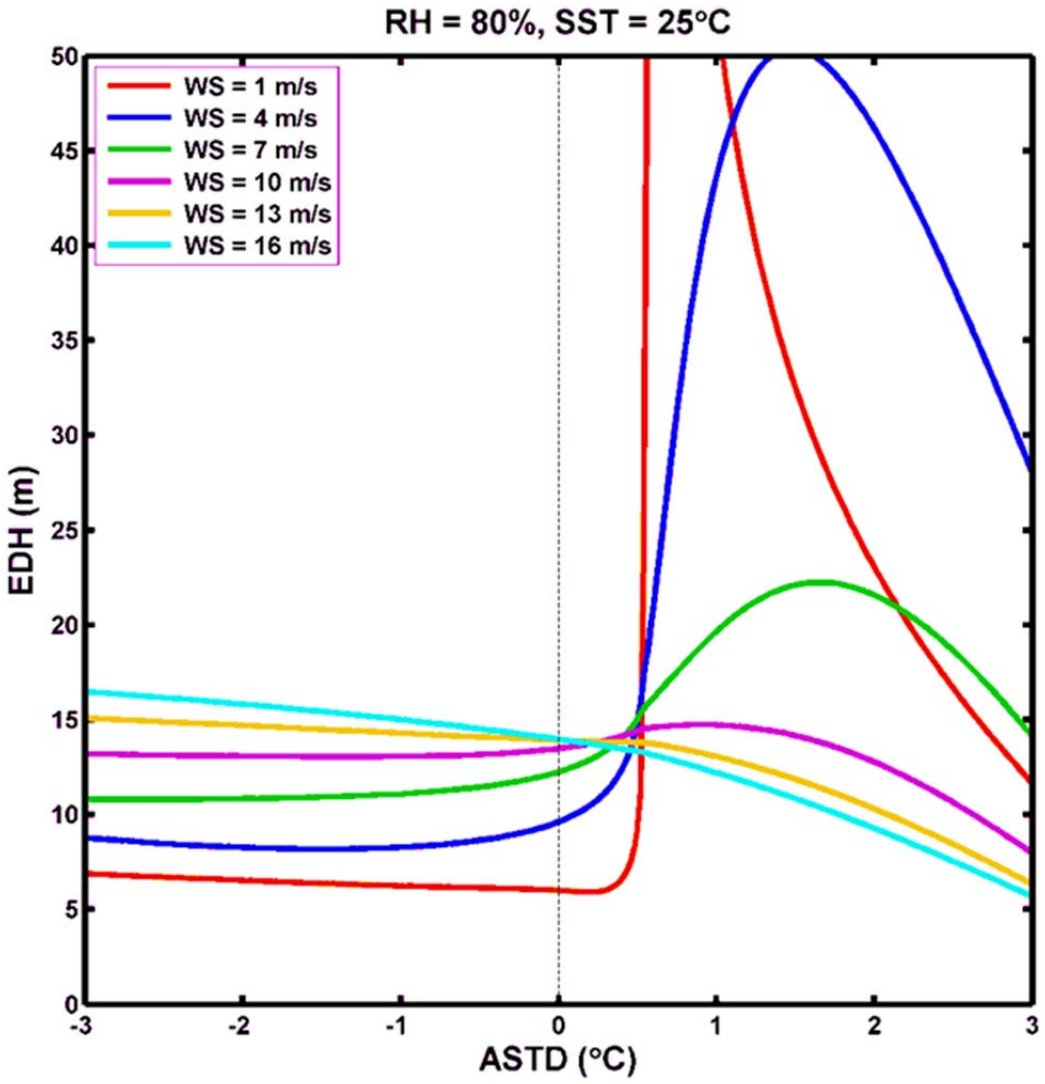

Figure 3. NAVSLaM plot of EDH versus air-sea temperature difference (ASTD) for various wind speeds (WS). Note the difference between positive and negative values of ASTD. Plot of NAVSLaM-modeled EDH courtesy of Paul Frederickson (October 2013).

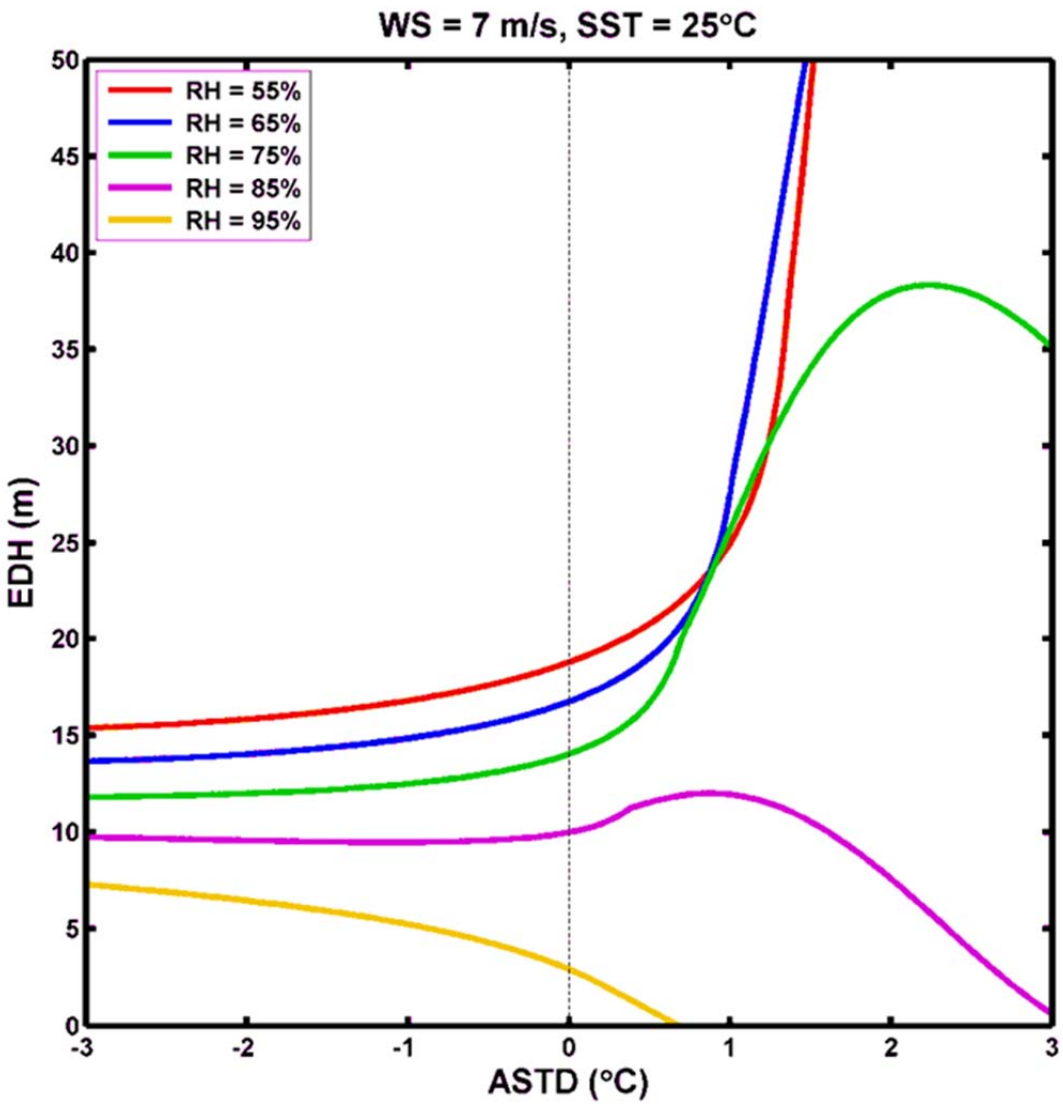

Figure 4. NAVSLaM plot of EDH versus air-sea temperature difference (ASTD) for various values of relative humidity (RH). Note the difference between positive and negative values of ASTD. Plot of NAVSLaM-modeled EDH courtesy of Paul Frederickson (October 2013).

3. Navy Atmospheric Vertical Surface Layer Model (NAVSLaM)

NAVSLaM is part of the U.S. Navy's Oceanographic and Atmospheric Library (OAML) and is a bulk evaporation duct model used operationally by the U.S. Navy to calculate vertical profiles of modified refractivity from near-surface environmental parameters. Model input can come from numerical weather model output, satellite, in-situ observations, or climate reanalysis data sets. It is primarily used to provide inputs to EM

propagation models and is the evaporation duct model used to calculate the EDH values in the data set within ACAF. NAVSLaM uses Monin-Obukhov similarity (MOS) theory which assumes that turbulent fluxes within the surface layer are nearly constant and that conditions are horizontally homogeneous and stationary. (Frederickson et al. 2000). NAVSLaM uses a modified version of the TOGA-COARE bulk algorithm to compute scaling parameters within the surface layer and the M profile up to 100 m. (Frederickson 2010a). The evaporation duct height is determined by the point at which the slope of M goes from negative to positive.

NAVSLaM validation testing confirmed it performs very well in the unstable conditions we typically observe in the SCS, but evaporation duct models utilizing MOS theory tend to have difficulty resolving evaporation ducts in stable conditions (Frederickson 2010d). Stable conditions in which the ASTD is positive, along with light winds and/or low relative humidity, can result in very high EDH to the point of being above the surface layer in which MOS theory is valid (Frederickson 2010d). Conditions such as these are extremely unusual in the tropical open ocean environment in which our study was conducted and is not a significant concern in this study. Refer to Frederickson (2010a-d) for more detailed information on NAVSLaM.

4. EM Propagation and Radar Detection Ranges

The presence of an evaporation duct of sufficient height is the single most important factor in determining near-surface propagation of EM waves and radar detection ranges (RDR; Ramsaur 2009). The heights of the evaporation duct, the antenna, and the target as well as the frequency in use are important factors in determining propagation loss and RDR (Twigg 2007).

An evaporation duct forms a “leaky” waveguide for EM waves (Frederickson et al. 2000), meaning some waves will escape the duct. If the frequency (wavelength) is high (low) enough to ‘fit’ within the duct (or the duct is high enough to accept the frequency) then the EM waves will be channeled over the horizon and experience reduced propagation loss within the duct. If the antenna and the target are both within the duct (or nearly within the duct), the reduced propagation loss will result in greater RDRs

for a given radar and target. The lowest frequency that will ‘fit’ within the duct is referred to as the cut-off frequency, but it is not an absolute cut-off. Since EM emissions propagating through the duct tend to pass though the upper boundary or “leak” in and out of the duct as they travel, the cut-off frequency is generally used to refer to the lowest frequency that will experience significant enhancement by a given EDH (Twigg 2007).

For many naval purposes, the EM frequencies of concern with regards to propagation through evaporation ducts are those higher than 3 MHz, and most often those above 3 GHz (see figure 5). The generally small heights of evaporation ducts means that evaporation ducts tend to have relatively large impacts on the performance of higher frequency radars. Figure 3 is a chart of frequency bands with their most common purposes and the evaporation duct width (same as EDH) necessary to allow enhanced propagation. Propagation enhancement will be observed at frequencies slightly lower than what is shown in Figure 5. This chart represents the minimum frequency required to observe highly significant propagation enhancement for a given EDH.

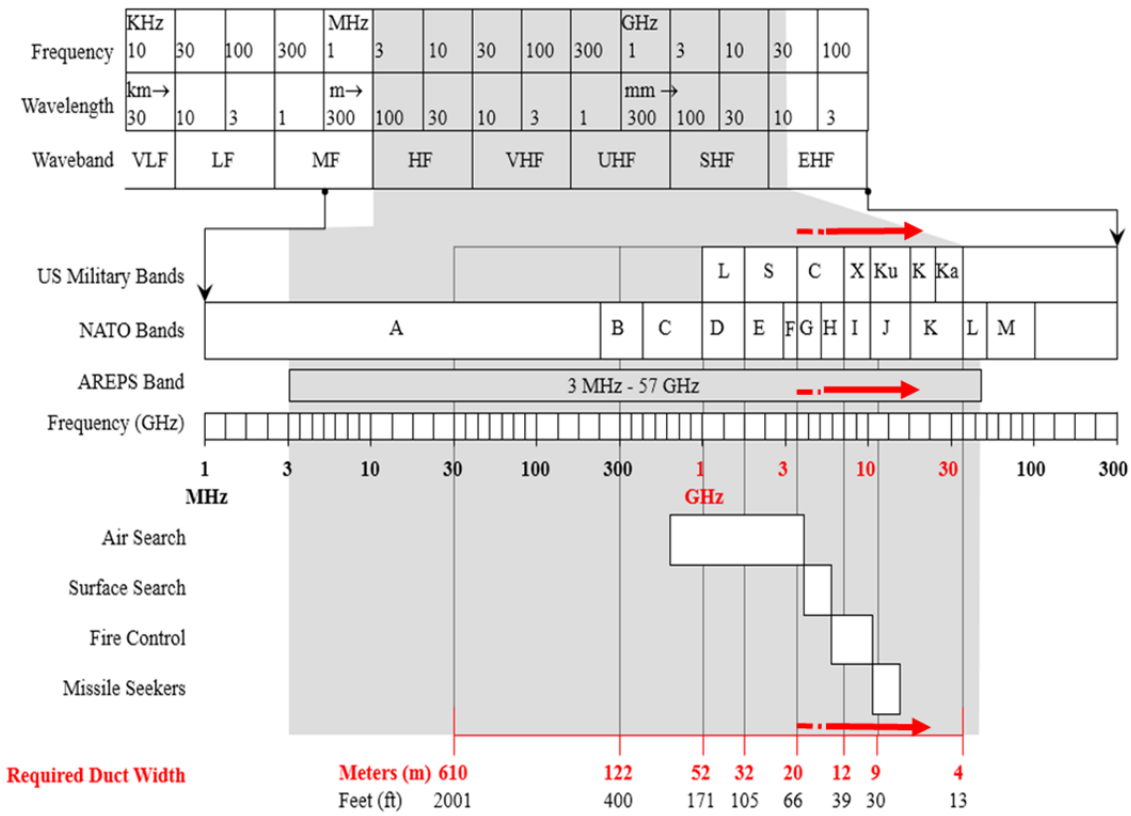

Figure 5. Radio frequency bands and the EDH (referred to as duct width in the figure) required to observe significant propagation enhancement. The red arrows highlight frequencies relevant to the ducting conditions most common in the SCS. Figure from P. Guest, MR3419 lecture 8 (2010a).

Significantly reduced propagation loss, or increased radar performance, occurs for a given radar frequency when the height of the evaporation duct is sufficient to cause waves at that frequency to be ducted. Figure 4 compares radar performance predictions for a standard atmosphere (Figure 6a) and for conditions in which a 12 m evaporation duct exists (Figure 6b). The presence of the 12 m evaporation duct significantly reduces propagation loss near the surface and increases the radar detection range for a given target that is within (or nearly within) the duct.

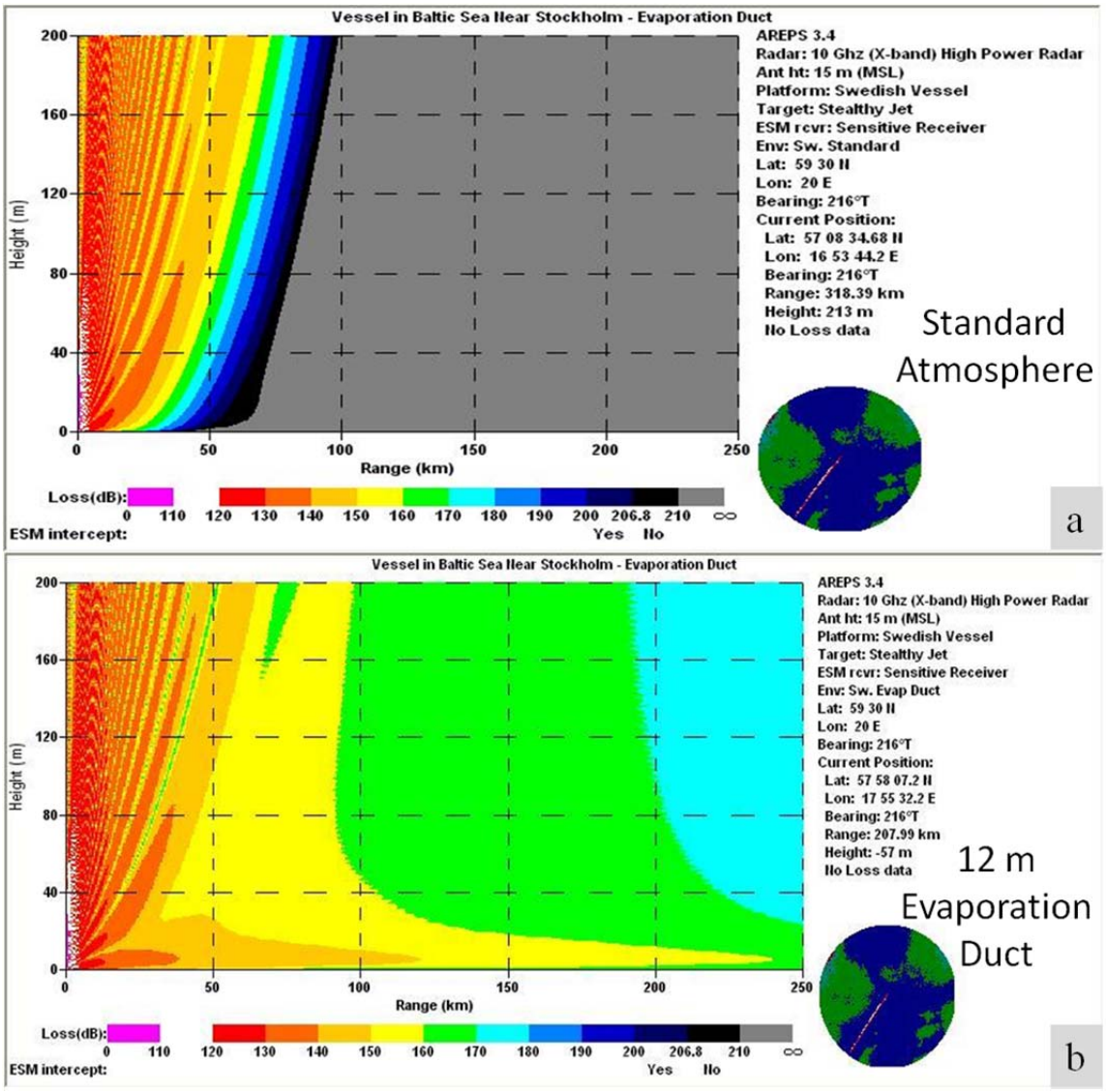

Figure 6. A comparison of the predicted propagation loss from an X-band radar at 15 m: (a) propagation loss in a standard atmosphere and (b) propagation loss with the presence of a 12 m evaporation duct. Warmer colors indicate a lower loss and greater radar return for a given target strength and distance. Note the significantly reduced propagation loss near the surface with the presence of an evaporation duct. Propagation loss is also reduced above the height of the duct indicating the "leaky" nature of the duct. Figures were generated with Advanced Refractive Effects Prediction System (AREPS) from P. Guest, MR3419 lecture 17 (2010b).

C. OVERVIEW OF THIS STUDY

The resources available to study evaporation ducts have increased greatly in the last decade, and especially the last five years. At the same time, both the U.S. Navy's need for further study of evaporation ducts and the strategic importance of the South China Sea have grown considerably, highlighting the need for our study.

Twigg (2007) for the Indian Ocean (IO) and Ramsaur (2009) for the western north Pacific (WNP) made significant steps forward in climate analysis of evaporation ducts. Our study is an additional step for a different region and using improved data sets and methods that were not available to Twigg and Ramsaur. Our analysis should be viewed as a demonstration of new techniques and tools for the climate analysis of evaporation ducts and is by no means complete. The spatial and temporal resolution of the reanalysis data sets now available allow for analyses more detailed and extensive than can be completed in any single work. As such, this study addresses the following focused set of research questions:

1. How does EDH in the SCS vary by month and by season?

2. Which environmental variables are most important in determining EDH in the SCS and how do these change seasonally?

3. To what regional and global scale climate variations are the variations in SCS EDH most closely related?

4. What is the potential to predict SCS EDH variations at long lead times (greater than 2 weeks)?

1. Area of Study: South China Sea

We conducted a basic analysis of the entire SCS to determine the most suitable area in which to focus our study. Figures of long-term mean (LTM) EDHs were created for a region from 5° N to 25° N and from 105° E to 125° E, for all 12 months. To get a sense of the variability of the region, LTM conditional composites for La Nina years (characterized by a Multivariate ENSO Index (MEI) value of -0.7 or less; see Chapter II,

section 3 for a description of MEI) and for El Nino years (characterized by MEI of 1.0 or more) were also created. A subjective, visual examination of these figures was made with consideration to the following area-selection criteria

1. Operational importance.
2. Must be > 100 km from coastlines (reasons for this will be discussed in Chapter III).
3. A simple geometric shape.
4. Large enough to be operationally relevant.
5. Relatively homogeneous EDH characteristics both spatially and temporally.

Figure 7 characterizes the spatial variation in EDH observed in the SCS. Note the clear differences in EDH between the northern and southern halves of the SCS in both February and October. This difference in behavior was observed in all but the summer months and necessitated a division between the northern and southern halves of the SCS (roughly denoted by the dotted black line) for our study. Due to its operational significance, we chose to focus on the northern half of the SCS four our study. We also chose to focus on open ocean conditions (> 100 km from coastlines) for our initial analysis of SCS EDH to avoid the complexities of the highly dynamic coastal environment.

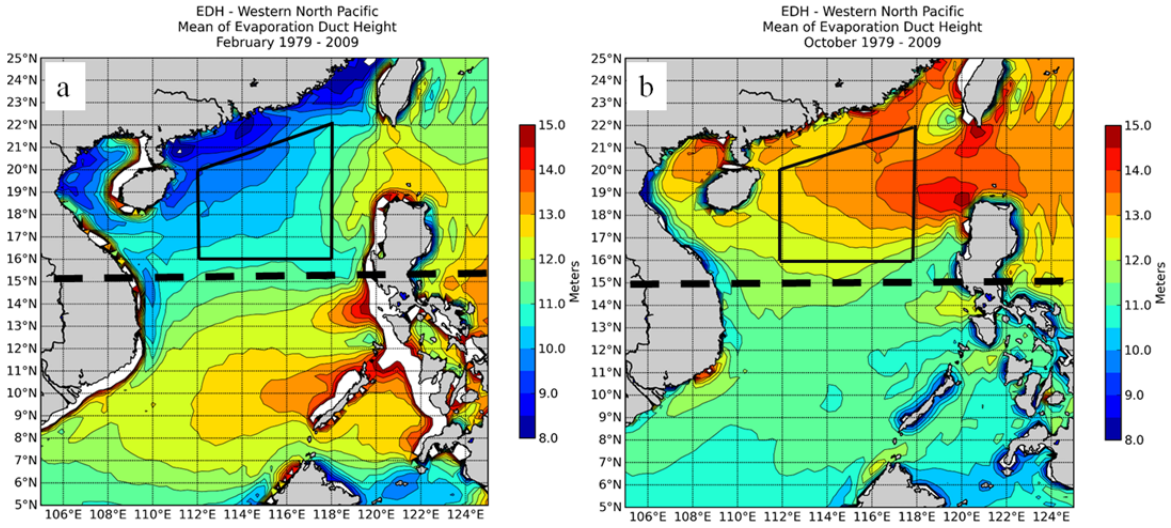

Figure 7. 1979–2009 LTM evaporation duct height (m) for (a) February and (b) October. The differences in EDH between the northern half and southern half of the SCS are significant in both figures. The boxed region shown was our primary area of study. Note: white color fill (most notable in Figure 7a) indicates EDH values outside the range of the color scale. All data in our study is from 1979–2009 unless otherwise noted. Figures created at the Advanced Climate Analysis and Forecasting (ACAF) website (October 2013).

Based on these considerations and the LTM EDH results, we chose as our study region a trapezoid-shaped box in the northern SCS (Figure 7). This box represents approximately 3100 square kilometers of ocean surface and is bounded by the following four corners: 16°N-112°E, 20°N-112°E, 22°N-118E, and 16°N-118°E. The area within this box met the aforementioned criteria and was relative homogeneous in space and time. Spatial variations in the LTM EDH within the box were less than 2 m in all months, and often 1 m or less across 90% of the area within the box. The two months depicted in Figure 7 were among the highest in EDH spatial variability, but were still relatively homogeneous within the selected area of study.

THIS PAGE INTENTIONALLY LEFT BLANK

II. DATA AND METHODS

A. DATA

We analyzed data from two global environmental reanalysis data sets as well as several climate variation indices.

1. NCEP/NCAR Reanalysis

The data used for comparison of SCS EDH with global environmental variables was obtained from the National Center for Environmental Prediction and the National Center for Atmospheric Research (NCEP/NCAR) Reanalysis data set (R1). The data was obtained between May and December 2013 via the Earth Systems Research Laboratory (ESRL) Physical Science Division (PSD) website (http://www.esrl.noaa.gov/psd). The data included a wide range of observed and derived environmental variables from historical observations and a forecast analysis using a T62 global atmospheric model. The R1 data has a 6-hour temporal resolution (00 Z, 06 Z, 12 Z, and 18 Z), a 1.875° / ~210 km horizontal resolution, 28 sigma levels, and is available from 1948 to present. Geopotential height (GPH), surface skin temperature (SST), and outgoing longwave radiation (OLR) from 1979 to 2009 were used in this study to investigate the relationship between EDH and global climate phenomenon. Previous work by Twigg (2007) and Ramsaur (2008) used this data to model EDH as well, but for this study, much higher resolution data sets are now available for modeling EDH. Refer to Kalnay et al., (1996) for more information on R1.

2. Climate Forecast System Reanalysis (CFSR)

The data set used for modeling of EDH and analyses involving the environmental variables that determine EDH was the Climate Forecast System Reanalysis (CFSR) data set recently developed by NCEP. The data was obtained between May and December 2013 via the Advanced Climate Analysis and Forecast (ACAF) tool, a common access card (CAC) enabled website available to Department of Defense (DoD) users (https://portal.fnmoc.navy.mil/climoportal/index.htm). This reanalysis is an improvement

over R1 in horizontal resolution (.3125° / ~38 km), vertical resolution (64 levels), temporal resolution (hourly), as well as an improvement in analysis methods including coupling of the ocean and atmosphere. This data set, however, is only available from 1979–2009, so our analysis of evaporative ducts was limited to this 31-year period. The modeling of EDH required the use of 10 m U and V wind components, 2 m specific humidity, 2 m air temperature, surface pressure, and sea surface temperature from this data set. All other variables necessary for modeling EDH were derived from these 6 variables from the CFSR data set. Refer to Saha et al. (2010) for more information on the CFSR data set.

CFSR data is available via ACAF for the Northern Indian Ocean, the Mediterranean Sea, and the Western North Pacific (WNP). The CFSR WNP data set used in this study extends from 90°E to 150°E, and 10°S to 50°N as depicted in Figure 8.

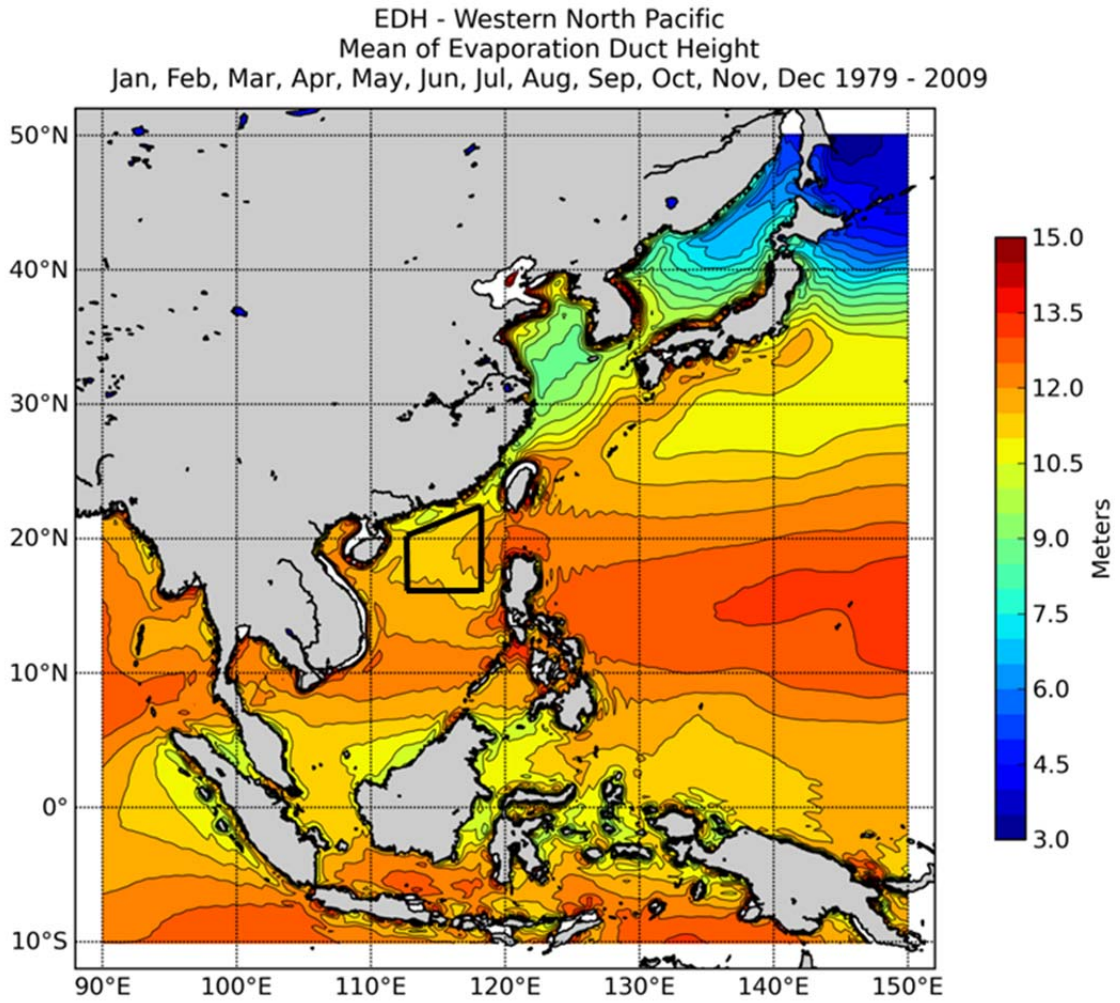

Figure 8. LTM EDH for all months and years in the Climate Forecast System Reanalyis (CFSR) data set. The white border indicates the spatial extent of the western North Pacific (WNP) data available from ACAF. Figure created at the ACAF website (October 2013).

A subset of this data falling within (or very nearly within) the borders of the specific area of study was used for all numerical calculations involving EDH or individual variables used to model EDH. Figure 9 depicts the specific area and data points used for these calculations. Two hundred ninety-four grid points fall within the area of study, with 24 time steps per day, resulting in approximately 211,768 individual data points averaged to create each monthly mean. The monthly means of EDH and its constituent environmental variables were then used for the calculation of conditional composites and correlations discussed in detail in Chapter III.

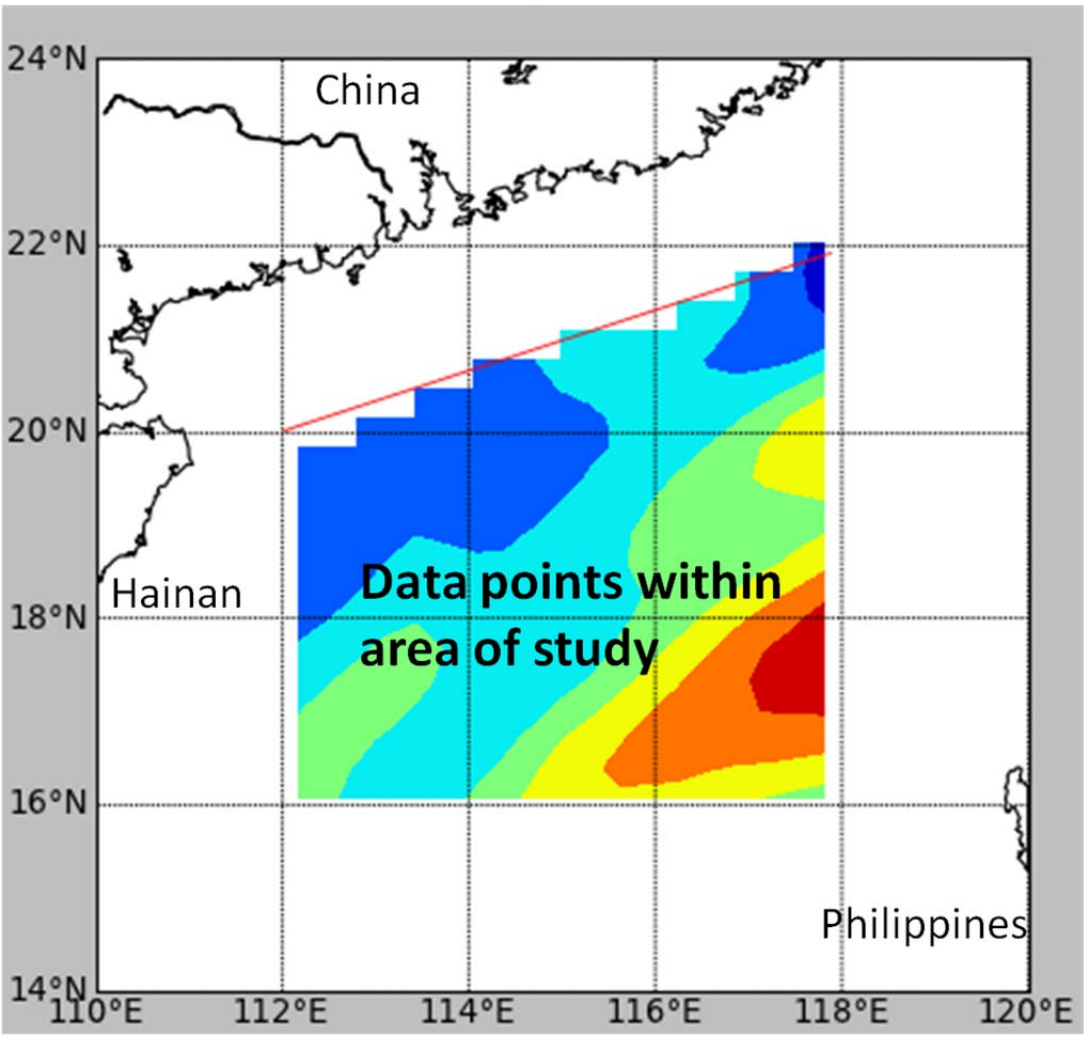

Figure 9. 294 CFSR grid points fall within the colored trapezoidal area of study shown in this figure. The colors in this figure are schematic only and are shown only to highlight the area of study. These grid points were averaged to create monthly means for the area of study as a whole which were then used for all additional analyses. Figure courtesy of Bruce Ford, Clear Science Inc. (August 2013).

3. Climate Indices

This study examined the relationship between SCS EDH and several climate variations that affect the SCS and nearby regions. To provide as much utility as possible to operational meteorology professionals who, at times, may have limited access to data, we focused on establishing relationships with commonly known and readily available climate variation indices where possible.

a. Multivariate ENSO Index (MEI)

The El Nino / La Nina /Southern Oscillation is the best known and perhaps the most influential global climate variation. This climate variation has been extensively researched under different names for several decades. El Nino La Nina (ENLN) or El Nino–Southern Oscillation (ENSO) are two more commonly accepted terms used to refer to this phenomenon. Though many indices (based primarily on tropical Pacific SST) have been developed to classify and measure the relative strength of this important global climate variation, we chose the Multivariate ENSO Index (MEI) for reference to compare with variations in SCS EDH. MEI incorporates a greater range of environmental variables including SST, U and V surface winds, sea level pressure (SLP), air temperature (AT), and total cloudiness fraction in the tropical Pacific. This greater range of variables is intended to reflect the importance of the coupled ocean-atmosphere in this climate variation and smooth out variations seen in any single environmental variable.

MEI is computed for bimonthly time periods (e.g., January/February, February/March) beginning with December/January 1950, but is updated every month shortly after the end of each bimonthly period. For the purpose of this paper, the monthly value of MEI referenced is the MEI value assigned to the month named and its preceding month. For example, reference to "November MEI" refers to the MEI value assigned to October/November. More information on MEI can be found at the ESRL website www.esrl.noaa.gov/psd/enso/mei/mei.html (2013f) or by referencing Wolter and Timlin (1993). MEI data was obtained between March and December 2013 from http://www.esrl.noaa.gov/psd/data/correlation/mei.data (2013b).

b. Nino 4 Index

Nino 4 is an SST index maintained by the Climate Prediction Center (CPC) and consists of mean SST in the tropical central Pacific from 5°N to 5°S and from 160°E to 150°E (see Figure 10). Monthly data is available from 1950 and is updated shortly after the end of each month. Nino 4 was used for comparison of EDH with a pure SST index however, our research indicated that similar results would have been observed from comparison with any of the Nino indices. Nino 4 data was obtained from the ESRL

website www.esrl.noaa.gov/psd/data/correlation/nina4.data (2013c) from March to December 2013.

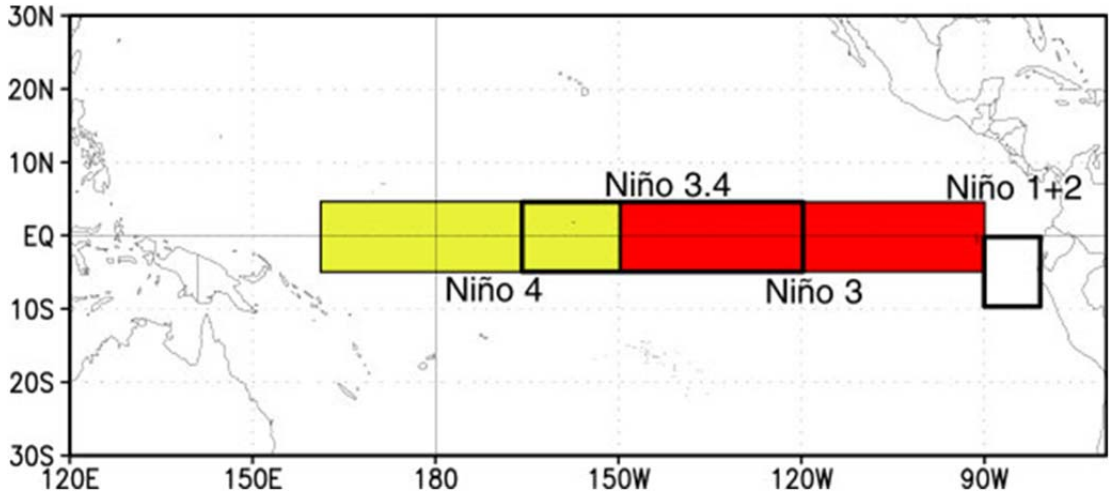

Figure 10. The Nino regions as they are divided across the topical Pacific. From the Climate Prediction Center website (November 2013).

c. Pacific Warm Pool (PWP)

The Pacific Warm Pool (PWP) is also known as the Indo-Pacific warm pool is an anomaly index of SST averaged over the region extending from 60°E to 170°E and 15°S to 15°N, spanning the western portion of the tropical Pacific Ocean, the maritime continent, and most of the tropical Indian Ocean. Data is monthly, available from 1948–2008, and was obtained from the ESRL website www.esrl.noaa.gov/psd/data/correlation/pacwarm.data (2013d) from March to December 2013.

d. Indian Ocean Dipole (IOD)

The Indian Ocean Dipole (IOD) or Indian Ocean Zonal Mode (IOZM) represents interannual variability in SST and related variables in the tropical Indian Ocean (IO). Opposing SST anomalies in the eastern and western tropical Indian Ocean produce anomalous zonal SST gradients. The positive (negative) phase is characterized by positive (negative) SST anomalies in the western tropical IO and negative (positive) SST anomalies in the eastern tropical IO and maritime continent. The temperature gradient

induces an atmospheric pressure gradient caused by ocean-atmosphere interactions and influences the wind patterns and location of convective activity in eastern Africa, southern Asia, the maritime continent, and Australia (Figure 11). The Dipole Mode Index (DMI) used in this study is calculated by taking the SST monthly mean anomaly in the western IO (50^0E-70^0E, 10^0S-10^0N) and subtracting the SST monthly mean anomaly in the eastern IO (90^0E-110^0E, 10^0S-equator). When the index is positive (more positive SSTs in the western IO than in the eastern IO), the IOD is in the positive mode, and vice versa. More information on the IOD can be found from the Japan Agency for Marine-Earth Science and Technology (JAMSEC) at www.jamstech.go.jp/frcgc/research/d1/iod/iod_home.html. Data was obtained from www.jamstech.go.jp/frcgc/research/d1/iod/data/dmi_hadisst.txt between March and December 2013.

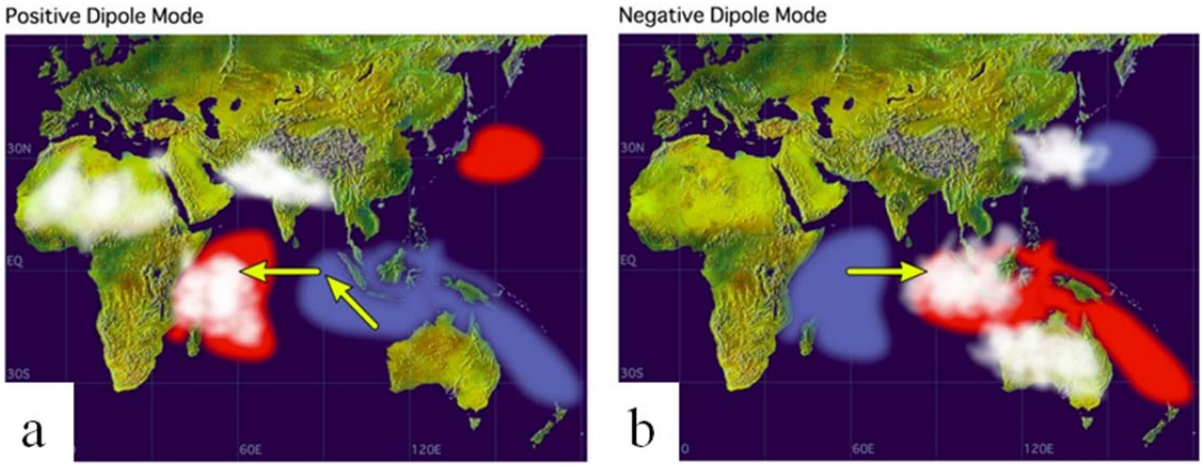

Figure 11. Diagrams of Indian Ocean Dipole (IOD) anomalies. The positive mode (a) is characterized by an anomalously warm (cool) western (eastern) tropical Indian Ocean (IO) and enhanced (suppressed) convection over the warm (cool) SSTs. The negative mode (b) is characterized by approximately opposite anomaly patterns. Arrows indicate lower tropospheric wind anomalies. Figures from the JAMSEC website (November 2013).

e. Summer Asian Monsoon OLR Indices (SAMOI)

Several of the Summer Asian Monsoon OLR indices (SAMOI) were used to compare SCS EDH to the strength of the Asian monsoon. The SAMOI use OLR to

represent the intensity of the Asian summer monsoon precipitation. The SAMOI consist of three indices which are created from differing combinations of OLR anomalies from different regions calculated for May through October. Negative OLR anomalies often occur where a convergence of surface winds cause an increase in convection, resulting in a decrease in OLR from Earth's surface. Figure 12 depicts the four regions in which OLR anomalies are area-averaged, and normalized by their standard deviations to create the SAMOI.

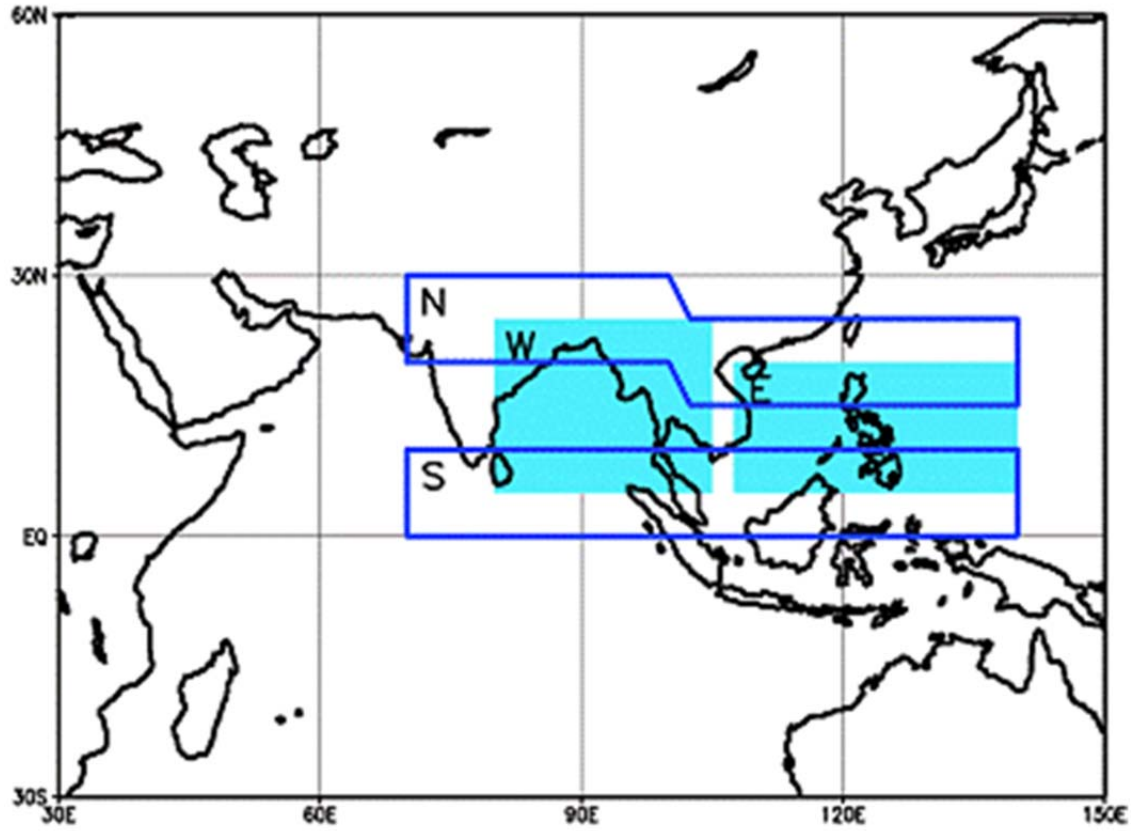

Figure 12. The north (N), south (S), east (E), and west (W) boxes in figure 12 represent the four regions in which an area-average OLR is taken. Values from these four areas are combined by different methods to create the three SAMOI sub-indices. From the Japan Meteorological Agency website (November 2013).

SAMOI-n is based on subtracting the OLR anomalies in the south region from those in the north region. SAMOI-w is based on subtracting the OLR anomalies in the east region from those in the west region. SAMOI-a, which showed the strongest relationship to SCS EDH, is based on adding the OLR

anomalies of the east and west regions. Additional information on SAMOI can be found at the Japan Meteorological Agency's Tokyo Climate Center http://ds.data.jma.go.jp/tcc/tcc/products/clisys/explanation.html (2013d). SAMOI data was obtained from http://ds.data.jma.go.jp/tcc/tcc/products/clisys/emi.html (2013a-c) between March and December 2013.

B. METHODS

1. Computing EDH

The previous works of Twigg (2007) and Ramsaur (2009) computed EDH by collecting R1 data for their area of interest, making necessary adjustments for grid spaces that encompassed land, and separately using the Naval Postgraduate School (NPS) bulk evaporation duct model to compute EDH for each grid space. With the advent of ACAF, all of these EDH values have been pre-computed and are available with much higher spatial and temporal resolutions.

The ACAF EDH values were calculated by Paul Frederickson of NPS using several CFSR variables. To determine 2 m relative humidity (RH), Frederickson used CFSR 2 m specific humidity (q), 2 m air temperature (AT), and surface pressure (Psfc). This derived 2 m RH (%) along with CFSR Psfc (hPa), SST (C), AT (C), and 10 m wind speed (WS) (m/s; derived from the U and V wind components), were used as input into the NAVSLaM model of EDH (similar to the NPS bulk EDH model). These EDH values, and the corresponding constituent environmental variables, are provided by ACAF. We used ACAF to create all the EDH figures in this study, as well as most of the figures involving the EDH constituent variables.

2. Computing Area LTMs

We computed area-averaged values of EDH, SST, AT, RH, and WS for our specific area of study for use in a number of our analyses, including correlations and conditional composites. The area-averaging was done outside of the ACAF environment and with the assistance of Bruce Ford of Clear Science, Inc.

3. Correlations

Linear correlation is a measurement of the relationship between two variables. The formula we used for correlation is:

$$\text{Correlation value} = \frac{\sum(xy)}{\sqrt{(\sum(x^2)(y^2))}}$$

where x and y are the values being correlated.

Correlation values range between -1.0 and +1.0. Positive correlations indicate the two variables both increase or decrease in value together. The wind speed and the power output of a wind turbine would be and an example of two variables with a highly positive correlation. Negative correlation values indicate the two variables tend to move in opposite directions. Outside air temperature and the use of home heating would be an example of two variables with a negative correlation. A zero or near zero correlation indicates that the two variables move independently of each other and may be completely unrelated. For the purpose of this study, the absolute value of the correlation is much more important than the sign.

The level of certainty in a correlation is also important. As the sample size of the comparison (n) increases, so does the certainty of the correlation. A two-tailed test was used to determine the significance at the 95% confidence interval. The significance test equation is:

$$Z = \frac{|z_{0.025}|}{|\sqrt{n}|}$$

where: Z is the test statistic ; $z_{0.025}$ = standard normal distribution = 1.96 and n = 31 for the 31 years in our study period (1979–2009). Therefore, in this study, correlation magnitudes of 0.352 or greater are significant at the 95% level. Refer to Wilks (2006) for further explanation of significance testing.

a. Correlations between EDH and Constituent Variables

Our initial numerical analyses of SCS EDH were comparisons of area-averaged EDH with area-averaged WS, SST, AT, RH, and ASTD in each of four selected

representative months (March, June, September, and November). Comparing EDH to each constituent variable was necessary in order to develop a broader understanding of the role played by each constituent variable in determining the EDH in a particular month. This information was used to (a) provide the end user with a conceptual model of EDH and (b) to aid in the explanation of apparent relationships between EDH and global climate phenomenon.

b. Correlations between EDH and Climate Indices

EDH was compared in the same manner with climate indices including MEI, Nino 4, IOD, SAMOI-a,w,n and the PWP. Correlations were calculated within the same month (e.g., September EDH with September MEI), and with the climate index leading by up to six months (e.g., September EDH with March IOD). A climate index with a significant correlation to EDH occurring months later is an indication that long-lead forecasts of monthly mean EDH may be skillful.

c. Correlations between EDH and Global Climate Variations

Analyses of the relationships between SCS EDH and specific global environmental variables can be useful in determining the climate variations and physical processes involved in producing EDH variations in the SCS. One example in this study is a relationship that we identified between EDH and El Nino / La Nina. Investigation into global SST anomalies revealed that stronger correlations existed with SST in specific locations in the tropical Pacific than with the MEI, which includes more variables over a large portion of the tropical Pacific. These types of correlation are an important step toward development of a tailored climate index for climate analysis and forecasting of SCS EDH.

The correlation portions of our study were made possible by the ESRL correlation analysis tools. The “Linear Correlations in Atmospheric Seasonal/Monthly Averages” plotting tool allows the user to upload a custom time series (area-averaged monthly SCS EDH in this case) and produce correlation maps with global climate variables such as SST, GPH, OLR, and many others. Figure 13 is an example of such a correlation map. More information on this capability can be found at the ESRL/PSD plotting and analysis

web page www.esrl.noaa.gov/psd/cgi-bin/data/correlation (2013a), accessed between March and December 2013.

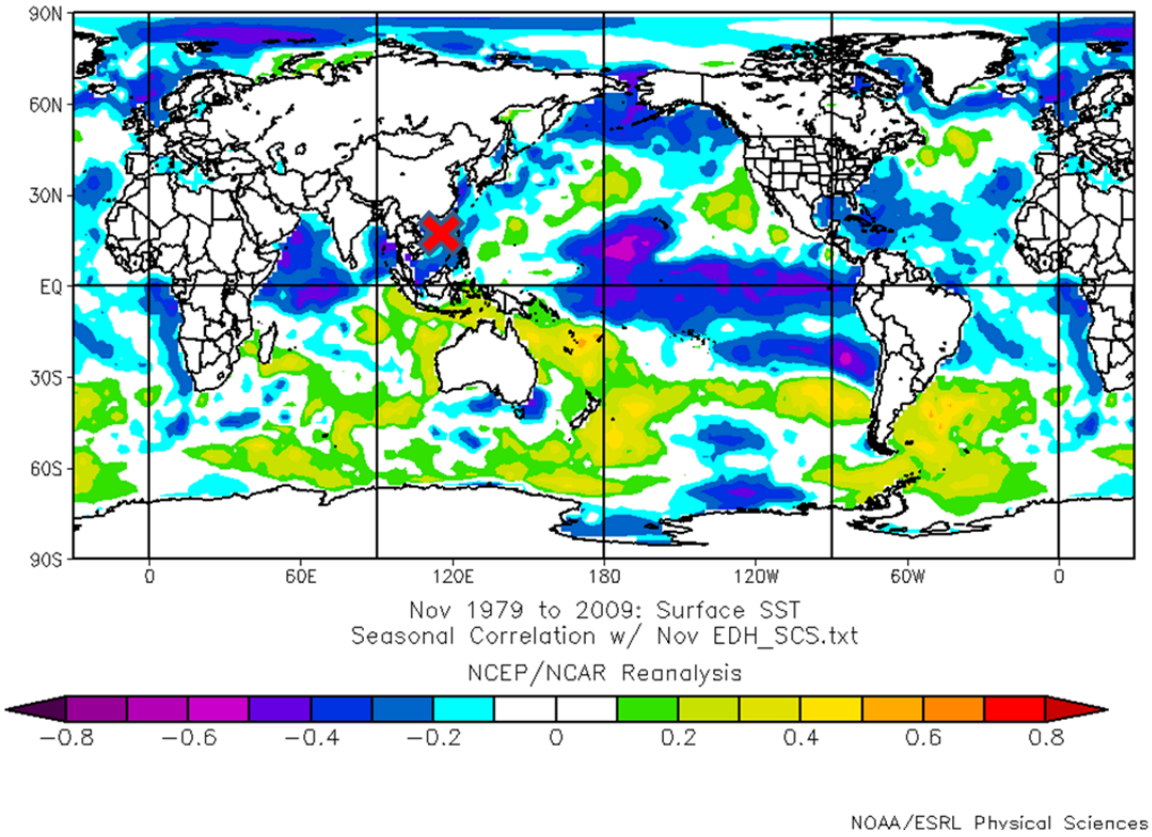

Figure 13. Example of a linear correlation map, in this case for November SCS EDH correlated with November global SST. The strongest correlation values are +0.71 (purple) and -0.55 (orange). The red "X" indicates our area of study. Figure created at the Earth Systems Research Laboratory (ESRL) website (October 2013).

4. Conditional Composites

Conditional composites were also used to examine relationships between EDH, climate indices, and global climate variables. Conditional composite analysis involves averaging together values for periods in which specified conditions were met (e.g., EDH values for EN periods or for periods in which EDH values were the most extreme). For our study, we averaged together the highest (and lowest) SCS EDH values in our study period (1979-2009) and compared them to the corresponding composite anomalies for other variables (e.g., SST). We chose as the most extreme EDH values the six-to-nine

highest EDH years (and lowest EDH years) during our study period and compared them to each other and to the composite anomalies for other variables for the highest (and lowest) EDH years (1979-2009). These comparisons allowed us to identify the characteristic anomaly patterns and processes associated with extreme EDH conditions. We also compared the conditional composite anomalies to the corresponding correlation maps to assess the physical processes that underlie the correlations.

a. EDH and Climate Indices

Conditional composites were created for months and for climate indices that showed significant correlations. Climate index values for a given month during the six-to-nine highest (lowest) EDH years were averaged, as well as the average for all 31 years in the study. This creates three values per monthly composite --- the mean anomaly of lowest EDH years, mean of all years, and mean anomaly of highest EDH years. The magnitude of the anomalies relative to the standard deviation of the index is an indication of the strength of the relationships between SCS EDH and the climate variation indices.

b. EDH and Global Climate Variables

The ESRL website plotting tool "Monthly/Seasonal Mean Composites" allows the user to plot the mean or the anomalous value of a climate variable (e.g., SST) for a given month (or months) and years selected. For the purpose of this study, the six-to-nine years of highest (or lowest) monthly mean SCS EDH were selected and global plots of SST and GPH were created. These plots show both the location and magnitude of the mean anomalies observed in the selected variable for the selected years. For example, Figure 14 indicates the equatorial Pacific had positive (negative) SST anomalies in the low (high) SCS EDH Novembers. These opposite anomalies indicate a characteristic relationship between SCS EDH and equatorial Pacific SST. More information on this capability can be found at the ESRL/PSD plotting an analysis web page http://www.esrl.noaa.gov/psd/cgi-bin/data/composites/printpage.pl (2013e), accessed between March and December 2013.

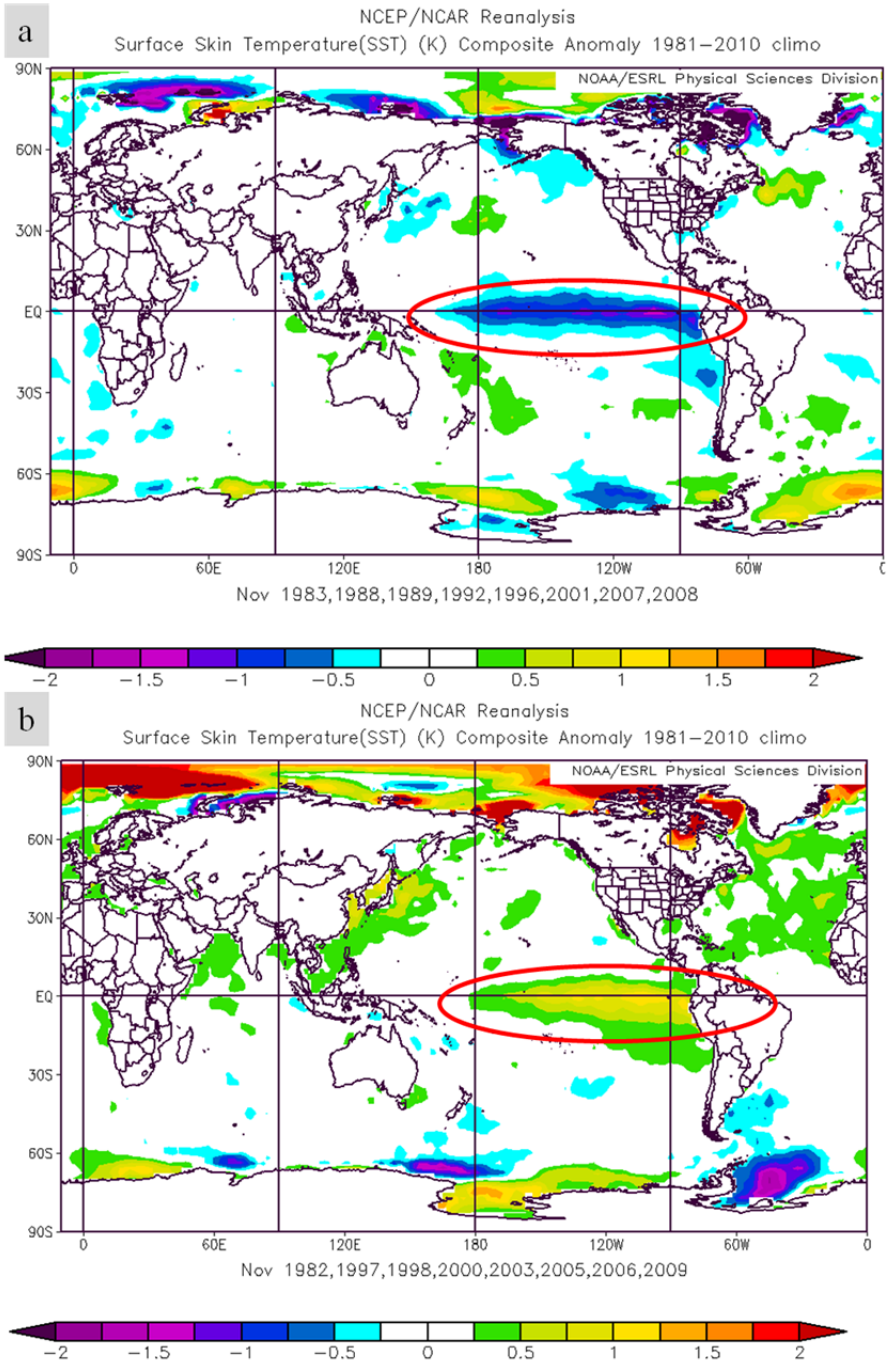

Figure 14. Conditional composite plots of global SST anomalies for: (a) the eight highest SCS EDH Novembers and (b) the eight lowest SCS EDH Novembers. The circled equatorial Pacific region shows opposite SST anomalies during the highest EDH Novembers verses the lowest EDH Novembers, indicating a characteristic relationship for November in which the variations of SCS EDH tend to be opposite to those of central-eastern equatorial Pacific SST. Figures created at the ESRL website (October 2013).

C. SUMMARY

The advanced data and methods used in this study represent significant progress in climate analysis and modeling since the prior studies by Twigg (2007) and Ramsaur (2009). The reanalysis data available is of much higher spatial and temporal resolution than what was available during these prior studies. Improvements in the modeling of EDH with NAVSLaM and advancements in analysis tools, such as ACAF, have made possible a much more robust climate analysis of evaporative ducts.

THIS PAGE INTENTIONALLY LEFT BLANK

III. RESULTS

A. LONG-TERM MEAN EDH SEASONAL CYCLE

We began our analyses by developing a baseline understanding of EDH in the SCS and how it changes throughout the year. This baseline understanding of seasonal variation provides a context for examining the influences of climate variations on EDH in particular months. We also analyzed variations in SCS EDH throughout all months of the year to determine the specific months on which to focus our study.

1. Monthly LTM EDH

Figures 15 and 16 depict the LTM (1979–2009) EDH for each of the 12 months. Note the high degree of spatial and temporal variability in SCS EDH. As discussed in Chapter I, the spatial variability led us to select the northern SCS as our area of study. For this area of study, a seasonal cycle in EDH is apparent in which a minimum EDH occurs in the early spring and a maximum EDH occurs in the late fall. A relative minimum occurs in September and a relative maximum occurs in June. These temporal variations are shown as a time series in Figure 21.

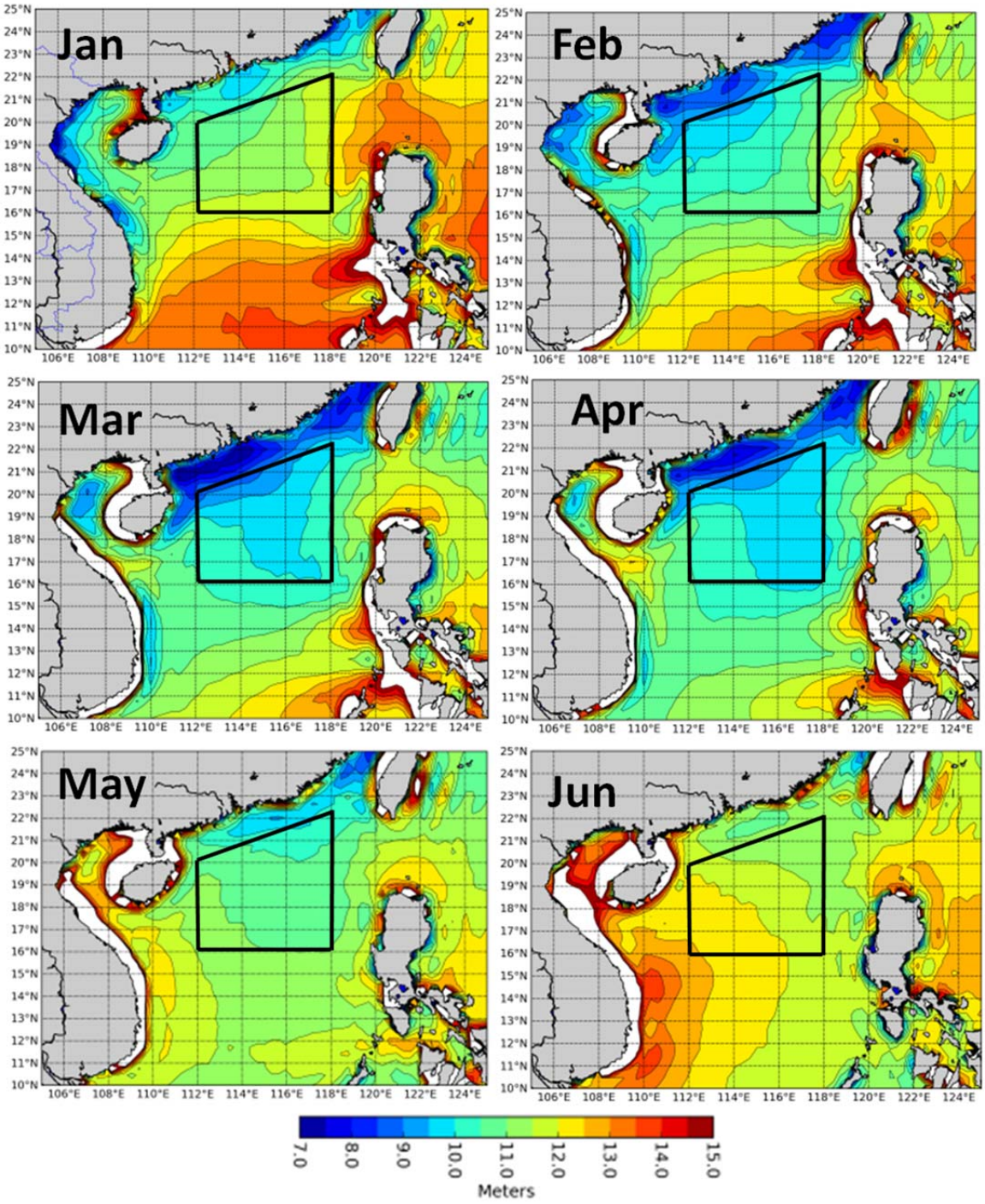

Figure 15. January-June LTM EDH. Within the area of study (in the trapezoidal box), the absolute minimum EDH occurs in March and a relative maximum occurs in June. Figures created at the ACAF website (October 2013).

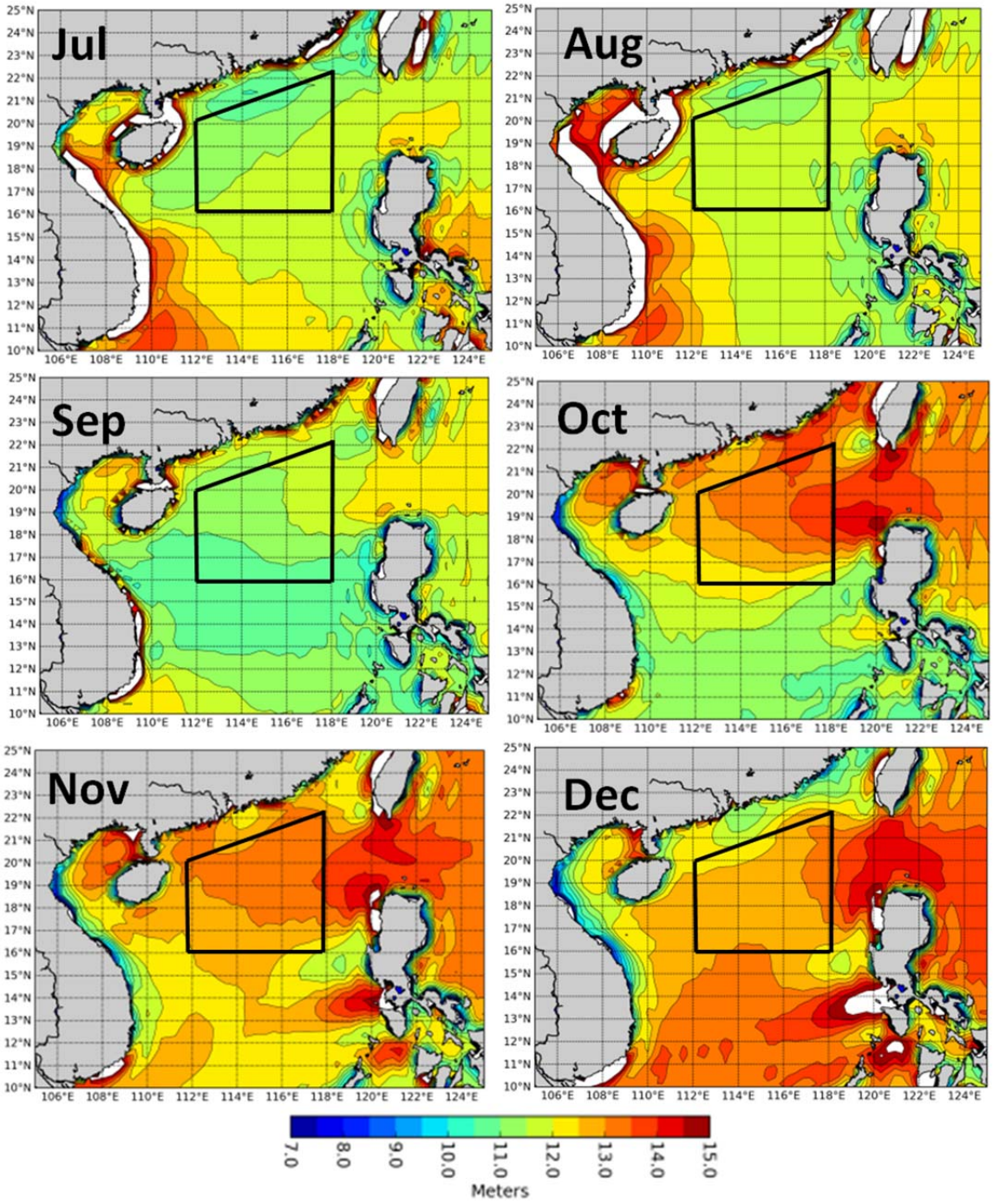

Figure 16. July-December LTM EDH. Within the area of study (in the trapezoidal box), the absolute maximum EDH occurs in November, and a relative minimum occurs in September. Figures created at the ACAF website (October 2013).

2. East Asian Monsoon

Analyses of the LTM wind field for each of the 12 months indicate that the seasonal cycle of EDH closely follows the seasonal changes in winds that are part of the East Asian Monsoon. Beginning between late September and early October, strong northeast winds are generated and bring cooler/dryer air from the WNP, East China Sea (ECS), and Philippine Sea into the SCS (Figure 17). This phase is called the winter or northeast (NE) monsoon.

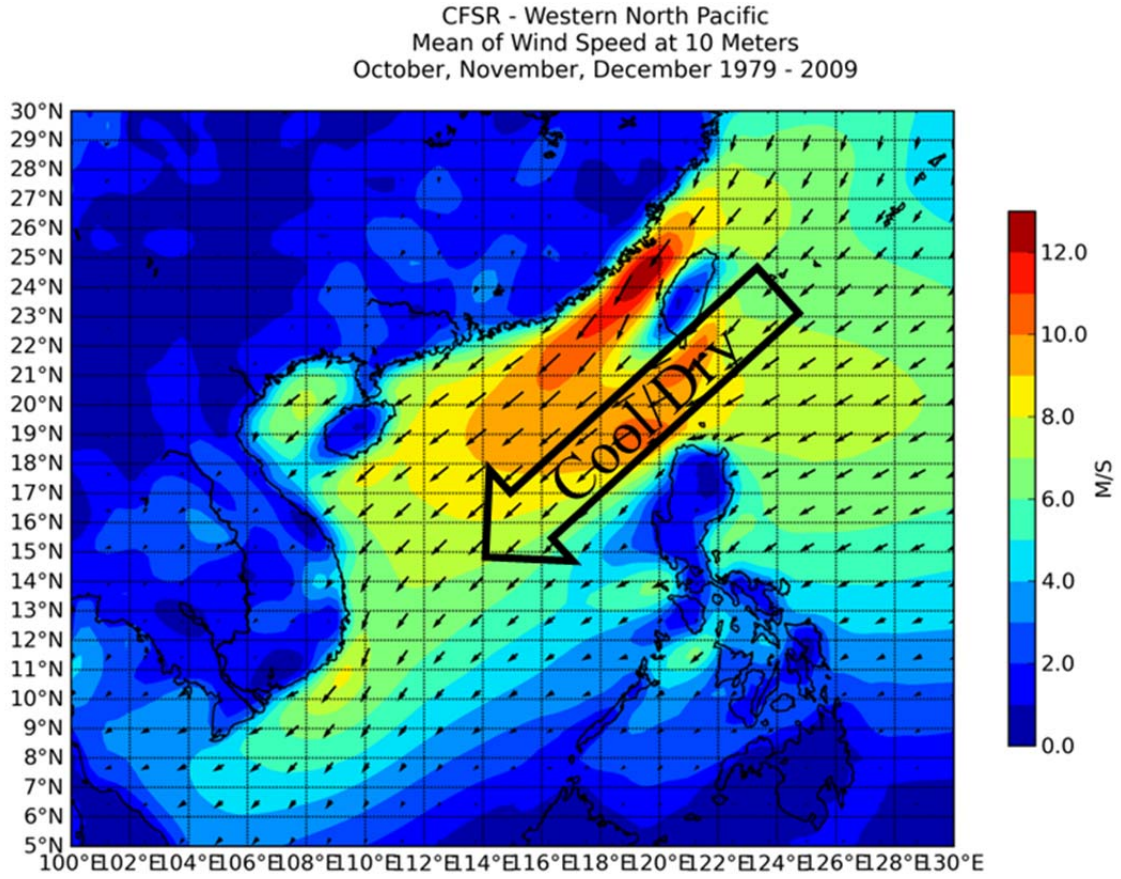

Figure 17. October-December mean near-surface wind speed and direction. Strong NE winds from the East China Sea (ECS) and Philippine Sea bring cool, dry air into the SCS. This causes an annual maximum in evaporation duct heights. Figure created at the ACAF website (October 2013).

These winds are driven by the semi-permanent Asian high that develops in early fall and remains a persistent feature through winter (Figure 18). The combination of high pressure over Asia with anticyclonic flow, and relatively low pressure over the tropical

western Pacific with cyclonic flow, force strong NE winds and cool/dry air into the SCS (Figure 18).

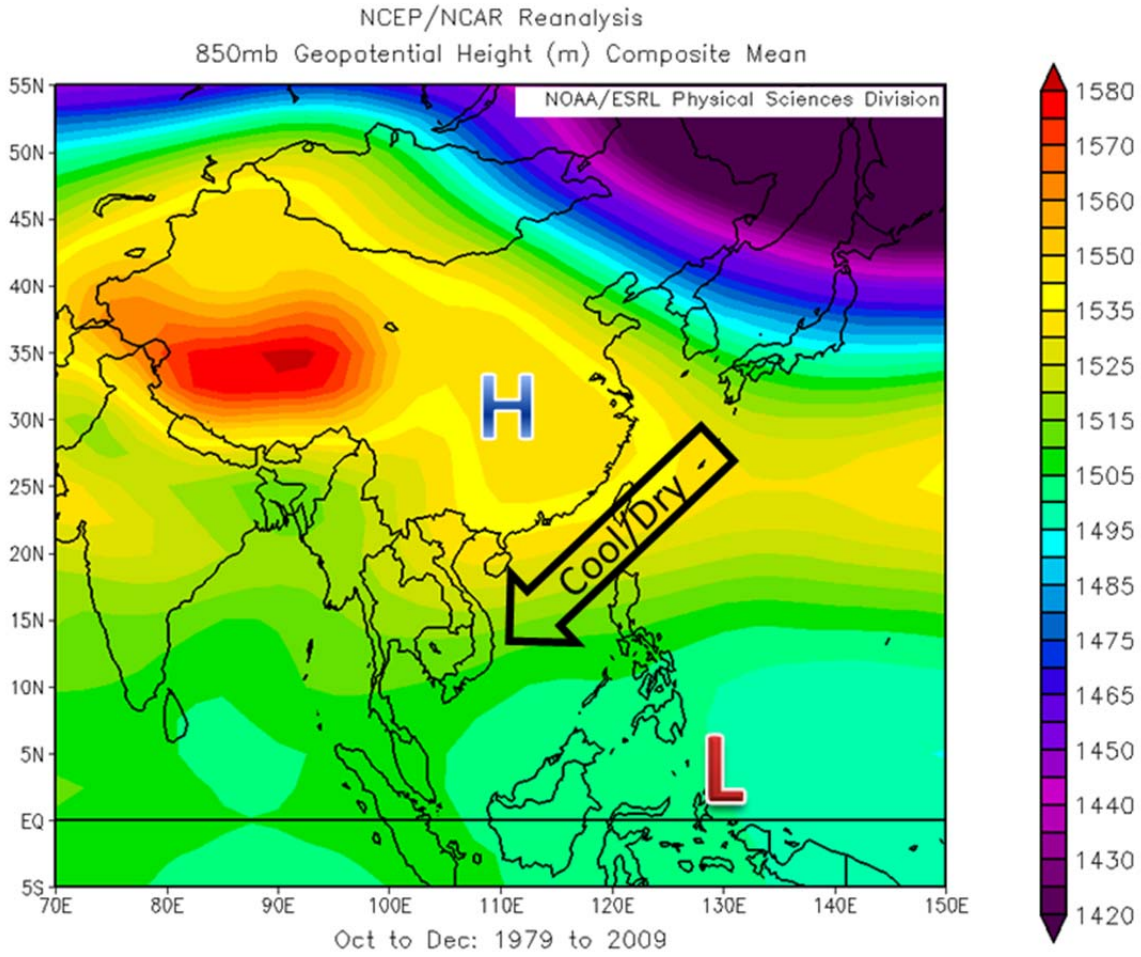

Figure 18. October-December 850 mb LTM geopotential heights (GPH). The high surface pressure over Asia combines with the low surface pressure over the western tropical Pacific to force strong NE winds into the SCS in the fall and initiate the Asian winter monsoon. Figure created at the ESRL website (October 2013).

The NE flow from the winter monsoon weakens as winter transitions to spring, and relatively weak winds occur in April. Usually beginning in late May, the weaker summer or southwest (SW) monsoon occurs (Figure 19).

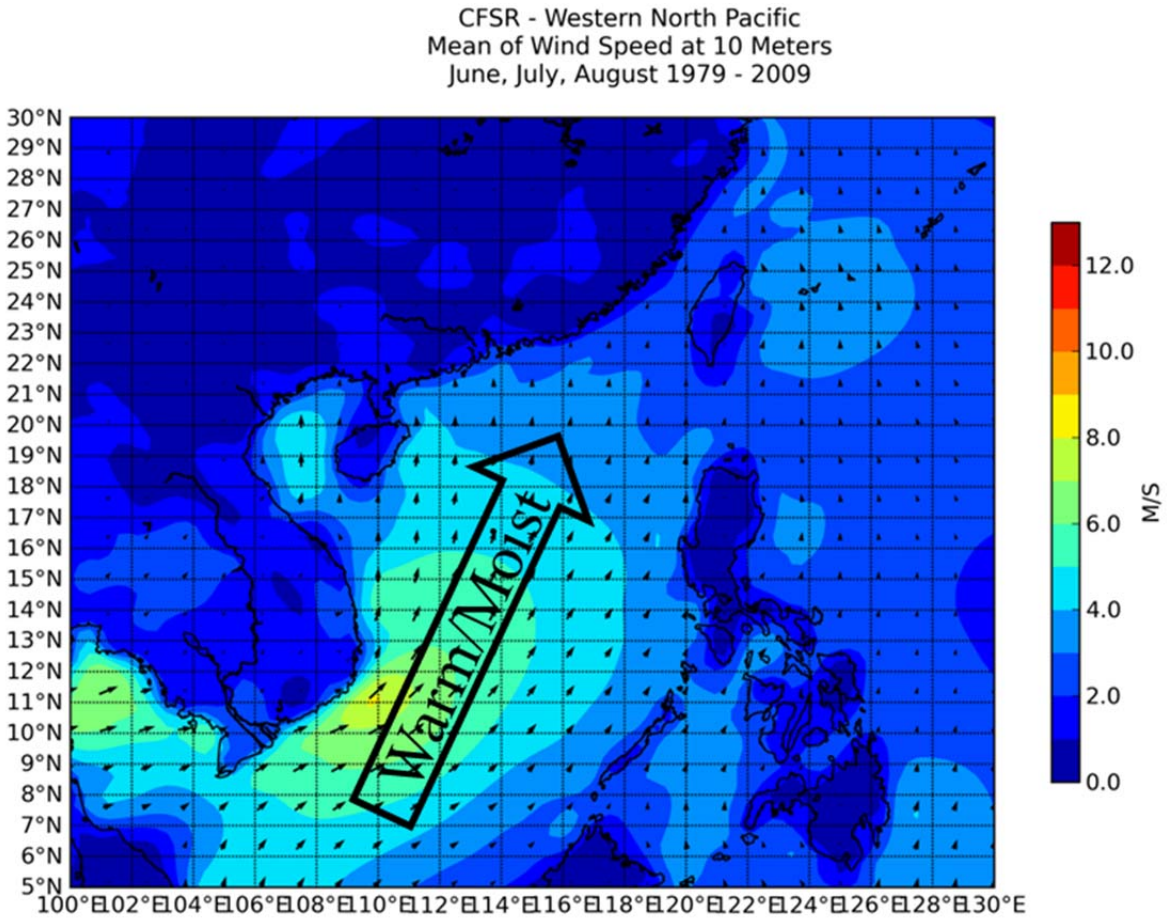

Figure 19. June-August mean near-surface wind speed and direction. Moderate SW winds into the SCS from the maritime continent bring warm, moist air into the SCS. This causes a local maximum in evaporation duct heights. Figure created at the ACAF website (October 2013).

This SW flow develops as the result of summer heating creating low surface pressures over the Asian continent and the occurrence of relatively high surface pressures over the subtropical western Pacific and maritime continent (Figure 20). The SW winds drive warm, moist air into the SCS.

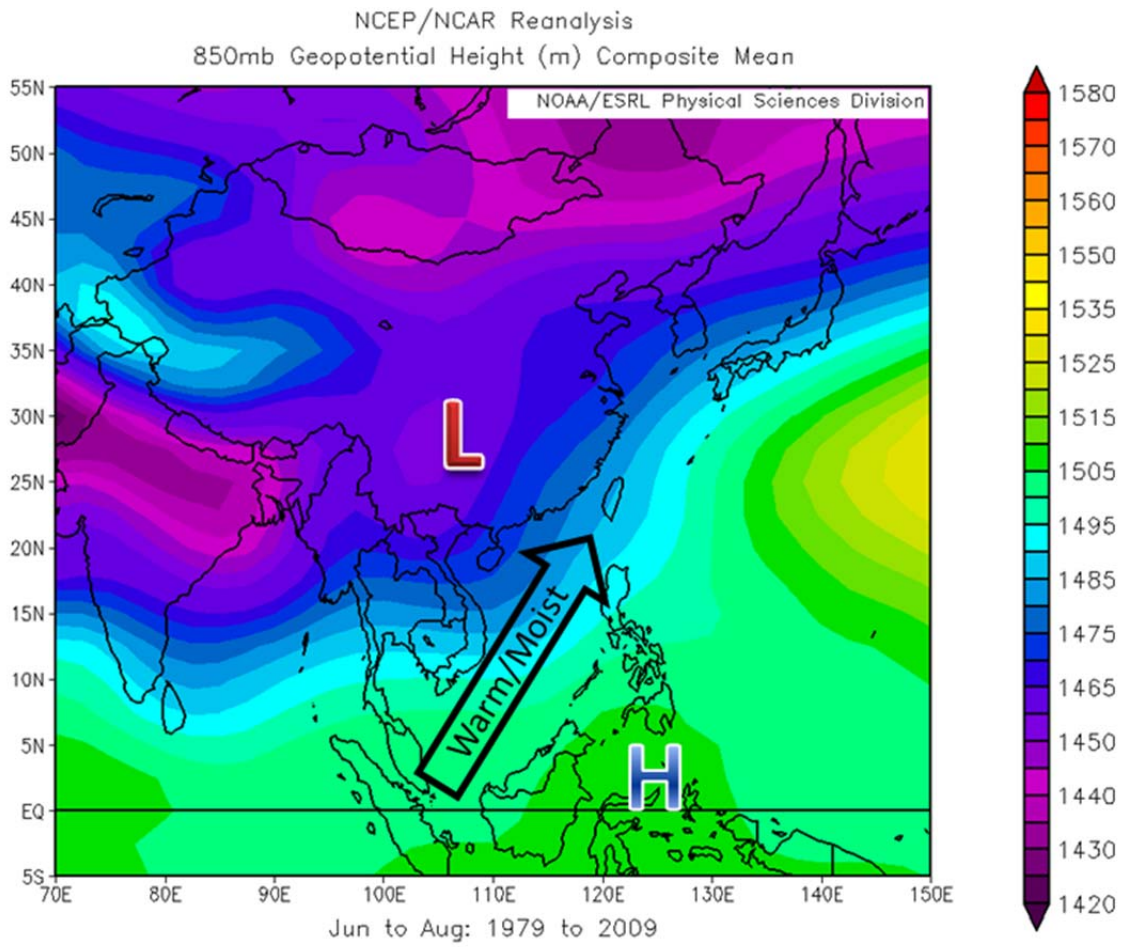

Figure 20. June-August 850 mb LTM geopotential heights (GPH). The low surface pressures over Asia, and the higher surface pressures over the subtropical western Pacific and maritime continent, combine to create the moderate SW winds of the Asian summer monsoon. Figure created at the ESRL website (October 2013).

When the ASTD is negative (or slightly positive) as seen throughout most of the year in the SCS, EDH increases with an increase in wind speed. The maximum EDH in November occurs when the peak winds are observed from the NE (or winter) monsoon. The local maximum EDH in June occurs when peak winds are observed from the summer monsoon. The EDH minimum in March coincides with a wind minimum and the shift from the winter monsoon with NE winds to the summer monsoon with SW winds. The local minimum in EDH in September occurs when calmer winds develop during the transition from the SW monsoon to the NE monsoon (Figure 21).

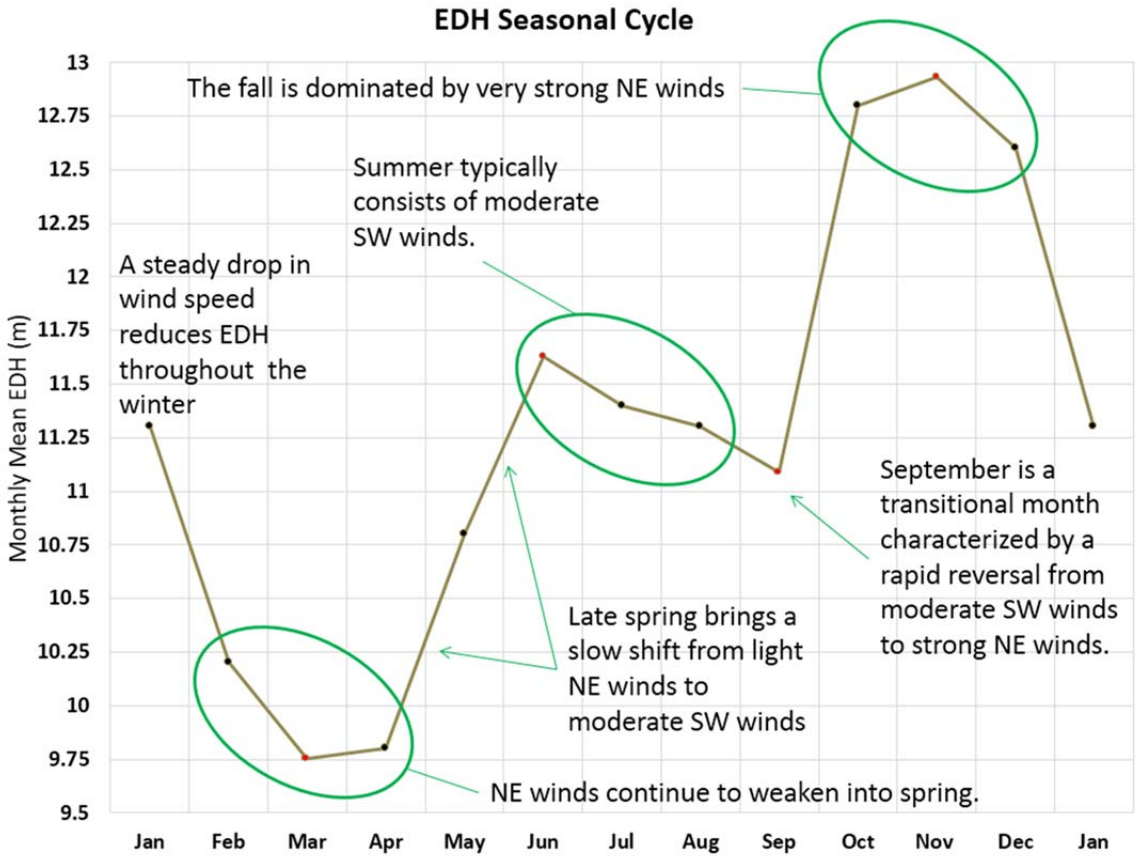

Figure 21. Time series of monthly LTM EDH for the area of study beginning and ending with January. The seasonal cycle of EDH is characterized by: (a) June and November maximums that occur during the peaks of the summer (SW) and winter (NE) monsoons, respectively; and (b) March and September minimums that occur during the spring and fall monsoon transitions, respectively.

3. Focus Months

We chose November and June as the focus months for our study because they represent maximums in EDH and the winter and summer extremes of the NE and SW monsoons, respectively. We also chose March and September as focus months because they represent minimums in EDH and the transitions between the winter and summer monsoon extremes. Analyses of these four months can be used to better analyze and understand the other eight months of the year.

B. ENVORONMENTAL VARIABLES THAT EFFECT EDH

1. Air Temperature (AT), Sea Surface Temperature (SST), and Air-Sea Temperature Difference (ASTD)

EDH is strongly affected by atmospheric stability conditions. In particular, EDH responds to changes in environmental variables differently for stable and unstable conditions. This is especially true for changes in wind speed. Stability conditions are typically described by the air-sea temperature difference (ASTD). Unstable conditions, indicated by negative ASTD, lead to enhanced vertical motions and atmospheric mixing due to positive buoyancy forces. Stable conditions, indicated by positive ASTD, lead to inhibited vertical motions and atmospheric mixing due to negative buoyancy forces. In typical SCS conditions, ASTD is negative (warmer SST than AT), indicating unstable conditions. This is important because in unstable conditions, EDH increases with an increase in wind speed. This remains the case until the ASTD climbs above approximately positive 0.4^0 C. In positive ASTD environments (stable conditions with warmer AT than SST), this wind-EDH relationship is often reversed so EDH declines with increased wind speeds. Figure 22 shows EDH versus ASTD for various wind speeds with the other environmental variables held constant at typical SCS values. Note that a reversal in the behavior of EDH and wind speed occurs at an ASTD of approximately 0.4^0 C.

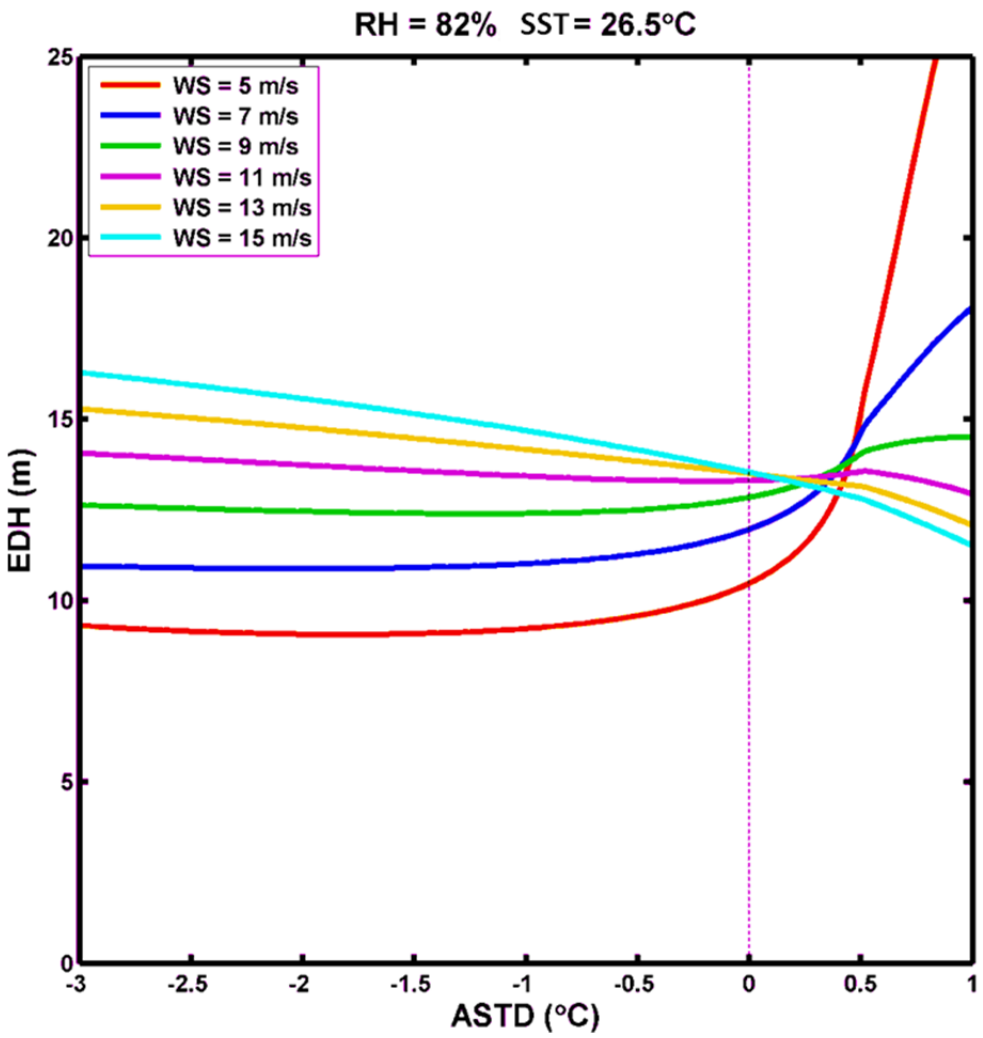

Figure 22. EDH versus ASTD for various wind speeds. Note the reversal in the behavior of EDH with wind speed at approximately 0.4° C. Plot of NAVSLaM-modeled EDH courtesy of Paul Frederickson (October 2013).

Figures 23–26 depict the SST and 2 m AT for March, June, September, and November, respectively. The ASTD is determined by subtracting the SST (color fill) from the AT (black contours). During our four focus months, LTM ASTD values range between -0.12^0 C in June and -0.93^0 C in November. Monthly mean EDH increases with monthly mean wind speed in all months due to unstable conditions. SST conditions in the SCS are relatively constant throughout the year, but an increase in SST will generally increase EDH.

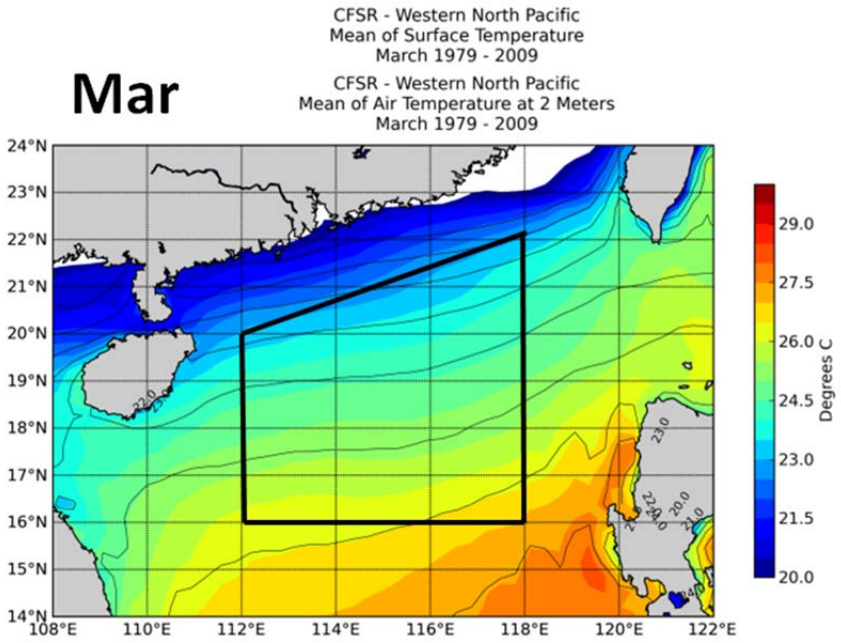

Figure 23. LTM SST (color fill) and 2 m AT (black contours). Area-averaged LTM: AT = 24.3^0 C, SST = 24.8^0 C, ASTD = -0.48^0 C. Area averaged monthly mean ranges: AT: 23.1^0 to 25.7^0, SST: 23.8^0 to 26.1^0, ASTD: -0.99^0 to -0.14^0. Figure created at the ACAF website (October 2013).

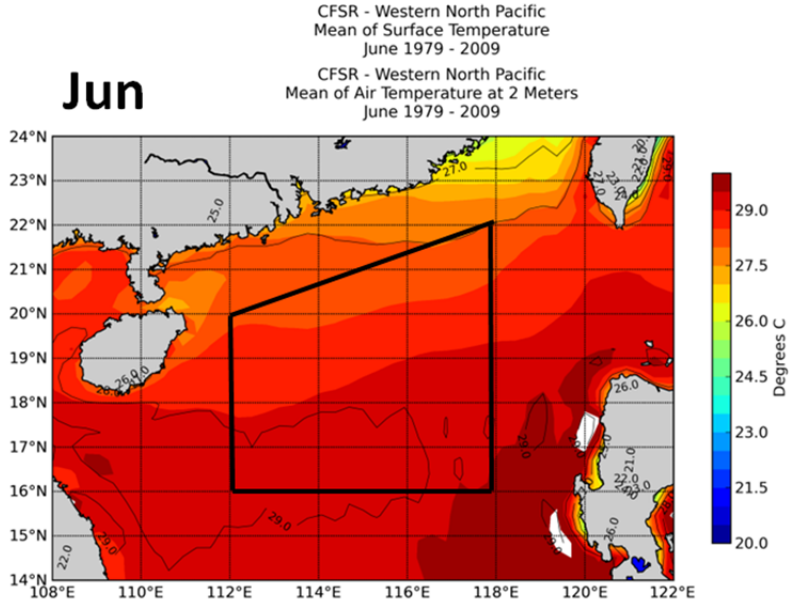

Figure 24. LTM SST (color fill) and 2 m AT (black contours). Area-averaged LTM: AT = 28.8º C, SST = 28.9º C, ASTD = -0.12º C. Area averaged monthly mean ranges: AT: 28.2º to 29.6º, SST: 28.1º to 29.7º, ASTD: -0.44º to 0.16º. Figure created at the ACAF website (October 2013).

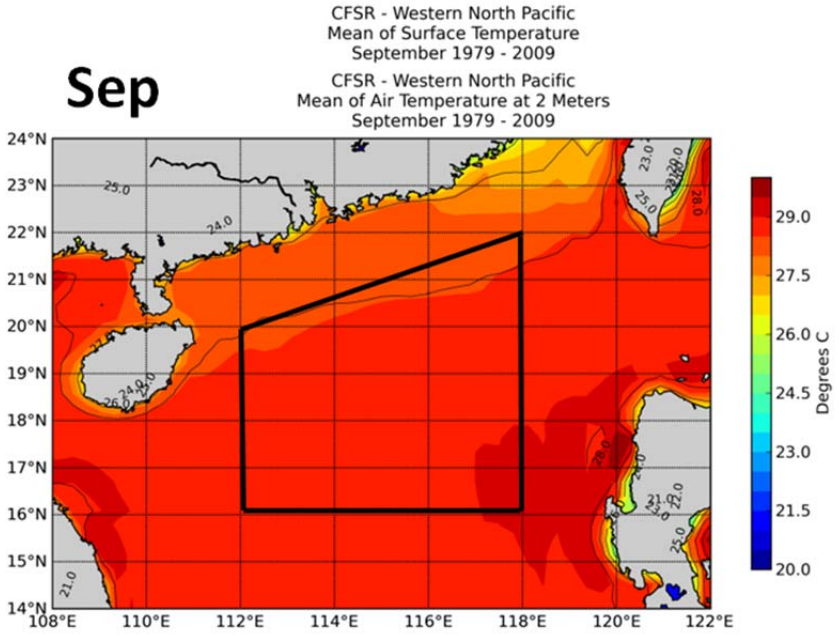

Figure 25. LTM SST (color fill) and 2 m AT (black contours). Area-averaged LTM: AT = 28.3º C, SST = 28.7º C, ASTD = -0.45º C. Area averaged monthly mean ranges: AT: 27.5º to 29.1º, SST: 27.6º to 29.8º, ASTD: -0.99º to 0.05º. Figure created at the ACAF website (October 2013).

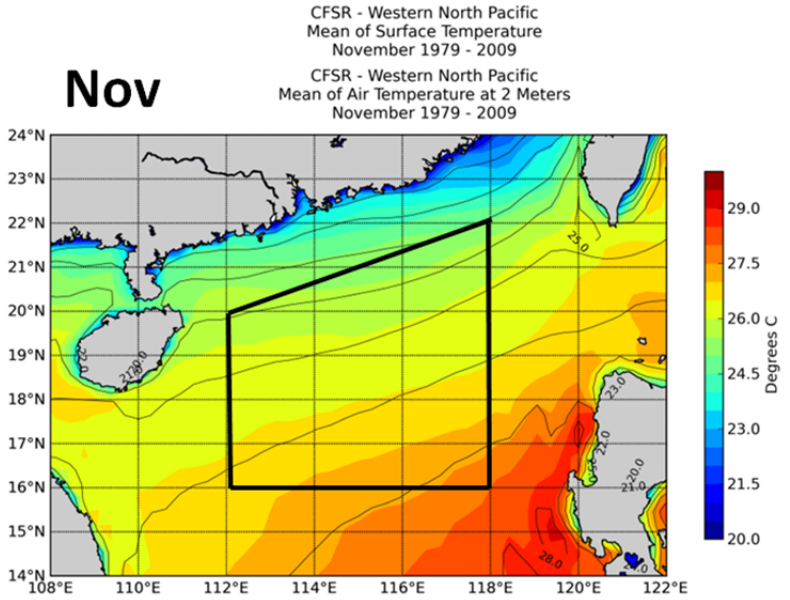

Figure 26. LTM SST (color fill) and 2 m AT (black contours). Area-averaged LTM: AT = 25.4º C, SST = 26.3º C, ASTD = -0.93º C. Area averaged monthly mean ranges: AT: 24.1º to 26.5º, SST: 25.1º to 27.4º, ASTD: -1.36º to -0.25º. Figure was created at the ACAF website (October 2013).

2. Relative Humidity (RH)

Monthly mean RH in the area of study ranges from approximately 78% to 86% during our months of focus. An 8% range in RH would not be considered significant in many atmospheric applications, but an 8% change in RH can change EDH by as much as 5 m in high wind conditions (with typical values of SST, AT, and ASTD observed in the SCS). Figure 27 depicts EDH versus RH for various wind speeds and conditions typical of the northern SCS. At higher wind speeds, EDH decreases more rapidly with increasing RH. Figures 28–31 depict RH for each of the four months of focus.

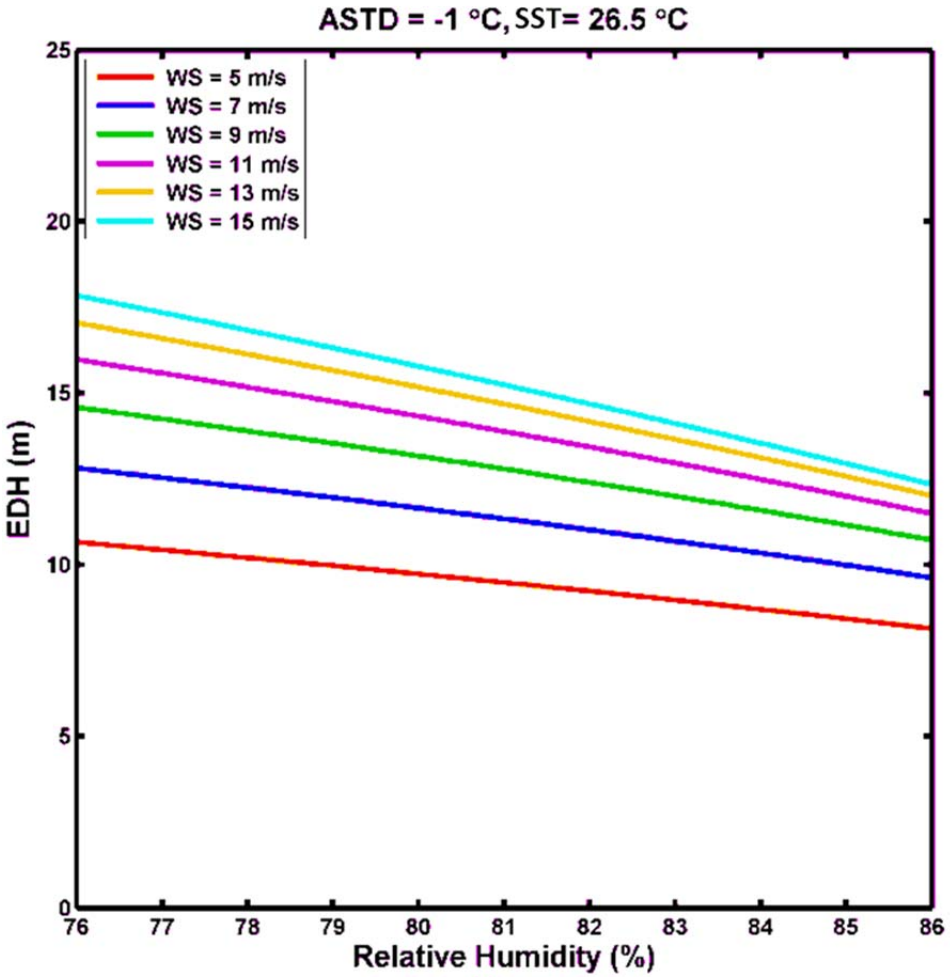

Figure 27. EDH versus RH for various wind speeds. Note the increased negative slope for higher winds speeds. Plot of NAVSLaM-modeled EDH courtesy of Paul Frederickson (October 2013).

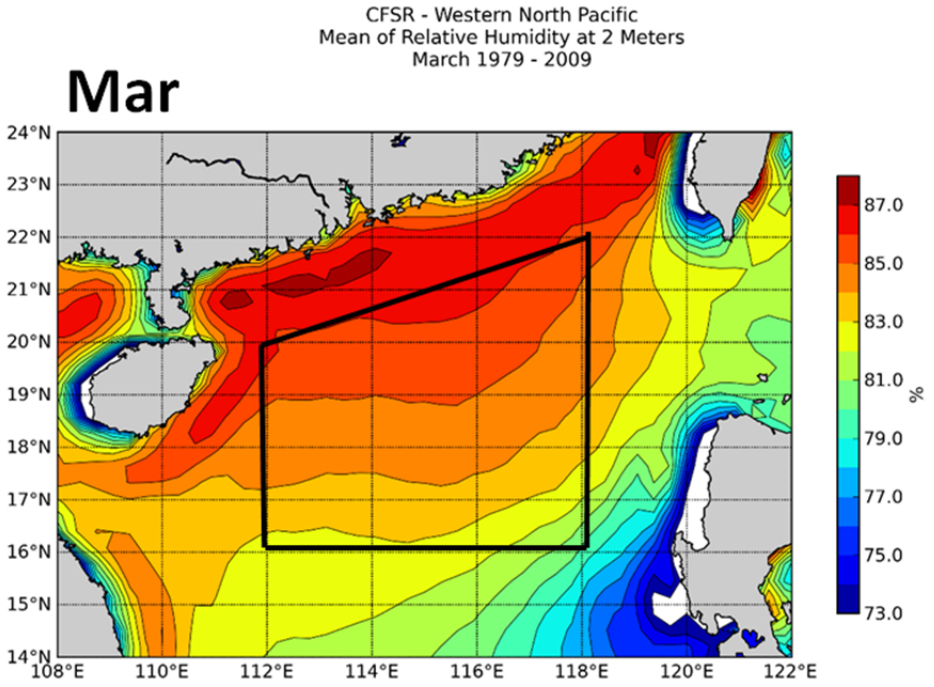

Figure 28. Area-averaged LTM RH in March is 84.5%. Area-averaged monthly mean ranges from 81.6% to 85.8%. Figure created at the ACAF website (October 2013).

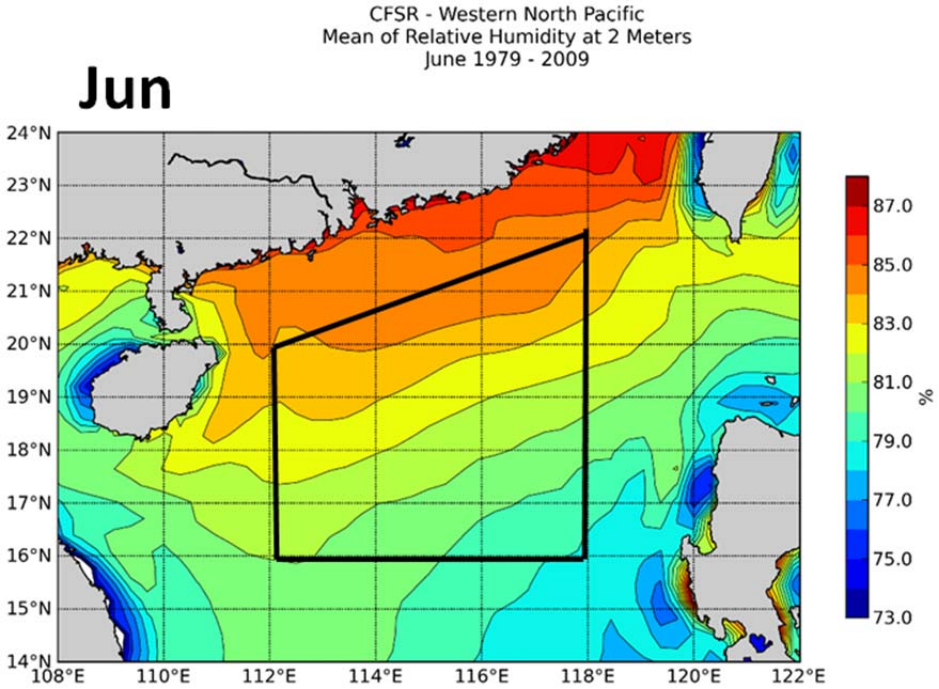

Figure 29. Area-averaged LTM RH in June is 82.1%. Area-averaged monthly mean ranges from 80.4% to 84.6%. Figure created at the ACAF website (October 2013).

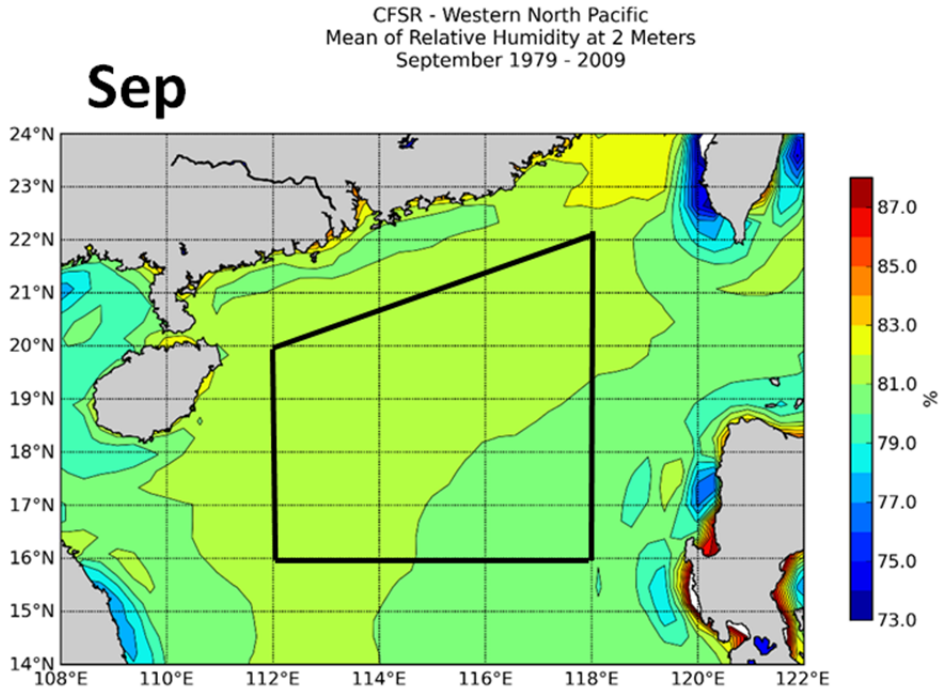

Figure 30. Area-averaged LTM RH in September is 81.2%. Area-averaged monthly mean ranges from 78.9% to 84.4%. Figure created at the ACAF website (October 2013).

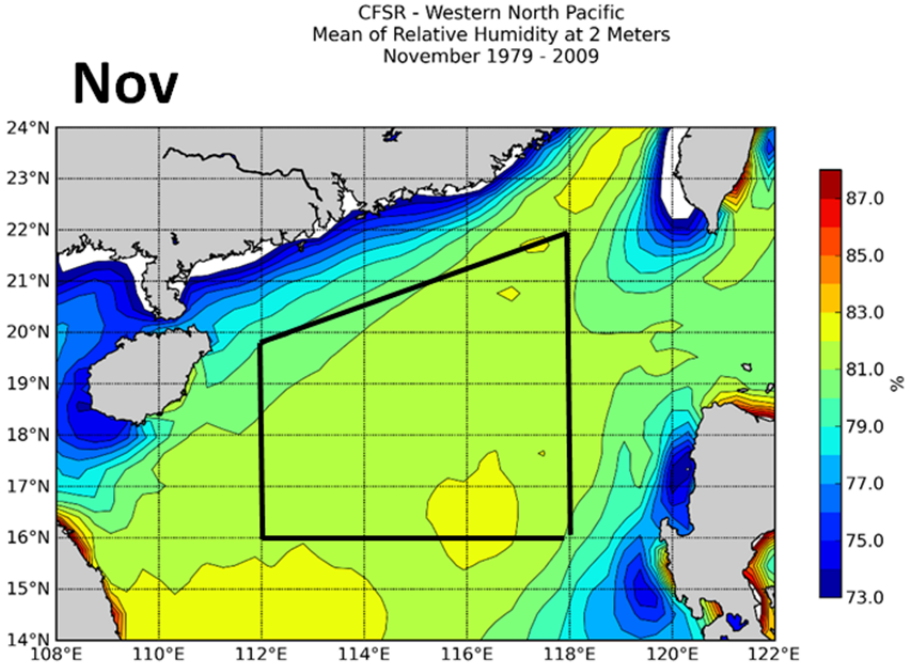

Figure 31. Area-averaged LTM RH in November is 81.7%. Area-averaged monthly mean ranges from 78.2% to 83.9%. Figure created at the ACAF website (October 2013).

3. Wind Speed (WS)

Near-surface wind speed plays a major role in determining EDH in the SCS. Isolated months in which other variables such as temperature or RH strongly influence EDH are months in which WS is at a minimum (e.g., September). Figure 32 depicts EDH versus WS at 10 m for various RH levels and conditions typical of the northern SCS. Figures 33–36 depict WS and direction for each of the four focus months. These figures provide a good characterization of the monsoonal flow in the SCS.

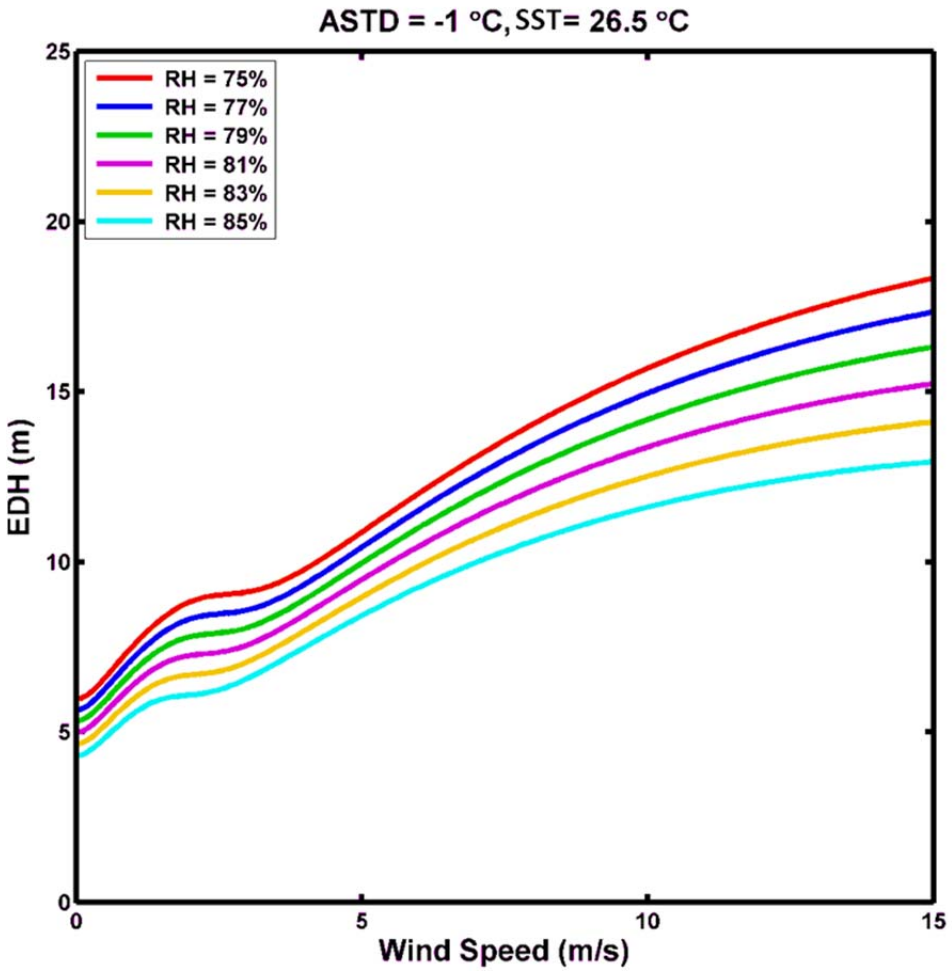

Figure 32. EDH versus WS for various levels of RH. Plot of NAVSLaM-modeled EDH courtesy of Paul Frederickson (October 2013).

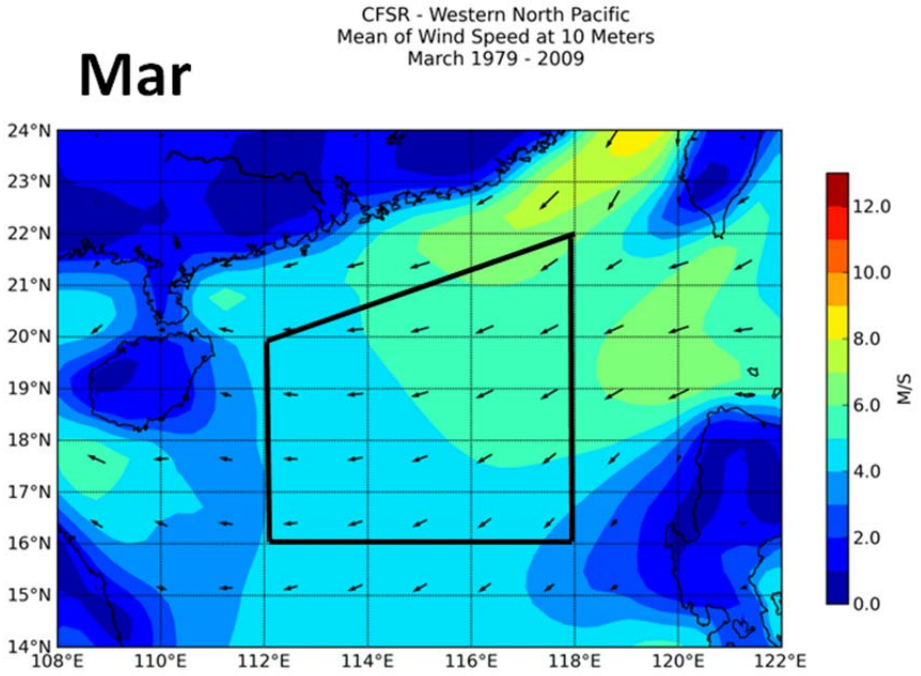

Figure 33. Area-averaged LTM WS in March is 5.0 m/s. Area-averaged monthly mean ranges from 3.2 to 7.6 m/s. Figure created at the ACAF website (October 2013).

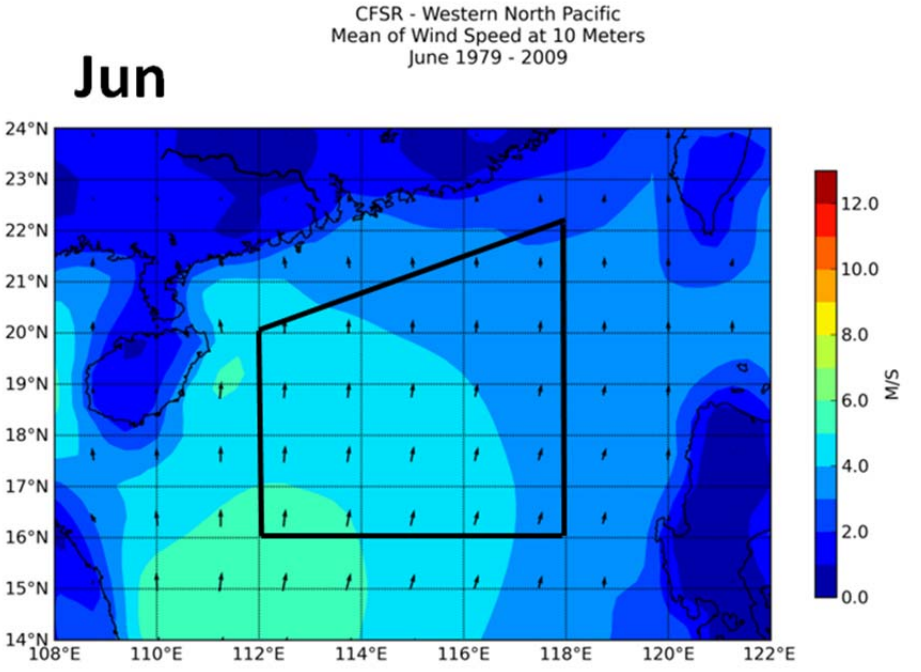

Figure 34. Area-averaged LTM WS in June is 4.4 m/s. Area-averaged monthly mean ranges from 1.3 to 6.4 m/s. Figure created at the ACAF website (October 2013).

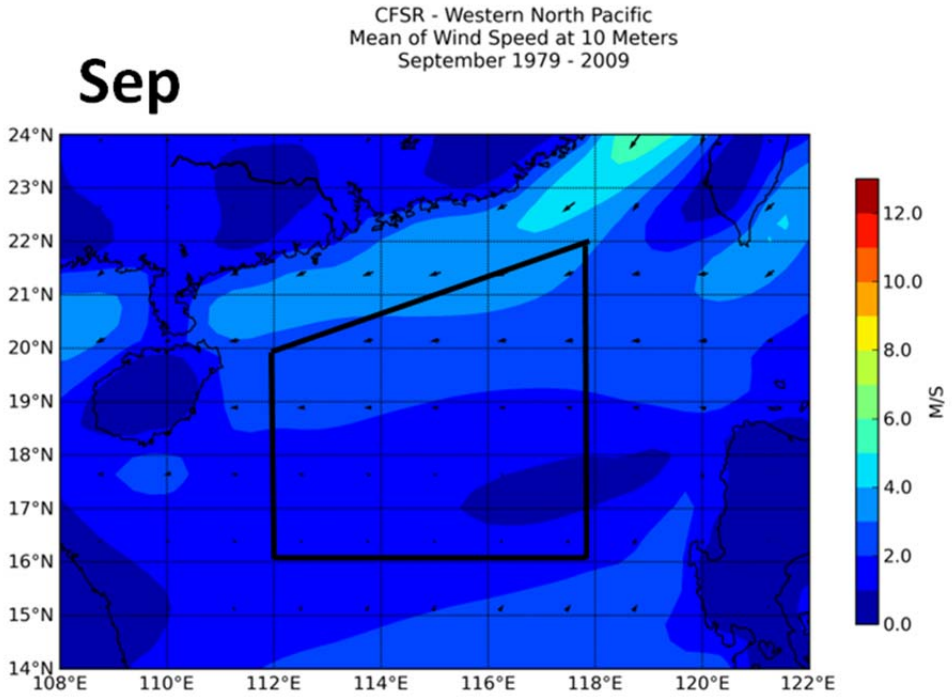

Figure 35. Area-averaged LTM WS in September is 2.0 m/s. Area-averaged monthly mean ranges from 0.8 to 4.4 m/s. Figure created at the ACAF website (October 2013).

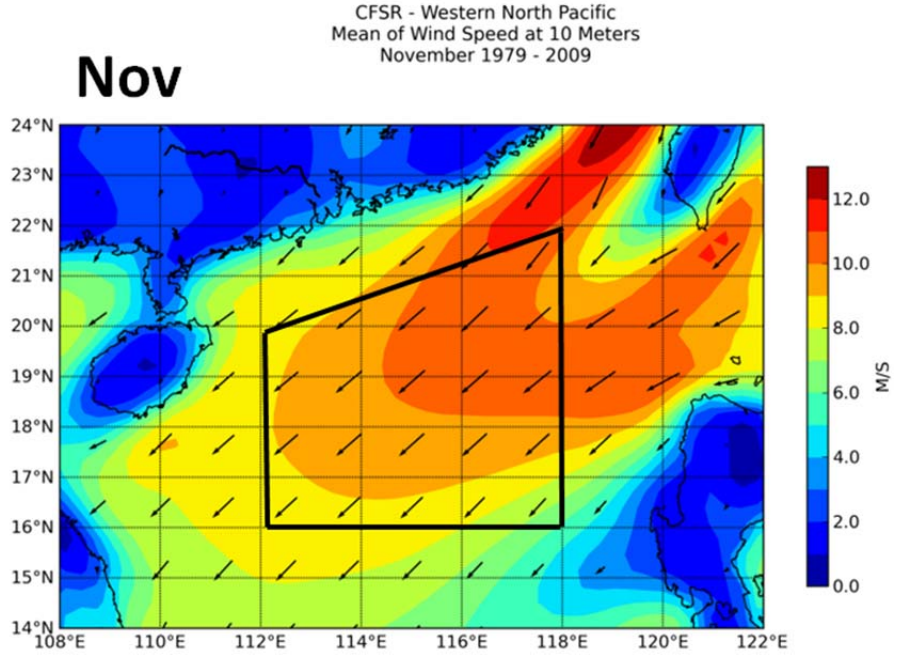

Figure 36. Area-averaged LTM WS in November is 9.6 m/s. Area-averaged monthly mean ranges from 6.3 to 11.5 m/s. Figure created at the ACAF website (October 2013).

Our correlation analyses of the relationships between SCS EDH and its constituent variables quantifies the importance of the role of each variable in each focus month (Table 1).

Table 1. Correlations of EDH with each constituent variable for each month. Significant correlations (above 0.352) are shaded in green. Particularly strong correlations (above 0.650) are shaded in dark green. These correlations are useful in determining which constituent variables are most important in each month.

Correlation of EDH with:	March	June	September	November
Wind Speed	0.559	**0.656**	-0.046	**0.800**
Sea Surface Temperature	-0.070	0.179	0.474	-0.107
Air Temperature	-0.175	0.464	0.494	-0.407
Air-Sea Temperature Difference	-0.341	0.503	-0.221	**-0.717**
Relative Humidity	**-0.658**	-0.042	-0.405	**-0.837**

C. IN-DEPTH CLIMATE ANALYSIS: NOVEMBER

We selected November for an in-depth climate analysis. This selection was based on the exceptionally strong correlations between EDH and several constituent variables in November, and the probable links between those variables and global climate variations (e.g., between ENLN and surface winds in the fall [Ramsaur 2009]). Figure 37 depicts November LTM EDH and the constituent variables. The spatial patterns of WS, AT, SST, ASTD, and RH can be used to derive the spatial pattern observed in EDH. For example, the effect of higher WS in the NE corner of the box is partially offset by the effects of cooler temperatures along the northern border of the box, which is why the

highest EDH values are observed along the eastern edge of the box instead of the NE corner where the wind field alone would suggest.

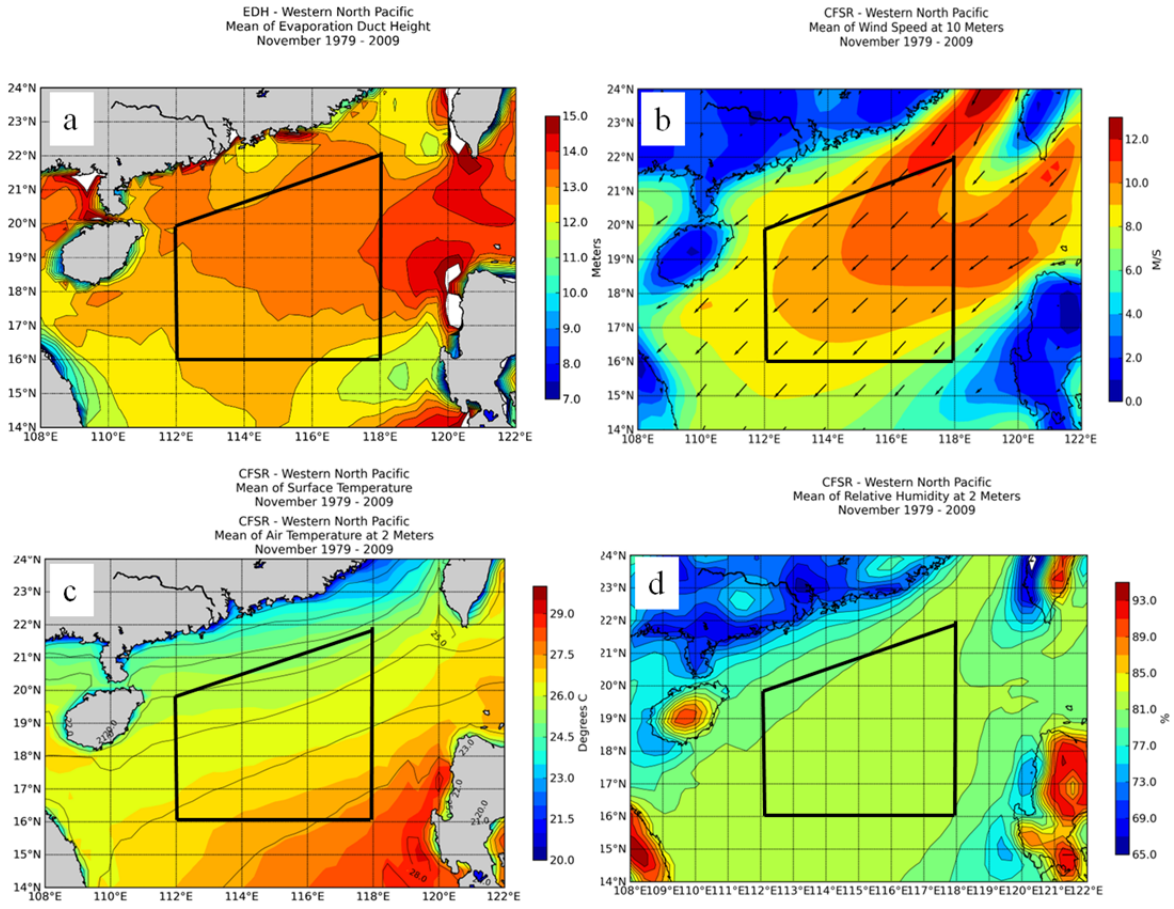

Figure 37. November LTM (a) EDH, (b) WS and direction, (c) SST in color shading and AT in black contours, and (d) RH. Figures created at the ACAF website (October 2013).

1. Interaction of EDH and Constituent Variables in November

The monthly mean ASTD in November is always negative (unstable), so the relationship between EDH and WS is positive, such that EDH increases (decreases) with an increase (decrease) in WS (see, for example, Figure 32).

The relationships between EDH and temperature in November are less straightforward. EDH shows a strong negative correlation with ASTD, and a weak negative correlation with SST (Table 1). Figure 38a shows that EDH decreases as ASTD

becomes less negative, but only for high wind speeds (winds speed above 9 m/s, which are commonly observed in November in the northern SCS). However, this probably only partially explains why there is a strong negative correlation between EDH and ASTD, since the change in EDH with ASTD is relatively small. This indicates that the dependence of EDH on ASTD is relatively complex.

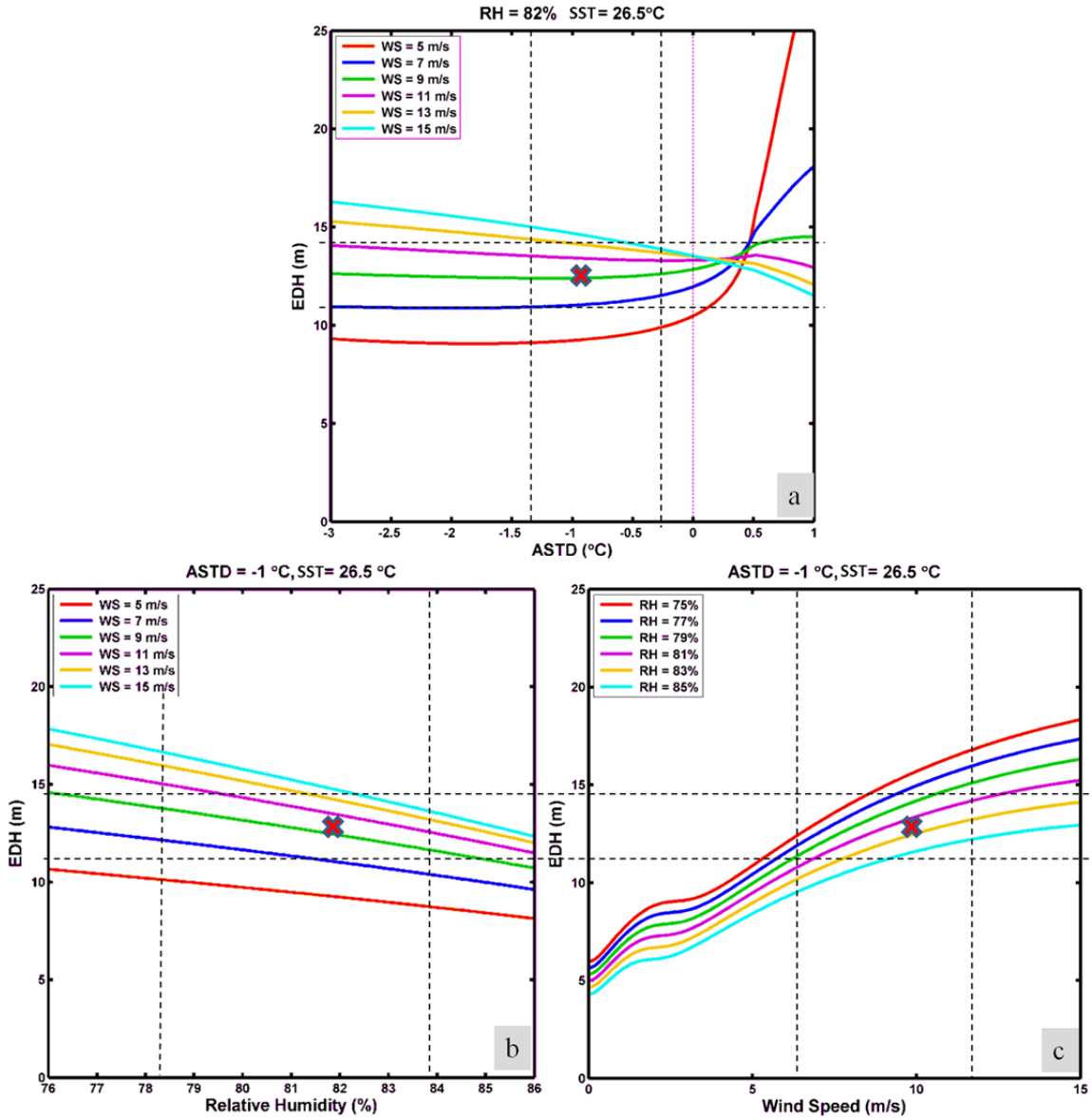

Figure 38. (a) EDH versus ASTD for various WS, (b) EDH versus RH for various WS, and (c) EDH versus WS for various RH. Dashed lines represent the extremes possible for area-averaged monthly means in November. The red "X" represents the November LTM. Plots of NAVSLaM-modeled EDH courtesy of Paul Frederickson (October 2013).

A likely explanation is that the negative correlations between EDH and AT (and ASTD) in November (Table 1) are closely related to the WS. November experiences strong NE winds which tend to advect colder air from the north into the SCS. So an increase in wind speed would likely correspond to a decrease in AT (and ASTD), which explains why the correlations of WS to EDH, and of AT (and ASTD) to EDH, are opposite to each other. It is also noteworthy that the correlations between EDH and AT (Table 1) are negative during months that experience northerly winds and cold air advection (November and March) and positive during months that experience southerly winds and warm air advection (June).

The strong negative correlation between EDH and RH in November (Table 1) is consistent with the results in Figure 38b. The strength of this correlation is likely related to the higher wind speeds from the NE in November that tend to advect drier air from Asia into the SCS (Figure 39). The combination of higher wind speeds and drier air significantly increase EDH and helps explain why the correlations of EDH with WS and RH (Table 1) are particularly strong in November in comparison to other months.

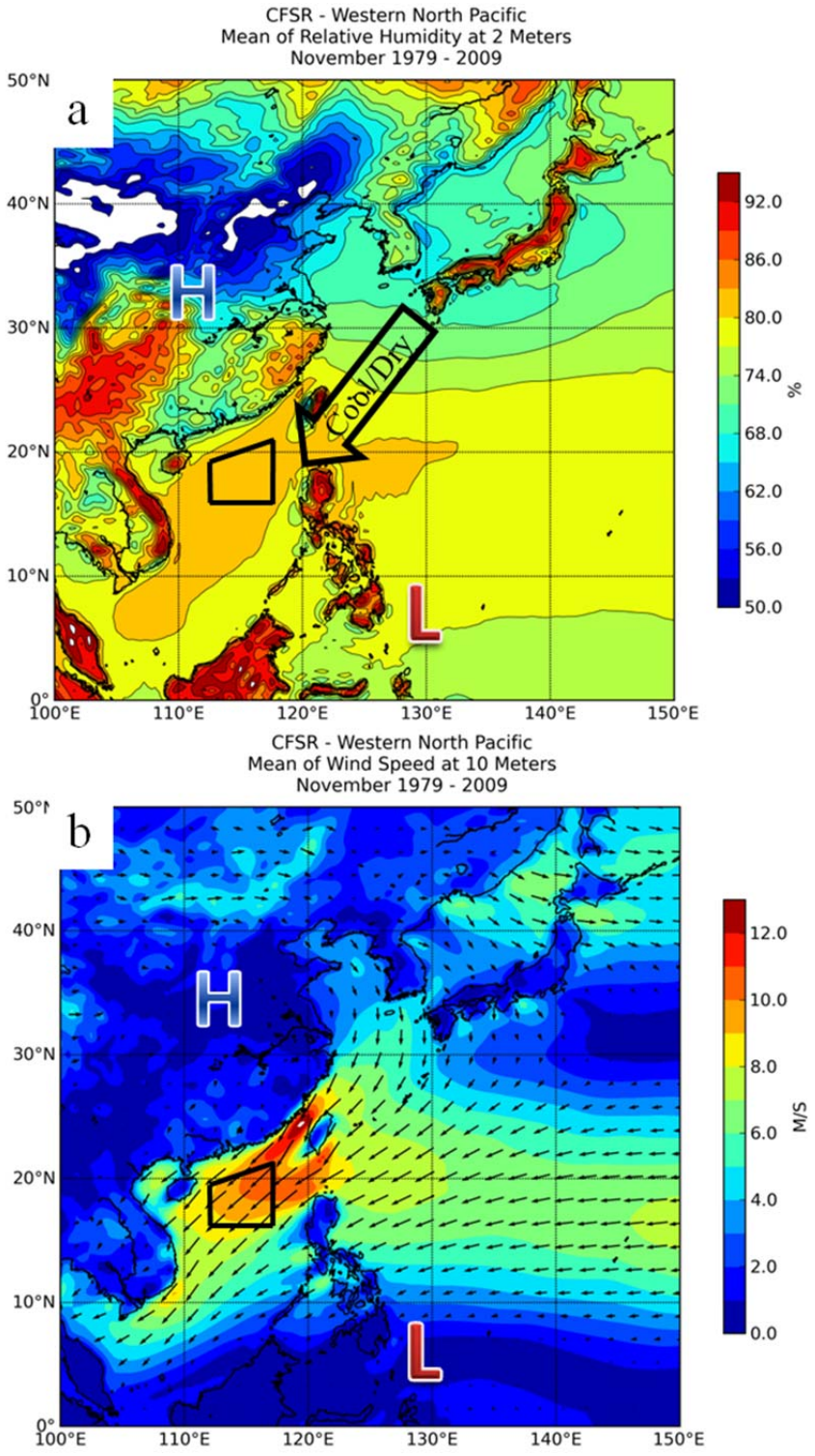

Figure 39. November (a) RH at 2 m and (b) WS at 10 m. The November winds advect low RH air from Asia into the SCS. The combination of low RH air and high wind speeds tends to increasing EDH in the northern SCS study region. Figures created at the ACAF website (October 2013).

2. Regional Climate Variables

We analyzed the relationships between SCS EDH variations and regional climate variables. Our primary motivation for these analyses was to determine the regional scale processes that lead to EDH variations and to lay a foundation for identifying potential predictors of the EDH variations at intraseasonal and longer scales. The geopotential height (GPH) anomalies associated with extremes in EDH can be very useful in identifying these processes and predictors—for example, regional circulation anomalies that alter the NE monsoon winds in Novembers with extremely high or low EDH values indicate the role of El Nino / La Nina (ENLN) or other climate variations in creating the EDH extremes. Figure 40a (b) shows conditional composites of the November 850 mb geopotential height anomalies for the eight Novembers during 1979-2009 that had the highest (lowest) EDH in our northern SCS study area. Note that the height anomaly patterns for the high and low ED composites are nearly opposite to each other. This is a strong indication that there is a robust, characteristic, and relatively linear relationship between the regional 850 mb GPH and northern SCS EDH.

Note also that the high (low) EDH height anomalies indicate anomalously strong (weak) NE monsoon winds, consistent with the prior results that indicate that EDH in November tends to increase when wind speed increases (Table 1, Figure 38). The opposite patterns for the two composites over large portions of the northern and southern hemispheres indicate that extremes in the northern SCS EDH are related to global scale climate variations.

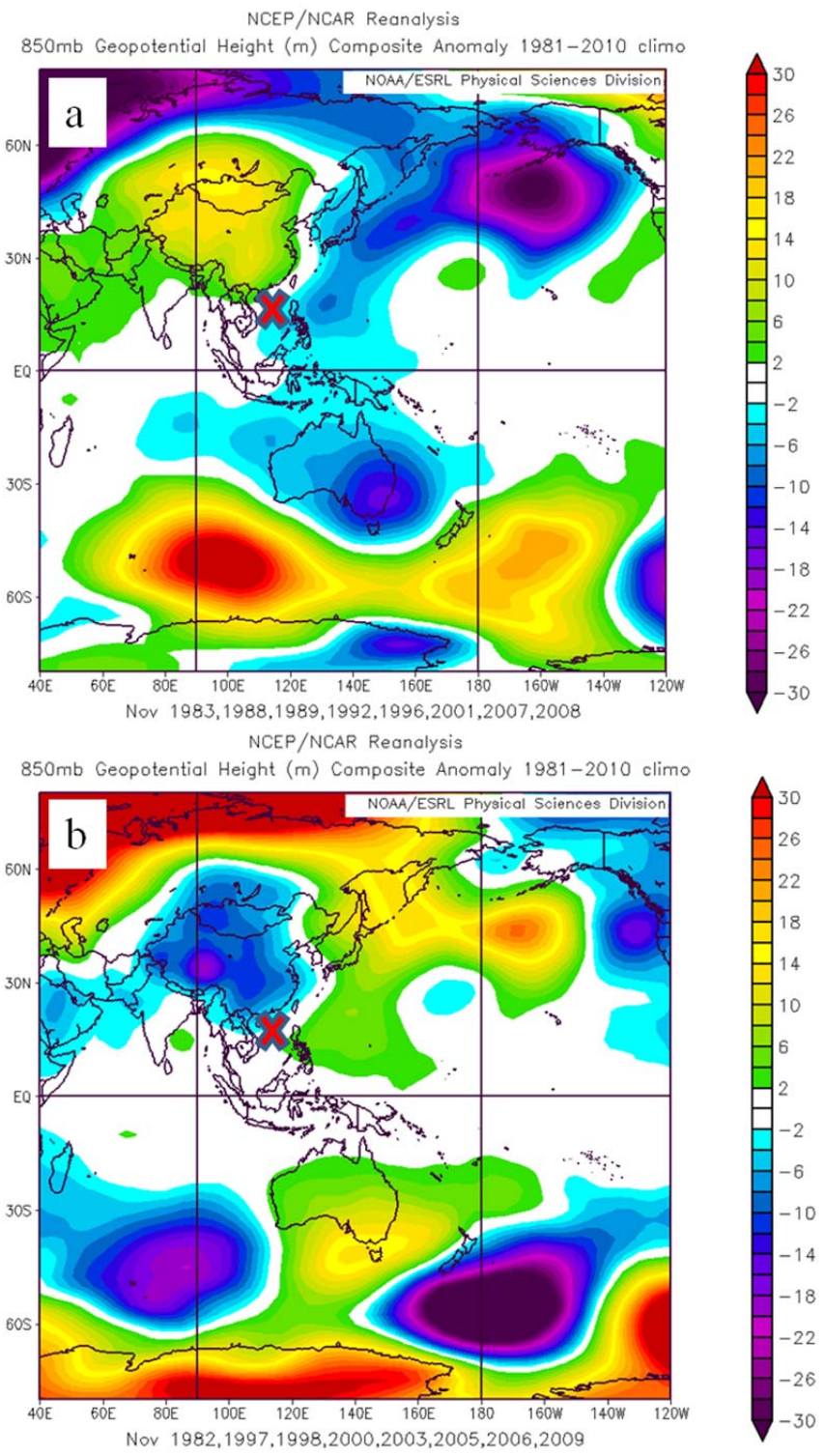

Figure 40. Conditional composite November 850 mb GPH anomalies for the eight Novembers in 1979-2009 with (a) the highest EDH and (b) the lowest EDH. The red X indicates the northern SCS study region. Figures created at the ESRL website (October 2013).

Figure 41 is a map of the correlation between November EDH in the northern SCS study region and November 850 mb GPH for all years (1979–2009). Positive (negative) correlations indicate that EDH increases (decreases) tend to be associated with 850 mb GPH increases (decreases). Correlations magnitudes that are equal to or greater than 0.352 are significant at the 95% level (see Chapter II, section B.3). Significant correlations occur in regions where strong and opposite anomalies were observed in the conditional composites (Figure 40). In particular, a positive correlation of 0.77 occurs in SE Asia and a negative correlation of -0.45 occurs in the WNP-Philippine Sea region. The similarities between the conditional composite results (Figure 40) and the correlations (Figure 41) indicate that: (a) the composites for the eight extremes provide are at least approximately representative of the relationships between EDH and 850 mb GPH during all the years; (b) the correlations represent real physical processes of the type discussed in the preceding paragraph; and (c) regional and global scale variations in 850 mb GPH play a major role in producing northern SCS EDH variations.

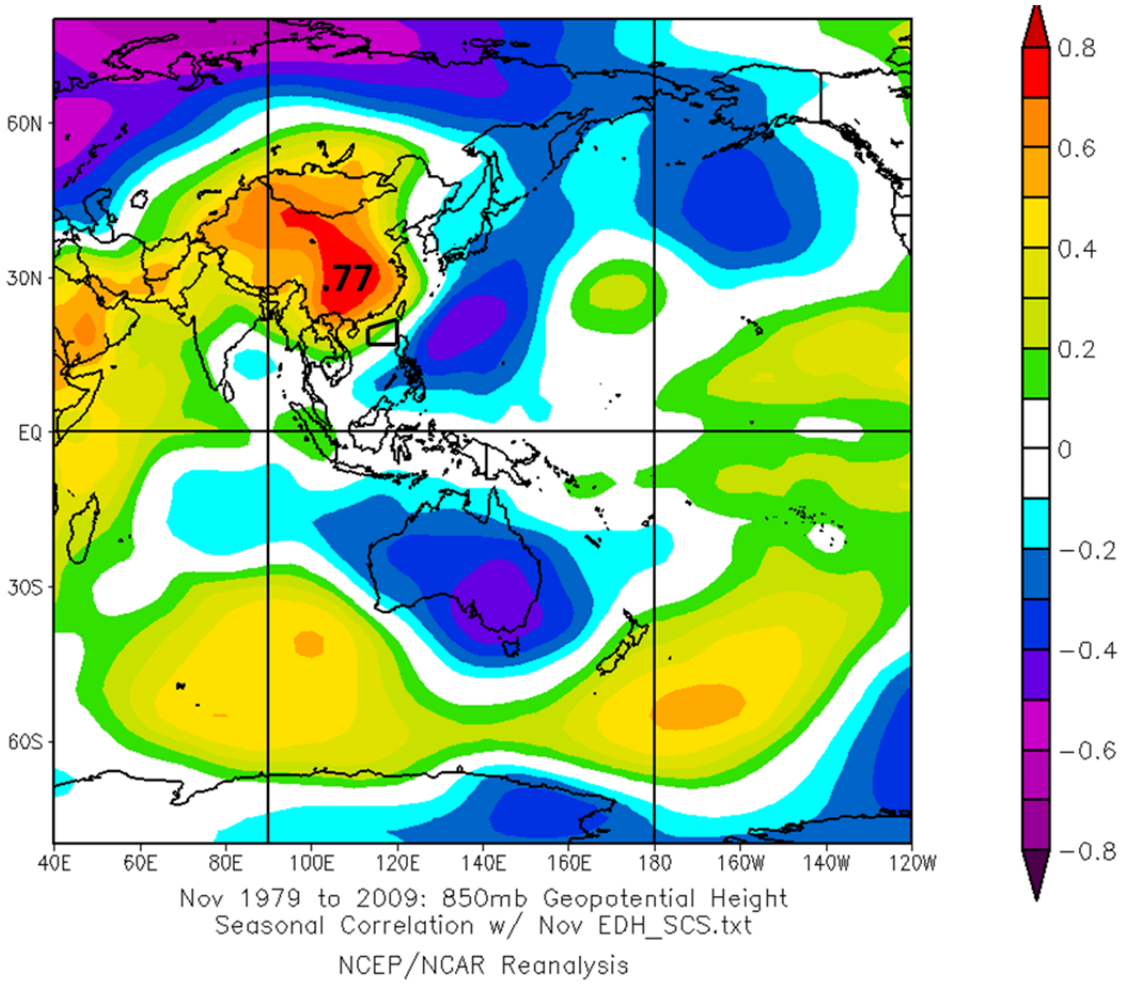

Figure 41. Correlation between November northern SCS EDH and 850 mb GPH for 1979-2009. The strongest correlations shown in this figure are +0.77 over China and -0.64 over the Arctic. Figure created at the ESRL website (October 2013).

Outgoing longwave radiation (OLR) can provide useful information about clouds and related quantities, such as precipitation. In the lower latitudes, OLR can be used to infer precipitation in deep convective systems, with, for example, lower values of OLR indicating deep convection and precipitation. Figure 42 is a map of the correlation between November EDH in the northern SCS study region and November OLR for all years (1979–2009). The strong negative correlations in the SCS-Philippine Sea region (shown in purple) indicate that increased (decreased) deep convection in this region is associated with decreased (increased) EDH in the northern SCS in November. This result,

combined with the wind-EDH results shown in Figures 40–41, indicate that increased (decreased) EDH in the northern SCS in November is associated with increased (decreased) NE monsoon winds that may contribute to more (less) intense deep convection in the tropical WNP. The significant positive and negative correlations with OLR over much of the western Pacific shown in Figure 42 indicate that the EDH variations are associated with large scale anomalies in convective activity in the northern and southern hemispheres.

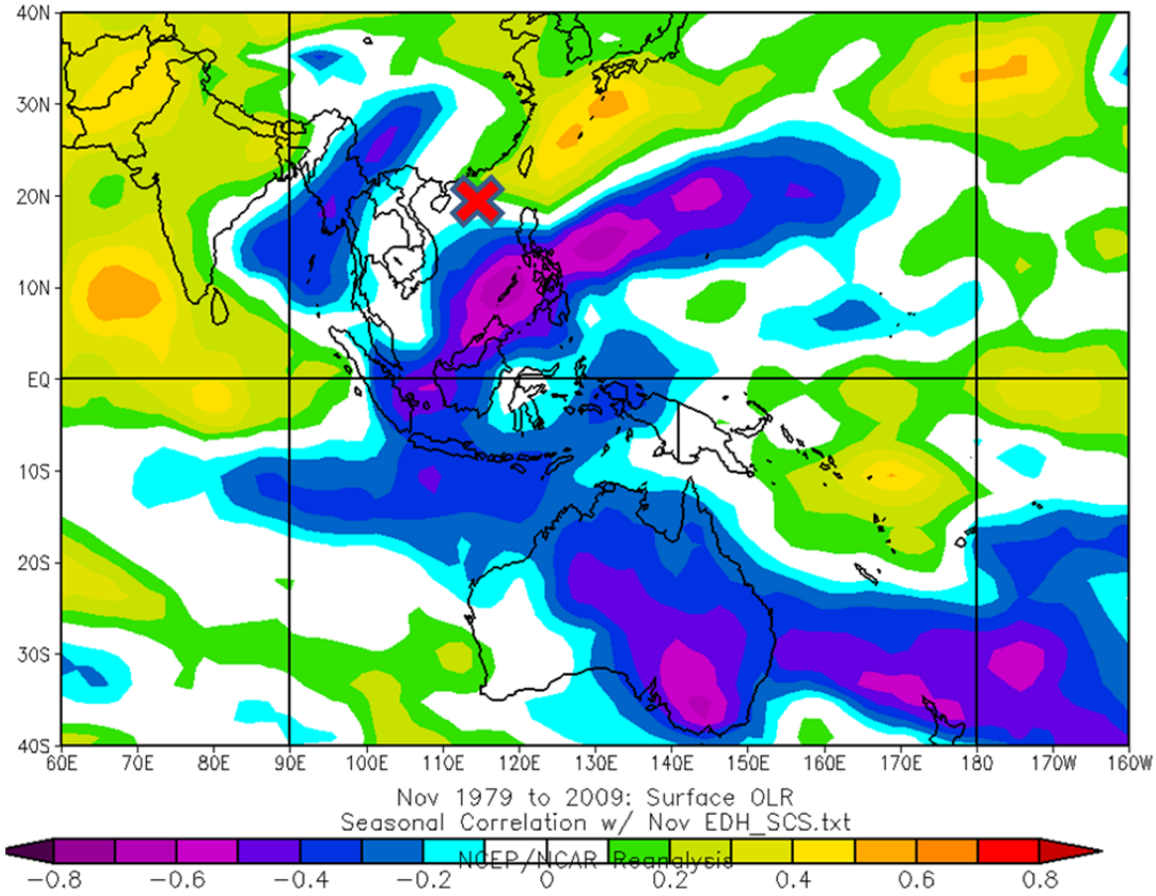

Figure 42. Correlation between November SCS EDH and OLR for 1979-2009. The strongest correlations are +0.56 and -0.70. The red X indicates the northern SCS study region. Figure created at the ESRL website (October 2013).

3. Global Climate Variations

Evidence of global scale climate variations can often be found in maps of 200 mb GPH anomalies, especially for variations that involve anomalies in extratropical and tropical atmospheric longwave patterns. Figure 43 shows the 200 mb GPH anomalies for the extreme EDH Novembers discussed in the prior section (see Figure 40). Note that the anomaly patterns in Figures 43 and 40 are very similar in the regions where the two figures overlap, especially in the extratropics (but with the 200 mb anomalies being slightly further to the west than those at 850 mb). This indicates that the upper and lower tropospheric GPH anomalies are physically related to each other and have an approximately equivalent barotropic structure. The global anomalies (Figure 43) show clear anomalous extratropical wave trains (e.g., the alternating positive and negative anomalies that extend across the North Atlantic, Asia, and North Pacific). In particular, there is an arching anomalous wave train extending from the North Atlantic into East Asia. Taken together, these results indicate that the 850 mb anomalies are part of a global scale pattern of anomalies and therefore are likely to be linked to global climate variations. Thus, northern SCS EDH variations are also likely to be driven to a significant extent by global climate variations. If so, then global scale anomalies and climate variations may be useful as intraseasonal to interannual predictors of northern SCS EDH.

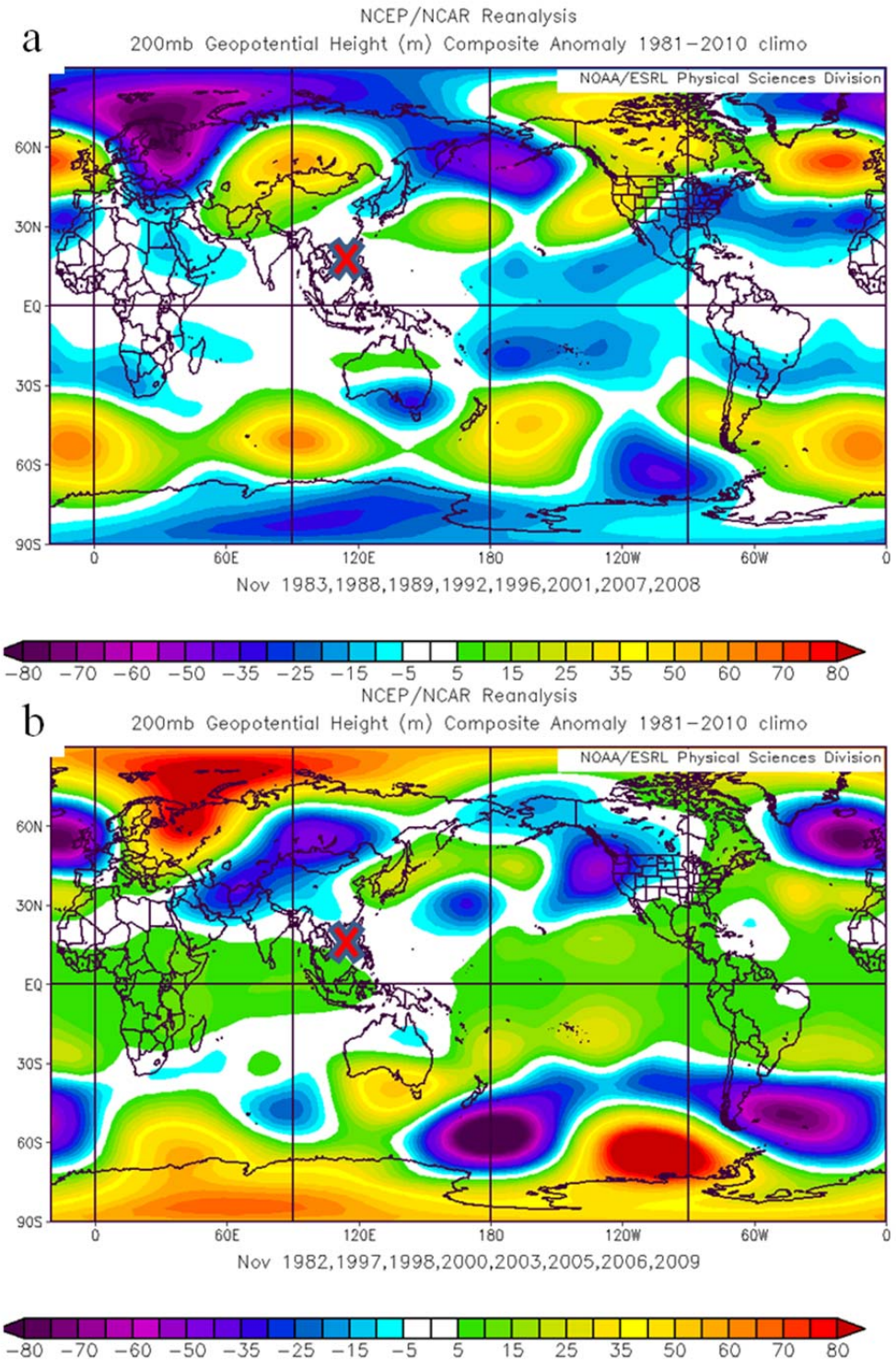

Figure 43. Conditional composite November 200 mb GPH anomalies for the eight Novembers in 1979-2009 with (a) the highest EDH and (b) the lowest EDH. The red X indicates the northern SCS study region. Figures created at the ESRL website (October 2013).

Large-scale variations in SST can have significant impacts on atmospheric conditions (e.g., Wolter and Timlin 1993). For example, warming of the eastern tropical Pacific (associated with El Nino) creates relatively unstable conditions, enhances convection, and alters lower and upper tropospheric GPH in that region. These GPH variations over the eastern tropical Pacific tend to produce corresponding GPH anomalies in nearby regions and globally via low frequency wave activity (Ford 2000). This large scale wave activity produces teleconnections or links between environmental conditions in widely separated parts of the globe. Figures 40, 41, and 43 suggest that northern SCS EDH variations in November are in part the result of global scale processes that set up anomalous wave trains that extend into East Asia that alter surface pressures over Asia and the western North Pacific that then alter the NE monsoon winds that then alter the northern SCS EDH. These figures do not explicitly provide information on what initial events cause which subsequent events. But physical reasoning suggests that the EDH variations are most likely driven by prior changes in circulation rather than the other way around. The lag-lead correlation results discussed in section 5 provide information about events that lead to the EDH variations and that may be useful in long-range forecasting of those variations.

Large scale and persistent changes in SST typically take place over the span of several months and have a long-lived influence on global atmospheric conditions. This makes SST anomalies useful for long-lead forecasting of other climate variables, if SST and those variables are well correlated. Figure 44 shows conditional composites of global SST anomalies during the eight highest and eight lowest EDH Novembers in 1979–2009. The opposite anomalies in the tropical central-eastern Pacific are very similar to characteristic ENLN SST anomalies, indicating that northern SCS EDH variations in November are related to ENLN. The strong and opposite SST anomaly patterns in the Arctic suggest that: (a) the Arctic SST anomalies may be related to the global scale climate variations indicated by the GPH anomalies shown in Figures 40, 41, and 43; and (b) the northern SCS EDH variations may be related to climate variations that influence the Arctic (e.g., ENLN, the Arctic Oscillation, the North Atlantic Oscillation).

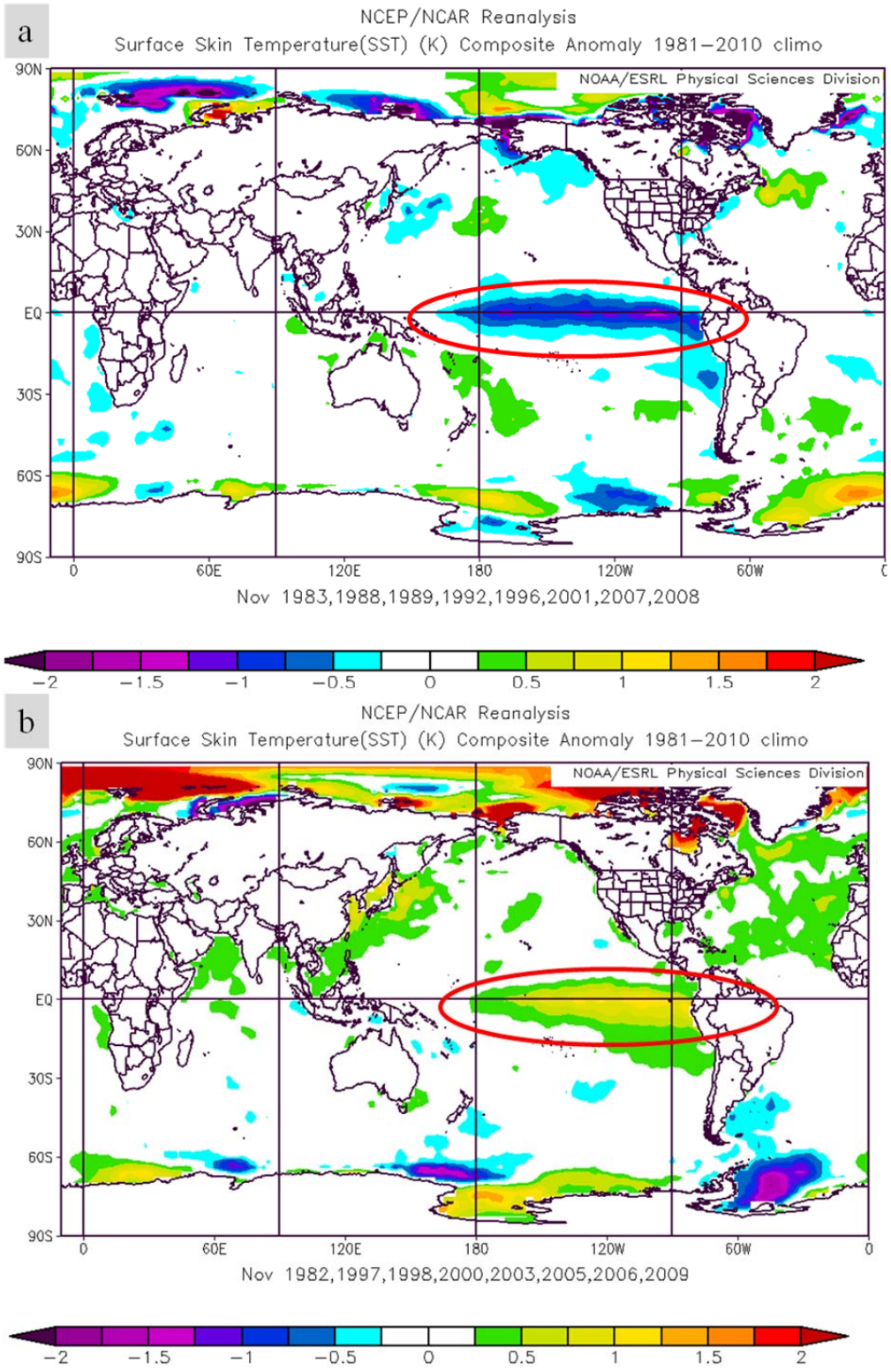

Figure 44. Conditional composite November SST anomalies for the eight Novembers in 1979-2009 with (a) the highest EDH and (b) the lowest EDH. Figures created at the ESRL website (October 2013).

The correlation between northern SCS EDH and SST in November for 1979–2009 is shown in Figure 45. Note the general agreement with the conditional composite anomalies in Figure 44. For example, the tropical central-eastern Pacific and the Arctic SST anomalies in Figure 44 are well represented in the correlations. Note though that the strongest correlation between northern SCS EDH and SST is located near 10^0N, 170^0W in the central tropical Pacific.

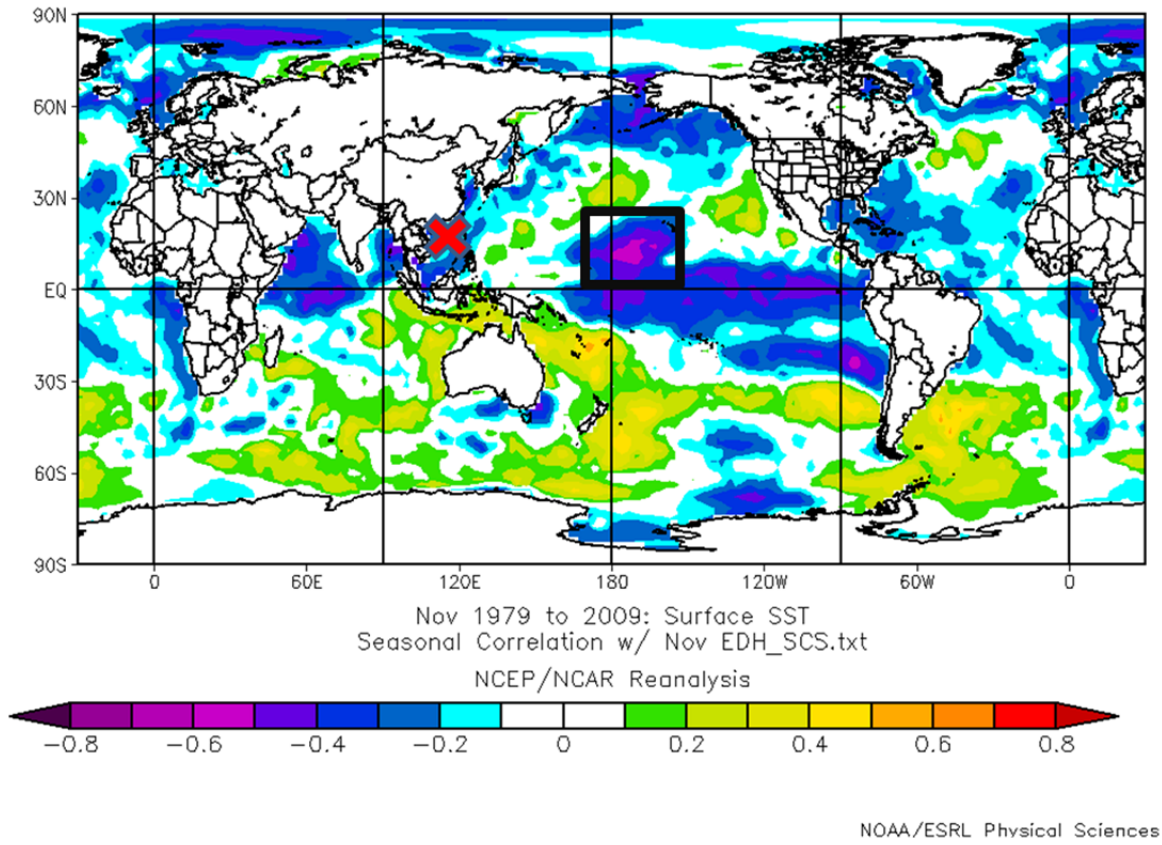

Figure 45. Plot of correlation between SCS EDH and SST in November. The global maximum correlation values are +0.55 and -0.71. The red X indicates the northern SCS study region. Figure created at the ESRL website (October 2013).

4. Climate Indices

We conducted analyses of the relationships between northern SCS EDH and global climate variations using indices of several climate variations. MEI was used to represent El Nino / La Nina / Southern Oscillation, Nino 4 was used to represent central

equatorial Pacific SST, the IOD index to represent the IOD (or IOZM), the PWP index to represent equatorial SST in the central-eastern IO and western Pacific, and the SAMOI for the strength of the summer Asian monsoon.

Table 2 provides an overview of the relationships between northern SCS EDH in November and the climate variation indices. The colored columns are conditional composite anomalies of EDH for the eight highest and eight lowest EDH Novembers. The right column shows the correlations between EDH and the climate indices. The LTM and standard deviation columns provide reference values for assessing the composite and correlation results. Oppositely signed anomalies for a given index indicate a possible relationship between EDH and the indicated climate variation. The strength of that relationship is suggested by the absolute value of the anomaly and the corresponding correlation value. Note that the SAMOI values are for the preceding October (SAMOI leading EDH by one month). The anomaly and correlation results in Table 2 indicate that northern SCS EDH in November is significantly related to ENLN and Nino 4 SST in November, marginally related to SAMOI-a in October and IOD in November, and poorly related to the November PWP, October SAMOI-w, and October SAMOI-n. These results are consistent with those shown in the prior composite and correlation figures.

Table 2. Relationships between northern SCS EDH in November and climate variation indices. The blue and orange columns show conditional composite EDH anomalies for the Novembers with the eight lowest and eight highest EDH values. The right column shows correlations between the EDH data and climate variation indices. The long term mean and standard deviation of the EDH data are provided as reference values. All values are based on 1979–2009 data, except for PWP for which 1979–2008 data was used.

Climate Variation Index	8 Lowest EDH Novembers	Long Term Mean	8 Highest EDH Novembers	LTM Standard Deviation	Correlation with EDH all Novembers
EDH (m)	-1.09	12.93	1.18	0.92	1.00
Nov MEI	0.40	0.29	-0.69	0.98	-0.37
Nov Nino4 (C)	0.22	28.70	-0.55	0.73	-0.40
Nov IOD	0.37	0.00	-0.53	1.11	-0.19
Nov PWP*	0.10	0.26	0.01	0.18	-0.08
Oct SAMOI-a	-0.19	-0.10	0.61	0.96	0.26
Oct SAMOI-w	-0.07	-0.11	0.04	1.17	0.08
Oct SAMOI-n	0.04	-0.05	-0.29	0.91	-0.10

5. Lead Correlations and Long-Lead Forecasting Potential

We analyzed correlations between November northern SCS EDH and variables for the preceding August, September, and October. We used these correlations to: (a) investigate cause-effect relationships and physical processes that produce EDH variations; and (b) identify potential long-lead predictors of EDH.

SST is often useful as a long-lead predictor due to its tendency to change much more slowly than atmospheric variables and the tendency of large regions of SST anomalies to influence global climate. Table 3 presents the correlations between November SCS EDH and the climate indices up to three months in advance. Significant correlations were found between November SCS EDH and both MEI and the Nino 4 up to two months in advance. Both MEI and Nino 4 are heavily based on tropical Pacific

SST anomalies. Weaker correlations were found for IOD, PWP, and SAMOI-a, none of which were significant at the 95% level.

Table 3. Correlations between November SCS EDH and climate variation indices, with the indices leading by one to three months. Green shading indicates correlations significant at the 95% level. N/A indicates the index is not available in that month.

Index	November	Oct (-1)	Sep (-2)	Aug (-3)
MEI	-0.37	-0.40	-0.38	-0.27
Nino 4	-0.40	-0.40	-0.38	-0.30
Indian Ocean Dipole	-0.19	-0.15	-0.11	-0.05
Pacific Warm Pool	-0.08	0.19	0.16	0.02
SAMOI-a	n/a	0.26	.06	
SAMOI-w	n/a	0.08		
SAMOI-n	n/a	-0.10		

These correlation results, in combination with the prior conditional composite and correlation results, indicate that sufficiently strong relationships exist to investigate the potential to develop skillful intraseasonal to seasonal lead forecasts of November SCS EDH. Some forecast skill is likely from the use of MEI and/or Nino 4 as predictors. But the development of indices designed specifically to represent the climate variations associated with northern SCS EDH variations would be especially useful in developing skillful forecasts. These indices might be based on, for example, SST and GPH predictors with especially strong statistical and dynamical links to EDH (see Chapter II, sections C.2-4).

D. COASTAL AND SUB-MONTHLY VARIAITONS OF SCS EDH

Skillful long–lead forecasts of the monthly mean SCS EDH would be useful for long–lead operational planning. There are, however, limitations inherent in long–lead forecasting of SCS EDH that must be addressed.

1. Coastal and Diurnal Variations in EDH

This study was limited to EDH in the open ocean (> 100 km from coastlines) because spatial and diurnal variations within 100 km of the coast can be extreme. The boundary layer air over continental land masses is often much drier than that of adjacent bodies of water. In contrast, large tropical islands often have relatively high moisture levels in the boundary layer due to large amounts of rainfall and evaporation from foliage. These contrasts can be observed in Figure 39a of relative humidity in the western Pacific and East Asia. Comparison of November RH levels in the SCS with the RH in southern China shows lower RH over the land, but in contrast, the RH over the Philippines is higher than over the SCS. These surface RH variations over land are also much more variable in time and space than the surface RH over the open ocean.

The different RH conditions over these land masses is important because the direction of the wind will determine RH characteristics near the coast. Offshore flow of warm dry air from southern China has the potential to increase the EDH at and near the coast by tens of meters or more over the course of hours. Conversely, onshore flow of maritime air can reduce the EDH. Diurnal land-sea breezes and synoptic weather events can force these kinds of onshore and offshore flows over the course of several hours to several days.

Diurnal variations in EDH far away from coastlines within our area of study were quite low, usually less than 0.5 m and often less than 0.25 m (not shown). For this reason, all monthly mean data was derived from the daily mean values which include all hours of the day. The monthly mean EDH values are valid for all hours of the day within the area of study because variations within a single day tend to be very small. But this is not true near coastlines where the EDH variation due to the land-sea breeze and other coastal dynamics make the daily mean value much less useful than in our open ocean study area.

Figure 46 provides examples of typical coastal and diurnal variations in EDH. Each panel of this figure shows marked variability in EDH near coasts. A comparison of Figures 46a and 46b shows very high diurnal variation as well. The circled regions in Figure 46 are examples of coastal regions where the diurnal variation exceeds 10 m.

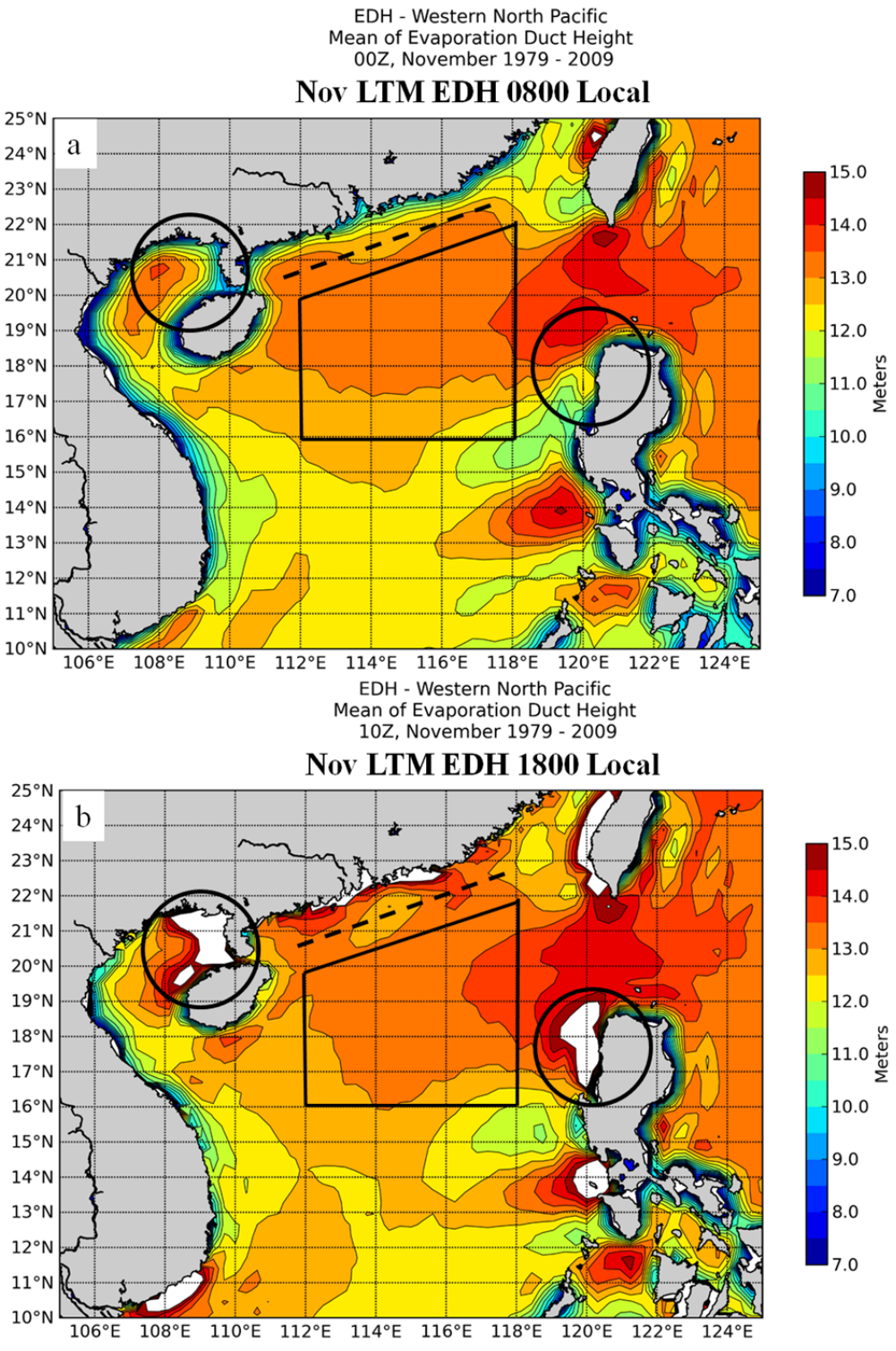

Figure 46. Diurnal and coastal variations in November LTM EDH. EDH at (a) 0800 local and (b) 1800 local show regions of significant coastal and diurnal variation (circled areas). The dashed line identifies a coastal region discussed in the main text. Figures created at the ACAF website (October 2013).

The dotted line along the coast of southern China in Figure 46 marks an example of coastal diurnal variability that could be important to naval operations concerned with whether EM emissions could be detected ashore. The EDH conditions at 1600 local time might allow emissions to propagate ashore while those at 0800 local might prevent emissions from reaching land-based receivers. Knowledge of this type of coastal and diurnal variability could be important in determining where and when during the day to conduct a particular operation.

2. Synoptic Variations in EDH

EDH is highly variable in space and time and changes as its constituent variables change. Synoptic systems that affect temperature, wind speed, and humidity will tend change the height of the evaporation duct. An analysis of monthly variations in EDH is useful. But information about daily and weekly variations in EDH would also be useful. The monthly mean is a good time-frame for examination of EDH on a seasonal basis or to examine the effects of climate variations, but it also filters out variation on any sub-monthly time scale.

Figure 47 depicts the daily mean EDH and daily mean wind field for two days in November 2004 (a fairly typical year in terms of climate conditions and SCS EDH). Figures 47a and 47c are the EDH and wind fields, respectively, on November 10th. Figures 47b and 47d are the EDH and wind fields nine days later. The wind fields are included to emphasize the importance of wind on EDH and that the significant change in EDH in this example is primarily due to a change in wind speed. Note that the EDH scale for this figure is 5–20 m, greater than for the prior monthly mean EDH figures. From November 10 to November 19, the EDH in our open-ocean area of study increased by approximately 10 m. This increase was closely associated with synoptic variations that led to a large increase in wind speed during that period.

In other cases, synoptic variations in EDH may be driven by surface heat flux variations that may force the ASTD to a positive value and reverse the effect of WS on evaporative ducts. An ASTD of +2° C has the potential to raise the EDH to over 50 m

when RH and WS are low. Those same conditions, but with 90% RH may make the evaporation duct disappear completely.

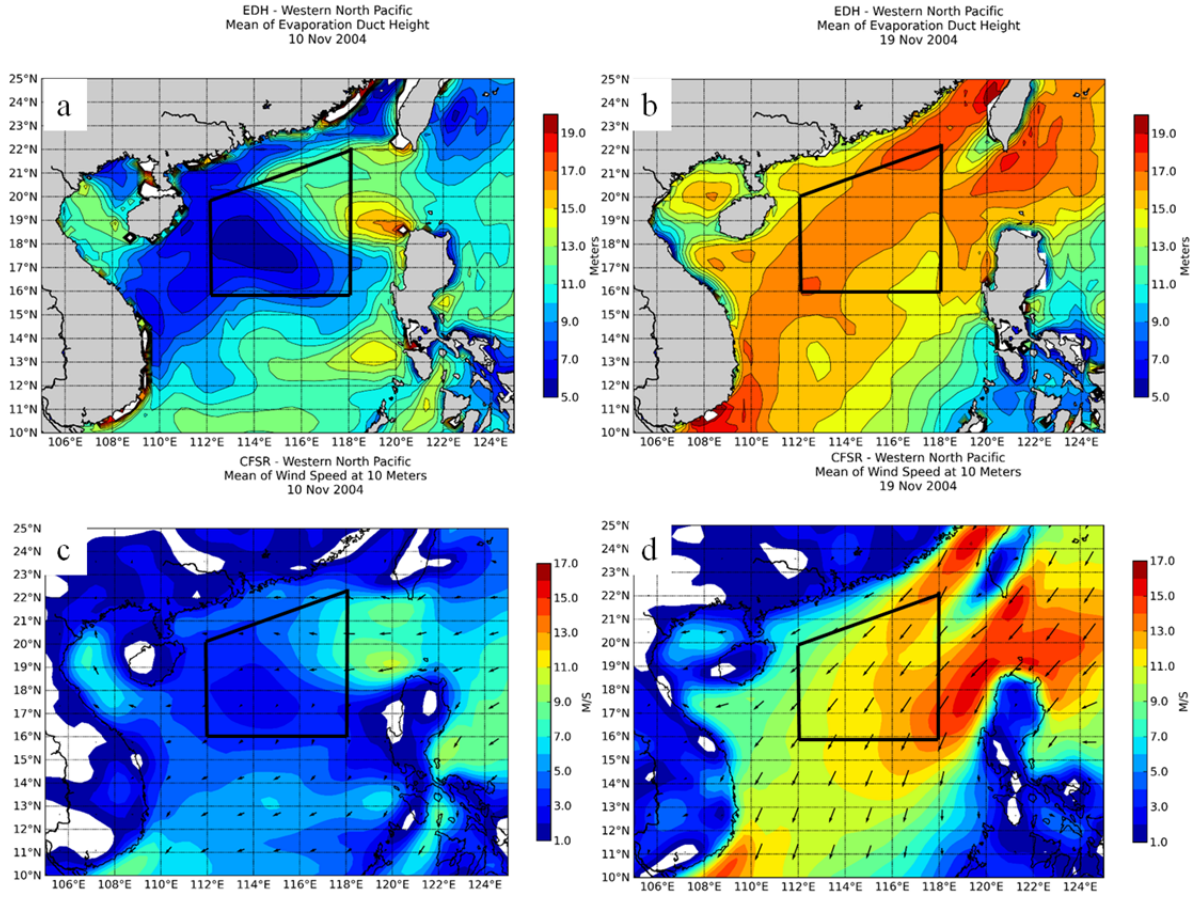

Figure 47. Example of daily variations of EDH in the SCS from November 2004. The November 10 daily mean EDH (a) and wind (c) compared to the November 19 daily mean EDH (b) and wind (d). The greater EDH on November 19 was associated with synoptic weather variations that led to stronger winds on that date. Figures created at the ACAF website (October 2013).

3. Tropical Cyclones and EDH in the SCS

Tropical cyclones (TCs) provide extreme examples of the effects of synoptic disturbances on EDH. TCs are relatively common occurrence in the SCS. Figure 48 is an example of the effects of a TC on November 1, 2006. Figure 48a depicts the surface winds and Figure 48b shows the corresponding EDH. U.S. Naval operations are not typically conducted in the vicinity of tropical cyclones, but this example demonstrates some of the potential impacts of a passing weather system on EDH conditions.

The wind field in Figure 43a shows much higher (lower) wind speeds and EDH on the west (east) side of the storm where the TC winds are blowing in the same (opposite) direction as the background NE Asian monsoon winds. Note that the TC winds both increase and decrease the EDH, depending on where, when, and how the TC winds combine with the background winds. In particular, note that the highest EDH is not co-located with the highest wind speeds, but is further west. The highest winds depicted in Figure 43a lie just east of 114^0E, but the highest EDHs occur west of 114^0E. This is a prime example of offshore flow of dry air from the Chinese mainland over the ocean. The elevated wind speeds in this area combination with decrease RH to produce a significant increase in EDH, and a much greater increase than what would have been produced by just the wind speed increase.

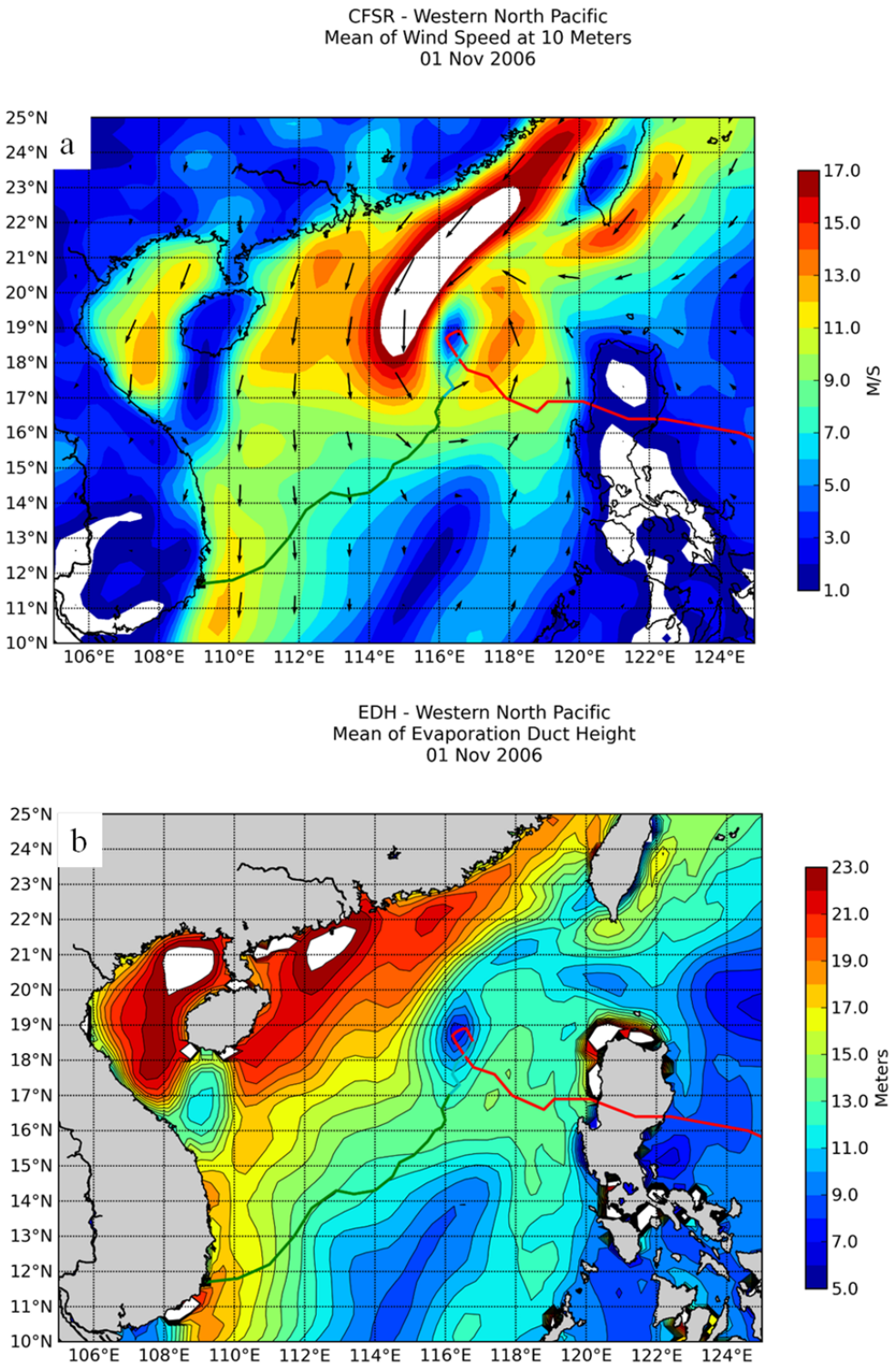

Figure 48. Impacts on SCS EDH of a tropical cyclone in the SCS on November 1, 2006. Figure 48a depicts the daily mean wind field and Figure 48b depicts the daily mean EDH. The red and green line shows the track of this TC. Figures created at the ACAF website (October 2013).

Analyses of the impacts of other TCs (not shown) indicate that TC impacts can extend well beyond the center of the TC. For example, a TC passing through the Philippine Sea created much stronger than normal NE winds blowing in the SCS as the TC approached the East China Sea (ECS), but then much weaker NE flow in the SCS as the TC made landfall in China. The passing of that TC influenced EDH in the SCS more than 1000 km away.

TCs provide extreme examples of the impacts of synoptic systems on EDH, but similar types of impacts occur for other types of synoptic weather systems.

IV. CONCLUSIONS AND RECOMMENDATIONS

A. SUMMARY AND CONCLUSIONS

We conducted climate analyses of spatial and temporal variations in evaporation duct height (EDH) in the northern South China Sea (SCS), including the relationships between EDH and global climate variations. Improved understanding of EDH in the SCS will aid in intraseasonal to interannual forecasting of EDH and related radar performance, and long–lead support for the planning of military operations and exercises. This type of support would have important implications for the detection of low-flying cruise missiles, submarine periscopes, and surface ships over the horizon.

Our study revealed that the variation in SCS EDH is strongly influenced on a seasonal basis by the East Asian Monsoon winds. EDH in our area of study reaches a maximum in June and November with the peaks of the summer and winter monsoons, respectively. EDH reaches minimums during the transition between the two monsoons in March and September. It is during these transitions where variables other than wind speed play a more important role in determining EDH.

The relationships we identified between northern SCS EDH and climate variations indicate: (a) a potential for developing skillful long–range forecasts of EDH for June, September, and November; and (b) that such forecasts would be more difficult in March. Relationships to El Nino / La Nina and the Multivariate ENSO Index (MEI) showed a potential for forecasting EDH in June and November. The Nino 4 index showed potential for forecasting EDH in November. The Pacific Warm Pool (PWP) and Summer Asian Monsoon OLR Index (SAMOI-a) showed potential for forecasting EDH in June and September.

Modern climate data sets, such as the Climate Forecast System Reanalysis (CFSR), and climate analysis tools, such as the Advanced Climate Analysis and Forecasting (ACAF) application, make a much more detailed analysis of EDH possible than in the previous studies of Twigg (2007) and Ramsaur (2009). Much higher spatial and temporal resolutions allow for more detailed examination of the impacts of synoptic

changes and climate variations on EDH. We conducted a detailed analysis of northern SCS EDH in November EDH in the SCS, but the same basic analysis techniques we used for November in the SCS can be applied to other months of interest, as well as to other regions of the world.

Evaporation ducts can be highly variable in space and/or time, which creates limits on the use of the type of climate analysis we conducted. Our climate analysis did not address the strength of evaporation ducting, other types of ducting, or other types of propagation paths due to the time constraints on our study and the limitations of the presently available reanalysis data (e.g., limited vertical resolution). But our study represents a significant step forward in climate analysis of evaporation ducts and provide a foundation for future studies that address additional scientific questions, data sets, and methods, and that extend the operational applications of climate analyses and long-lead forecasts.

B. RECOMMENDATIONS FOR FUTURE RESEARCH

The previous studies by Twigg (2007) and Ramsaur (2009) noted the limitations placed on evaporation duct studies by the limited horizontal, vertical, and temporal resolution of the available reanalysis data sets. These limitations have been significantly reduced, but the limited vertical resolution is still significant. The vertical resolution available in the current reanalysis data sets is not high enough to resolve the presence and attributes of evaporation ducts, or upper-air ducts such as elevated ducts, surface ducts, or surface-based ducts. We recommend development of reanalysis data sets with much higher vertical resolution in the boundary layer to aid in analyses of electromagnetic ducting.

Our study focused on an in-depth analysis of November EDH conditions, but similar analyses for other months are needed (e.g., for June and September for which we identified potential long-lead predictors of EDH). Our results showed or implied connections between northern SCS EDH and climate variations across the northern hemisphere and in the Arctic that need to be further investigated. Our research also suggested but did not directly address the possibility that the Madden-Julian Oscillation

(MJO) may play a role in determining SCS EDH. More research is needed on this topic, and identifying the climate variations, and the climate processes, that are most strongly related to EDH variations in all months of the year.

There is substantial potential for improved understanding and long-lead forecasting of SCS EDH through the development and application of climate variation indices tailored to the analysis and forecasting of EDH. Our analyses of geopotential height (GPH), outgoing longwave radiation (OLR), and SST indicate that there are significant global scale correlations to, and teleconnections with, SCS EDH that can be exploited to better understand and predict SCS EDH. Our results suggest that skillful long–lead forecasts of EDH based on standard climate variation predictors are possible up to two months in advance in some situations. Tailored indices have the potential to extend the lead time even further and to improve forecast skill at shorter lead times.

Several regions of emerging geopolitical importance are in need of evaporation duct analysis. CFSR data sets are available from ACAF for the northern Indian Ocean, the Mediterranean Sea, and the entire western North Pacific (WNP). To our knowledge, detailed climate analysis such as this has not been conducted in these regions since CFSR and ACAF have become available.

Our study demonstrated the potential for using CFSR and ACAF to study the impacts of tropical storms, cold surges, and other synoptic systems on EDH. We found that: (a) these impacts can be substantial and potentially predictable; and (b) the spatial and temporal resolutions of reanalysis data sets are now high enough to make detailed studies of these synoptic impacts more feasible.

Research is sorely needed into methods for collection of near-surface observations for the calculation of more accurate M-profiles, especially in-situ. Development of a system for ships at sea to make accurate measurements of near surface atmospheric parameters (wind speed, air temperature and relative humidity) at a single level and of the sea surface temperature for input to NAVSLaM, would greatly enhance the accuracy of the modified refractivity profiles used for radar performance predictions.

ACAF has demonstrated the utility of having high–resolution plan–view plots of evaporation duct height. The NAVSLaM model input requires only basic near–surface variables that can be readily obtained from current numerical weather prediction model analysis fields (Frederickson 2010b). Development of an ACAF–like map of real-time (or forecast) evaporation duct heights should be a logical next step. Similar products are already being produced for use in visualizing sonic layer depth and have shown utility in anti–submarine warfare. Evaporation ducts have implications for so many types of U.S. Naval operations, that development of such a product would be a logical and very useful next step forward.

APPENDIX

Table 4. March LTM, minimum monthly mean, and maximum monthly mean of EDH and its constituent variables.

March	Min	LTM	Max
EDH (m)	9.1	9.8	11.2
AT (C)	23.1	24.3	25.7
SST (C)	23.8	24.8	26.1
ASTD (C)	- 0.99	- 0.48	- 0.14
RH (%)	81.6	84.5	85.8
WS (m/s)	3.2	5.0	7.6

Table 5. June LTM, minimum monthly mean, and maximum monthly mean of EDH and its constituent variables.

June	Min	LTM	Max
EDH (m)	10.4	11.6	13.1
AT (C)	28.2	28.8	29.6
SST (C)	28.1	28.9	29.7
ASTD (C)	- 0.44	- 0.12	0.16
RH (%)	80.4	82.1	84.6
WS (m/s)	1.3	4.4	6.4

Table 6. September LTM, minimum monthly mean, and maximum monthly mean of EDH and its constituent variables.

September	Min	LTM	Max
EDH (m)	9.9	11.1	12.1
AT (C)	27.5	28.3	29.1
SST (C)	27.6	28.7	29.8
ASTD (C)	- 0.79	- 0.45	0.05
RH (%)	78.9	81.2	84.4
WS (m/s)	0.8	2.0	4.4

Table 7. November LTM, minimum monthly mean, and maximum monthly mean of EDH and its constituent variables.

November	Min	LTM	Max
EDH (m)	10.9	12.9	14.4
AT (C)	24.1	25.4	26.5
SST (C)	25.1	26.3	27.4
ASTD (C)	- 1.36	- 0.93	- 0.25
RH (%)	78.2	81.7	83.9
WS (m/s)	6.3	9.6	11.5

Table 8. Correlations between March SCS EDH and climate variation indices, with the indices leading by one to three months. No significant correlations were found.

Index	**March**	Feb (-1)	Jan (-2)	Dec (-3)
MEI	-0.09	-0.11	-0.15	
Nino 4	-0.20	-0.19		
Indian Ocean Dipole	0.12	-0.04		
Pacific Warm Pool	-0.07			
SAMOI-a	n/a			
SAMOI-w	n/a			
SAMOI-n	n/a			

Table 9. Correlations between June SCS EDH and climate variation, with the indices leading by one to three months. Green shading indicates correlations significant at the 95% level.

Index	**June**	May (-1)	Apr (-2)	Mar (-3)
MEI	0.23	0.38	0.40	0.45
Nino 4	0.01	(verified)		
Indian Ocean Dipole	0.21	0.12	0.02	
Pacific Warm Pool	0.36	0.28	0.34	0.30
SAMOI-a	-0.36	-0.18		
SAMOI-w	0.29	0.06		
SAMOI-n	0.21	-0.17		

Table 10. Correlations between September SCS EDH and climate, with the indices leading by one to three months. Green shading indicates correlations significant at the 95% level.

Index	**September**	Aug (-1)	Jul (-2)	Jun (-3)
MEI	-0.16	-0.16	-0.10	
Nino 4	-0.10	-0.12		
Indian Ocean Dipole	-0.26	-0.28	-0.32	-0.32
Pacific Warm Pool	0.30	0.39	0.47	0.40
SAMOI-a	0.18	-0.37	-0.13	
SAMOI-w	0.12	0.33	-0.02	
SAMOI-n	n/a	-0.10		

Table 11. Correlations between November SCS EDH and climate variation, with the indices leading by one to three months. Green shading indicates correlations significant at the 95% level.

Index	**November**	Oct (-1)	Sep (-2)	Aug (-3)
MEI	-0.37	-0.40	-0.38	-0.27
Nino 4	-0.40	-0.40	-0.38	-0.30
Indian Ocean Dipole	-0.19	-0.15	-0.11	-0.05
Pacific Warm Pool	-0.08	0.19	0.16	0.02
SAMOI-a	n/a	0.26	.06	
SAMOI-w	n/a	0.08		
SAMOI-n	n/a	-0.10		

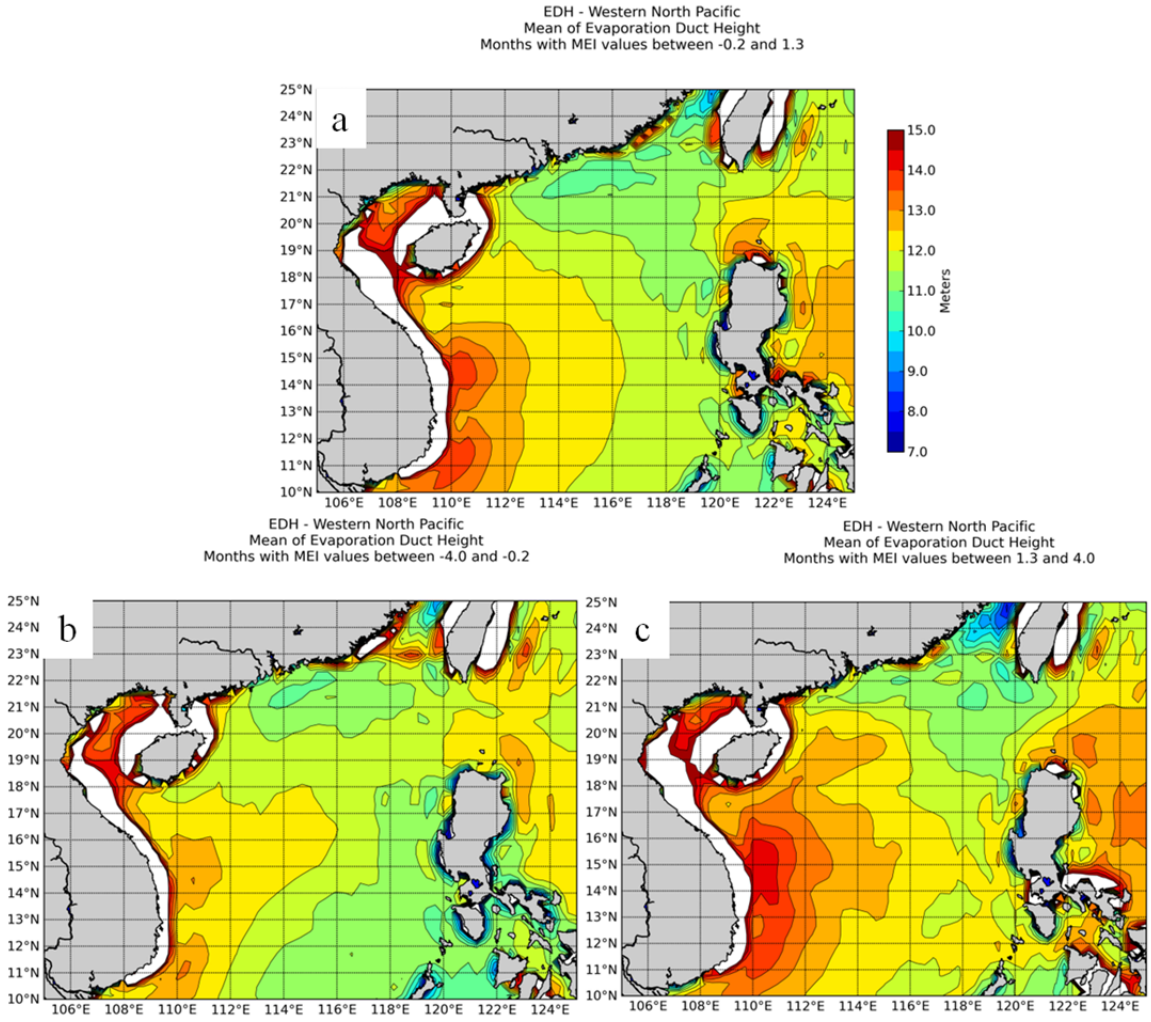

Figure 49. Conditional composite plots of June EDH for (a) 21 years of relatively neutral MEI between -0.2 and 1.3, (b) the five Junes with the lowest June MEI (-0.2 or less), and (c) the five Junes with the highest June MEI (1.3 or greater). June SCS EDH in our area of study had significant positive correlation with MEI. Note: La Nina years (negative MEI values) since 1979 have been relatively weak La Nina years on average in comparison to the strength of the El Nino years (positive MEI values) since 1979. Figures were created at the ACAF website (October 2013).

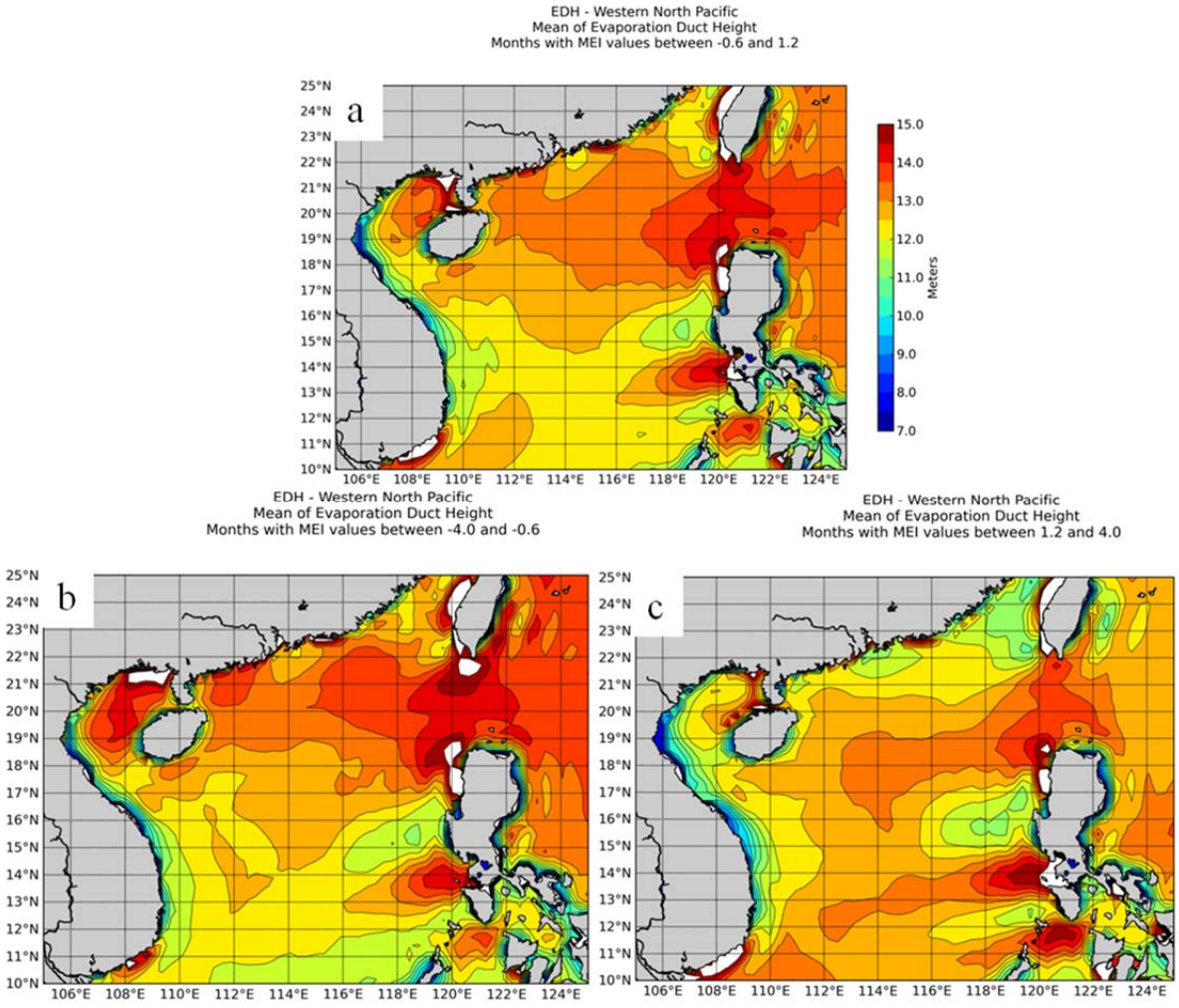

Figure 50. Conditional composite plots of November EDH for (a) 21 years of relatively neutral MEI between -0.6 and 1.2, (b) the five Novembers with the lowest November MEI (-0.6 or less), and (c) the five Novembers with the highest November MEI (1.2 or greater). November SCS EDH had significant negative correlation with MEI. Note: La Nina years (negative MEI values) since 1979 have been relatively weak La Nina years on average in comparison to the strength of the El Nino years (positive MEI values) since 1979. Figures were created at the ACAF website (October 2013).

LIST OF REFERENCES

Earth System Research Laboratory, Physical Science Divisions, 2013a: *Linear Correlations in Atmospheric Seasonal/Monthly Averages.* Accessed from http://www.esrl.noaa.gov/psd/data/correlation/

Earth System Research Laboratory, Physical Science Divisions, 2013b: *Climate Indices: Monthly Atmospheric and Ocean Time Series* [mei.data]. Retrieved from http://www.esrl.noaa.gov/psd/data/correlation/mei.data

Earth System Research Laboratory, Physical Science Divisions, 2013c: *Climate Indices: Monthly Atmospheric and Ocean Time Series.* [nina4.data]. Retrieved from http://www.esrl.noaa.gov/psd/data/correlation/nina4.data

Earth System Research Laboratory, Physical Science Divisions, 2013d: *Climate Indices: Monthly Atmospheric and Ocean Time Series* [pacwarm.data]. Retrieved from http://www.esrl.noaa.gov/psd/data/correlation/pacwarm.data

Earth System Research Laboratory, Physical Science Divisions, 2013e: *Monthly/Seasonal Climate Composites.* Accessed from http://www.esrl.noaa.gov/psd/cgi-bin/data/composites/printpage.pl

Earth System Research Laboratory, Physical Science Divisions, 2013f: *Multivariate ENSO Index (MEI).* Accessed from http://www.esrl.noaa.gov/psd/enso/mei/mei.html

Fleet Numerical Meteorological and Oceanographic Center Climatology Portal, 2013: *Advanced Climate Analysis and Forecast.* Accessed from http://www.esrl.noaa.gov/psd/data/correlation/

Ford, B. W., 2009: El Nino and La Nina Effects on tropical cyclones: The mechanisms. M.S. thesis, Dept. of Meteorology, Naval Postgraduate School, Monterey, California, 120 pp.

Frederickson, P. A., K. L. Davidson, and A.K. Goroch, 2000: *Operational bulk evaporation duct model for MORIAH*, Version 1.2. Naval Postgraduate School, 70 pp. (Available from P. A. Frederickson, Naval Postgraduate School, 589 Dyer Road, Monterey, CA 93943–5114).

Frederickson, P. A., and K. L. Davidson, 2008: *Operational bulk evaporation duct model.* Naval Postgraduate School, 55 pp. (Available from P. A. Frederickson, Naval Postgraduate School, 589 Dyer Road, Monterey, CA 93943–5114).

Frederickson, P. A., 2010a: Software Design Description for the Navy Atmospheric Vertical Surface Layer Model (NAVSLaM) CSCI, Version 1.0. Prepared for the Naval Oceanographic Office, Systems Integration Division, 7 July 2010. 36 pp.

Frederickson, P. A., 2010b: Software Requirements Specification for the Navy Atmospheric Vertical Surface Layer Model (NAVSLaM) CSCI, Version 1.0. Prepared for the Naval Oceanographic Office, Systems Integration Division, 7 July 2010. 38 pp.

Frederickson, P. A., 2010c: Software Test Description for the Navy Atmospheric Vertical Surface Layer Model (NAVSLaM) CSCI, Version 1.0. Prepared for the Naval Oceanographic Office, Systems Integration Division, 18 pp., 7 July 2010. 18 pp.

Frederickson, P. A., 2010d: Validation Test Report for the Navy Atmospheric Vertical Surface Layer Model (NAVSLaM) CSCI, Version 1.0. Prepared for the Naval Oceanographic Office, Systems Integration Division, 7 July 2010. 32 pp.

Guest, P., 2010a: *MR3419 Course Lecture 8,*[PowerPoint slides]. Department of Meteorology, Naval Postgraduate School, Monterey, California.

Guest, P., 2010b: *MR3419 Course Lectures 17*, [PowerPoint slides]. Department of Meteorology, Naval Postgraduate School, Monterey, California.

Japan Agency for Marine-Earth Science and Technology, 2013: *Indian Ocean Dipole, IOD, Home.* Accessed from www.jamstech.go.jp/frcgc/research/d1/iod/iod_home.html

Japan Agency for Marine-Earth Science and Technology, 2013: *Indian Ocean Dipole* [dipole%20mode%20index.html]. Retrieved from www.jamstech.go.jp/frcgc/research/d1/iod/html/dipole%20mode%20index.html

Japan Meteorological Agency, Tokyo Climate Center, WMO Regional Climate Center in RA II (Asia), 2013a: *ENSO and Asian Monsoon Monitoring Indices* [samoi-a.txt] Retrieved from http://ds.data.jma.go.jp/tcc/tcc/products/clisys/emi/samoi-a.txt

Japan Meteorological Agency, Tokyo Climate Center, WMO Regional Climate Center in RA II (Asia), 2013b: *ENSO and Asian Monsoon Monitoring Indices* [samoi-n.txt]. Retrieved from http://ds.data.jma.go.jp/tcc/tcc/products/clisys/emi/samoi-n.txt

Japan Meteorological Agency, Tokyo Climate Center, WMO Regional Climate Center in RA II (Asia), 2013c: *ENSO and Asian Monsoon Monitoring Indices* [samoi-w.txt]. Retrieved from http://ds.data.jma.go.jp/tcc/tcc/products/clisys/emi/samoi-w.txt

Japan Meteorological Agency, Tokyo Climate Center, WMO Regional Climate Center in RA II (Asia), 2013d: *Explanatory Notes.* Accessed from http://ds.data.jma.go.jp/tcc/tcc/products/clisys/explanation.html

Kalnay, E., Kanamitsu, M., Kistler R., Collins, W., Deaven D, Gandin L, Iredell M, Saha S, White G, Woollen J, Zhu Y, Chelliah M, Ebisuzaki W, Higgins W, Janowiak J, Mo CK, Ropelewski C, Wang J, Leetmaa A, Reynolds R, Jenne R, Joseph D., 1996: The NCEP/NCAR 40-year reanalysis project. *Bull. Amer. Meteo. Soc.* 77: 437–471.

National Weather Service, Climate Prediction Center, 2013: *El Nino regions.* Accessed from http://www.cpc.ncep.noaa.gov/products/analysis_monitoring/ensostuff/nino_regions.shtml

Ramsaur, D., 2009: Climate analysis and long range forecasting of radar performance in the Western North Pacific. M.S. thesis, Dept. of Meteorology, Naval Postgraduate School, Monterey, California, 93 pp.

Twigg, K.L., 2007: A smart climatology of evaporation duct heights and surface radar propagation for the Northwest Indian Ocean and nearby regions. M.S. thesis, Dept. of Meteorology, Naval Postgraduate School, Monterey, California, 131 pp.

Saha, S., and Coauthors, 2010: The NCEP climate forecast system reanalysis. . *Bull. Amer. Meteo. Soc.* 91: 1015–1057.

Wilks, D.S., 2006: *Statistical Methods in the Atmospheric Sciences.* 2nd ed. Academic Press, 627 pp

Wolter, K., and M.S. Trimlin, 1993: Monitoring ENSO in COADS with seasonally adjusted principal component index. *Proc. Of the 17th Climate Diagnostics Workshop,* Norman, OK, NOAA/N MC/CAC, NSSL, Oklahoma Clim. Survey, CIMMS and the School of Meteor., Univ. of Oklahoma, 52–57.

THIS PAGE INTENTIONALLY LEFT BLANK

INITIAL DISTRIBUTION LIST

1. Defense Technical Information Center
   Ft. Belvoir, Virginia

2. Dudley Knox Library
   Naval Postgraduate School
   Monterey, California